University of New Mexico
UNM Digital Repository

Fall 11-15-2016

SEARCHING NEUROIMAGING BIOMARKERS IN MENTAL DISORDERS WITH GRAPH AND MULTIMODAL FUSION ANALYSIS OF FUNCTIONAL CONNECTIVITY

Hao He
University of New Mexico

Follow this and additional works at: https://digitalrepository.unm.edu/ece_etds

Part of the Electrical and Computer Engineering Commons, Psychiatric and Mental Health Commons, and the Statistics and Probability Commons

Recommended Citation

Hao He
Candidate

Electrical and Computer Engineering
Department

This dissertation is approved, and it is acceptable in quality and form for publication:

Approved by the Dissertation Committee:

Vince D. Calhoun , Chairperson

Vincent P. Clark

Marios S. Pattichis

Jing Sui

**SEARCHING NEUROIMAGING BIOMARKERS IN
MENTAL DISORDERS WITH GRAPH AND
MULTIMODAL FUSION ANALYSIS OF
FUNCTIONAL CONNECTIVITY**

by

HAO HE

B.S., Computer Science and Technology,
Shanghai Jiao Tong University, 2007

M.S., Computer Engineering
The University of New Mexico, 2010

DISSERTATION

Submitted in Partial Fulfillment of the
Requirements for the Degree of

**Doctor of Philosophy
Engineering
with transcripted minor in Statistics**

The University of New Mexico
Albuquerque, New Mexico

December, 2016

DEDICATION

To

Wenhui Du

For her everlasting love

ACKNOLEDGEMENT

SEARCHING NEUROIMAGING BIOMARKERS IN MENTAL DISORDERS WITH GRAPH AND MULTIMODAL FUSION ANALYSIS OF FUNCTIONAL CONNECTIVITY
Hao He

B.S., Computer Science and Technology,
Shanghai Jiao Tong University, 2007

M.S., Computer Engineering,
University of New Mexico, 2010

Ph.D., Engineering,
University of New Mexico, 2016

ABSTRACT

Mental disorders such as schizophrenia (SZ), bipolar (BD), and major depression disorders (MDD) can cause severe symptoms and life disruption. They share some symptoms, which can pose a major clinical challenge to their differentiation. Objective biomarkers based on neuroimaging may help to improve diagnostic accuracy and facilitate optimal treatment for patients. Over the last decades, non-invasive in-vivo neuroimaging techniques such as magnetic resonance imaging (MRI) have been increasingly applied to measure structure and function in human brains. With functional MRI (fMRI) or structural MRI (sMRI), studies have identified neurophysiological deficits in patients' brain from different perspective. Functional connectivity (FC) analysis is an approach that measures functional integration in brains. By assessing the temporal coherence of the hemodynamic activity among brain regions, FC is considered capable of characterizing the large-scale integrity of neural activity.

In this work, we present two data analysis frameworks for biomarker detection on brain imaging with FC, 1) graph analysis of FC and 2) multimodal fusion analysis, to better understand the human brain. Graph analysis reveals the interaction among brain regions based on graph theory, while the multimodal fusion framework enables us to utilize the strength of different imaging modalities through joint analysis. Four applications related to FC using these frameworks were developed. First, FC was estimated using a model-based approach, and revealed altered the small-world network structure in SZ. Secondly, we applied graph analysis on functional network connectivity (FNC) to differentiate BD and MDD during resting-state. Thirdly, two functional measures, FNC and fractional amplitude of low frequency fluctuations (fALFF), were spatially overlaid to compare the FC and spatial alterations in SZ. And finally, we utilized a multimodal fusion analysis framework, multi-set canonical correlation analysis + joint independent component analysis (mCCA+jICA) to link functional and structural abnormalities in BD and MDD. We also evaluated the accuracy of predictive diagnosis through classifiers generated on the selected features. In summary, via the two frameworks, our work has made several contributions to advance FC analysis, which improves our understanding of underlying brain function and structure, and our findings may be ultimately useful for the development of biomarkers of mental disease.

Table of Contents

List of Figures

List of Tables

Chapter 1   Introduction

1.1   Motivation

Mental disorders including schizophrenia(SZ), bipolar disorder (BD) and major depressive disorder (MDD, or unipolar depression) rank among the most debilitating illnesses worldwide (Murray, Lopez et al. 1996; Hirschfeld and Vornik 2005). They share similar clinical symptoms, which often lead to misdiagnosis. Objective neuroimaging markers that distinguish disorders may significantly improve diagnostic accuracy, especially in the early phases of the illness (Strakowski, Adler et al. 2012), and may facilitate optimal clinical and functional outcome for individuals suffering from these disorder (Cardoso de Almeida and Phillips 2013).

In the two decades, both functional (Delvecchio, Fossati et al. 2012; Cerullo, Eliassen et al. 2014) and structural (Konarski, Mcintyre et al. 2008; Kempton, Salvador et al. 2011) brain abnormalities in patients with mental disorders have been extensively studied in the literature of magnetic resonance imaging (MRI). In general, functional MRI shows the brain activation in different regions. Functional connectivity (FC) analysis is an approach that assesses temporal coherence of the hemodynamic activity among brain regions (Friston 2002). FC calculated from fMRI images is capable of characterizing large-scale integrity of neural activity and provides insight into the functional integration and segregation of the brain (Van Dijk, Hedden et al. 2010). Graph analysis treats FC map across multiple brain regions as a whole network. Analyses of FC by computing graph theory metrics, such as clustering coefficient, characteristic path

length, local efficiency and global efficiency, further assess the topological properties of brain graphs, and provides a useful measure of how effectively information is passed and processed between different brain regions either locally (within one or several regions or connectivity) or globally (overall network structure of whole brain) (Rubinov and Sporns 2010). Graph organizational properties may reveal disease-related abnormalities in functional brain networks among psychiatric patients from resting-state as well as task-related neuroimaging data (Achard, Salvador et al. 2006; Stam, Jones et al. 2007; Liu, Liang et al. 2008; He, Chen et al. 2009; Lynall, Bassett et al. 2010; Wang, Metzak et al. 2010; Yu, Sui et al. 2011; Yu, Sui et al. 2011; He, Sui et al. 2012).

Generally, each neuroimaging modality provides a certain perspective on brain function or structure. For example, although fMRI contains both spatial and temporal information, its spatial resolution is relative low. On the other hand, structural MRI provides static images on tissue distributions in high spatial resolution. By intuition, the brain anatomical structures shape its function. This hypothesis has been supported by previous neuroimaging studies (Greicius, Supekar et al. 2009; van den Heuvel, Mandl et al. 2009; Mars, Jbabdi et al. 2011). However, the relationship between altered brain function and structure in mental disorders is still unclear. A conventional multimodal practice is firstly to analyze each modality separately, and then to compare the results side by side (Rigucci, Serafini et al. 2010). However, such an approach is not able to capture the joint information directly (Sui, Adali et al. 2012; Calhoun and Sui 2016). Data fusion through a joint analysis not only capitalizes on the strengths of each imaging modality, but also reveals underlying inter-relationships, providing comprehensive understanding of brain deficits in psychotic disorders (Calhoun, Adali et al. 2006; Sui,

2

Adali et al. 2012; Calhoun and Sui 2016). Associated FC maps and structural patterns derived from multimodal fusion analysis may be useful to differentiate patients with mental disorders.

1.2   Thesis Statement

In this dissertation, we introduce two data analysis frameworks on functional connectivity in human brains: graph analysis and multimodal fusion. By applying these analyses to functional connectivity, the underlying interaction patterns across brain regions, as well as the relationship between functional and anatomical attributes, can be revealed. Both functional and structural deficits may be characterized in different patients with mental illnesses like schizophrenia, bipolar and major depression disorders, thus could be served as objective biological markers to distinguish these disorders.

1.3   Outline

The dissertation is organized as follows:

Chapter 2 provides the background of the conducted research. The definition of biomarkers for mental disorders is introduced first. The basics of MRI for functional and structural brain imaging are explained, followed by a brief description to a common signal processing technique in medical imaging, independent component analysis. Introduction to functional connectivity, graph analysis, and multimodal fusion analysis are given too. In the end, the information of three clinical datasets used for dissertation work is provided.

Chapter 3 includes a study of functional connectivity from model-based approach, with application to find the altered brain functionality in schizophrenia during working

memory performance. A special type of graph structure called small-world network were built and analyzed using graph metrics. The findings characterize the effects of dysfunctional neural circuitry and variations in impaired connectivity across levels of working memory demands in SZ.

Chapter 4 demonstrates another graph analysis study that constructing functional network connectivity with data-driven method on resting-state fMRI from bipolar and major depression disorders. Both global and local graph measures show different functional network connectivity related to distinct mood control schemes between these mood disordered subgroups.

Chapter 5 introduces an attempt to combine information from two measures of fMRI, functional network connectivity and fractional amplitude of low frequency fluctuations to examine the functional correlates of cognitive dysfunction in schizophrenia during resting-state. Each measure were measured and correlated with the cognitive scores separately. The results from each measure were then overlaid to compare the results side by side, showing the findings of abnormalities related to cognitive impairment in schizophrenia from two methods are consistent.

Chapter 6 describes a multimodal fusion framework called mCCA+jICA, which combine information of multiple imaging modalities through a joint analysis. We describe the assumption and the mathematical model in detail. Simulation is then presented to show the performance of the framework under different scenarios.

Chapter 7 presents an application of the mCCA+jICA framework on functional network connectivity and structural MRI from subjects with bipolar or major depression

disorders. Graph analysis was also applied to the fusion results. Related functional and structural changes specific to disorders were found. In addition, high accuracy achieved by trained classification models imply that features extracted from our fusion analysis may be ultimately served as potential biomarkers.

Chapter 8 summarizes and concludes the projects and provides some perspective of potential future works.

Chapter 2   Background

2.1   Biomarkers for Mental Disorders

According to World Health Organization, mental disorders including schizophrenia, bipolar disorder (or manic depressive) and major depressive disorder (or unipolar depressive) rank among the most debilitating illnesses worldwide (Murray, Lopez et al. 1996; Hirschfeld and Vornik 2005), causing disabilities and early death. In specific, schizophrenia is a severe mental disease usually characterized by disintegration in perception of reality, cognitive problems, and chronic impairment in emotion and behavior (Heinrichs and Zakzanis 1998). Both bipolar and major depressive disorders are mental disorders that cause unusual shifts in mood, energy, activity levels, and the ability to carry out day-to-day tasks. However, major depressive disorder patients suffer from sad or "empty" moods, while bipolar patients often experience extreme euphoric or irritable moods called "mania" in addition to depression(Mitchell, Wilhelm et al. 2001). Prevalence estimates suggest that lifetime risk of schizophrenia is about 1% in general population, while the number is 1.5–3.0% for bipolar disorder, and more than 6% for suffering from major depressive disorder for more than 12 months (Narrow, Rae et al. 2002). However, these mental disorders share similar clinical symptoms, and misdiagnosis often lead to inappropriate and longer medication trials, a poorer prognosis, and greater health care expenses (Ho and Andreasen 2001; Strakowski, Adler et al. 2012; Dudek, Siwek et al. 2013). Unfortunately, the causes for these mental disorders are little known, and there is no clinical test available. Based on *Diagnostic and Statistical Manual of Mental Disorders* (DSM) published by the American Psychiatric Association, the

criteria for diagnosis are usually based on self-reported symptoms and abnormalities in behavior.

In contrast to medical symptoms or subjective descriptions, biomarkers or biological markers, refer to a broad subcategory of medical signs that are objective indications of medical state observed from outside the patient, and can be measured accurately and reproducibly (Strimbu and Tavel 2010). Over the last decades, non-invasive in-vivo neuroimaging techniques such as magnetic resonance imaging (MRI) open a new window to understand mental disorders. Neuroimaging have been increasingly applied to measure structure and function in human brains. With functional MRI (fMRI) or structural MRI (sMRI), studies have identified neurophysiological deficits in patients' brain from different perspective. Objective markers derived from neuroimaging might help improve accuracy in differentiating the mental disorders, and ultimately optimize clinical and functional outcome for all individuals suffering from the disorders (de Almeida and Phillips 2013).

2.2　Magnetic Resonance Imaging

Magnetic resonance imaging (MRI) is a medical imaging technique to measure the anatomy and physiology processes of body. MRI takes advantage of nuclear magnetic resonance properties of atomic nuclei. This non-invasive imaging method generates relatively high resolution compared to other imaging techniques, providing a powerful tool for medical diagnosis and biomedical research. Hydrogen atoms can generate a detectable radio-frequency signal during the imagin process. The abundance of hydrogen atoms in human bodies, particularly in water and fat, make MRI for anatomy and functional imaging possible.

For a single proton of hydrogen, thermal energy makes the proton to spin about itself and orient randomly under normal conditions. The spin motion of the proton generates an electric current that causes have a small dipolar magnetic field with an angular momentum – a property known as a spin or magnetic moment. When an external magnetic field is applied, the spinning proton will initiate a gyroscopic motion, known as precession, where the spin axis rotates around a central axis aligned to the external magnetic field. If an additional radio-frequency (RF) energy pulse is applied at a certain frequency called resonant frequency, the protons will absorb energy and disturb the alignment away from the external magnetic field. After turning off the RF pulse, the behavior of protons is once again determined by the external magnetic field only and they try to come back to their original alignment. There are two processes of realignment that occur simultaneously, T1 relaxation and T2 relaxation (Figure 2.1). The T1 relaxation of protons realigns themselves parallel to the external magnetic field and the longitudinal magnetization increases. For T2 relaxation, the protons lose their previous coherent precession and begin to diphase, as the spins realign parallel to the external magnet axis. During these two processes, the protons emit a radio frequency signal (MRI signal), which is detected via a receiver coil of MRI scanner.
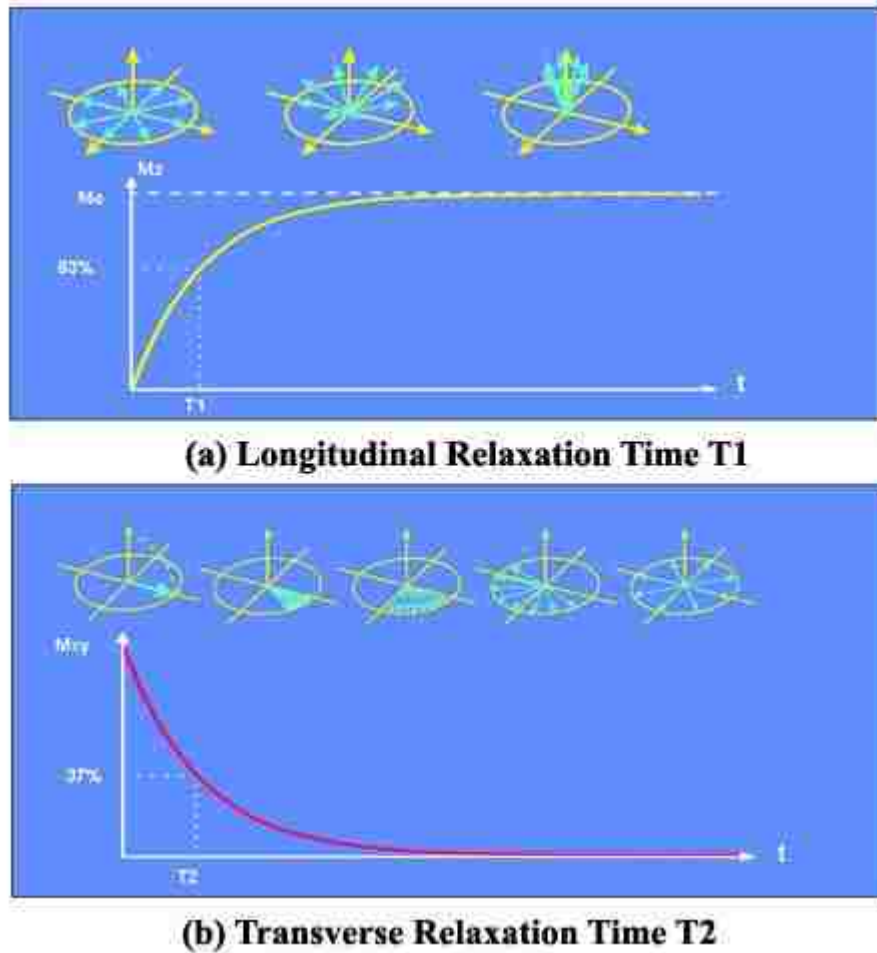
Figure 2.1 Schematic illustration of spin relaxation. (a) longitudinal/T1 relaxation; (b) transverse/T2 relaxation (Hashemi, Bradley et al. 2003)

MRI can be versatilely configured to emphasize contrasts reflecting different tissue characteristics for neroimaging. The recovery of longitudinal magnetization varies between tissues with different T1 constants allow different levels of T1-contrast to be obtained by adjusting the repetition time (TR, the time interval between successive excitation pulses). Given a T1 constant of ~900ms for gray matter (GM), ~600ms for white matter (WM) and 4200ms for cerebrospinal fluid (CSF), T1-weighted images are the most commonly used to study anatomical brain structures. Meanwhile, T2-contrast reflects the difference in T2 constants among the tissues and can be adjusted through the

9

echo time (TE, the time interval between the excitation and data acquisition). T2*-contrast is commonly used in functional MRI (fMRI), where brain functions are approximated by the associated changes in blood flow.

The superior resolution at less than 1 mm^3 of structural MRI (sMRI) allows gray and white matter to be clearly distinguished. It not only provides excellent assessment of main structures such as the corpus callosum, hippocampus and amygdala, but also permits visualization of subcortical structures, such as the caudate and thalamus which are considered to be associated with many psychiatric disorders.

On the other hand, fMRI is an MRI procedure that detects changes in blood flow or oxygenation in response to neural activation. The most popular fMRI technique measures blood oxygenation level dependence (BOLD) contrast. This approach takes advantage of the phenomenon that neural activity are accompanied by local changes in perfusion. In specific, when neurons in a certain region become more active, the local blood flow increases to support the increased oxygen consumption, results in a local decrease in the concentration of deoxyhemoglobin. As deoxyhemoglobin is paramagnetic, a reduction in its concentration results in an increase in the homogeneity of the static magnetic field, which yields stronger in the MRI signal. Therefore, fMRI images measures brain activities indirectly via hemodynamic response, which is temporally delayed relative to neural activation by about 1 to 2 seconds. FMRI acquires a volume (or scans) a spatial resolution of 1 to 3 mm^3 every few seconds (Smith 2004). Capable of revealing both temporal and spatial perspectives of brain, fMRI has been used extensively to study functionality of the brain system in the past two decades.

2.3 Independent Component Analysis

Independent component analysis (ICA) is a technique that separates multivariate signals into statistically independent components or "sources". A typical ICA model assumes that the observed signals are formed by the independent source signals through an unknown linear mixing process. Mathematically ICA formulation can be written as:

$$X = AS \tag{2.1}$$

where X denotes the observed random vectors, S is the spatial component map whose elements are assumed independent sources, and A is the unknown mixing matrix. There are several algorithms have been implemented for solving ICA problems, such as Infomax, fastICA, JADE, EVD, and AMUSE (Bell and Sejnowski, 1995a; Cardoso and Soloumiac, 1993; Georgiev and Cichocki, 2001; Hyvarinen and Oja, 1997; Tong et al., 1990).

Since the measured biomedical signals are often mixtures of signals from different underlying "sources" including both noise and signals of interest, ICA has been applied to fMRI data widely (McKeown, Makeig et al. 1998; Calhoun, Adali et al. 2001; Calhoun, Adali et al. 2001; Beckmann, DeLuca et al. 2005). In fMRI data, ICA is capable to separate sources that are the artifacts-related and the sources from neural physiological activity (Du, Allen et al. 2016). Each non-artifact independent component (IC) reflects brain regions which exhibit temporal coherence components are maximally independent and linearly mixed. Also, ICA can used to discover differences in temporal dynamics and changes with respect to spatially distributed brain networks where the source signals that are not observable.

2.4   Functional Connectivity

The description of brain function can be divided into two categories: functional segregation and integration (Friston 2011). Functional segregation in the brain demonstrate the ability for specialized processing to occur within densely interconnected groups of brain regions, while functional integration refers the ability to rapidly combine specialized information from distributed brain regions.

Functional connectivity (FC) analysis is an approach that assesses temporal coherence among brain regions (Friston 2002). This method is capable of characterizing large-scale integrity in human brain, and provides insight into functional integration and segregation of the brain (Van Dijk, Hedden et al. 2010). Functional MRI is a powerful tool to study FC since fMRI captures spatial resolution and corresponding temporal information, assessing FC, make assessing FC possible by calculating correlation between the activities of specialized regions. Analyses of FC by treating collection of FC between brain regions as a whole, and measure it using graph theory metrics, such as clustering coefficient, characteristic path length, local efficiency and global efficiency, summarizes the topological properties of brain networks, and provides a useful measure of how effectively information is passed and processed between different brain regions (Rubinov and Sporns 2010).

There are two widely used types of approaches to estimate FC in the brain: regions of interest (ROI) based and independent component analysis (ICA) methods. The ROI-based methods calculate FC between ROIs that are selected based on an initial hypothesis. For example, selecting task-dependent regions based on stimuli onset time by using general linear regression model, or using parcellation templates like Automated

Anatomical Labeling (AAL) (Tzourio-Mazoyer, Landeau et al. 2002). This type of method has been widely adopted for the study of mental disorders (Raffo, Hampson et al. 2004; Foland, Altshuler et al. 2008; Chepenik, Raffo et al. 2010; Tang, Kong et al. 2013), however, it may be limited by the shapes, locations and inter-subject variability (Du, Li et al. 2012). On the other hand, ICA is a multivariate data-driven approach that identifies a set of maximally spatially-independent components (i.e. temporally coherent networks), each with associated time course (McKeown, Makeig et al. 1998; McKeown and Sejnowski 1998; Calhoun, Adali et al. 2001; Calhoun, Adali et al. 2001; Du and Fan 2013). Without the need of a specific model, ICA is ideal for analyzing resting-state data (Kiviniemi, Kantola et al. 2003). Based on the results from ICA, the interrelationship among multiple brain components is defined as functional network connectivity (FNC) (Jafri, Pearlson et al. 2008; Arbabshirani, Kiehl et al. 2013).

To measure the functional connection strength between brain regions, pair-wise statistics (i.e. correlations, coherence, etc) between ICA time courses can be calculated. In most common cases, Pearson's correlation or partial correlation are adopted to construct the connectivity matrices of the networks.

The element r_{ij} of Pearson's correlation matrix is the correlation coefficients between two random variables (x_i, x_j), or the time courses of brain regions i and j here. Correlation coefficient is defined as

$$r_{ij} = \frac{\text{cov}(x_i, x_j)}{\text{cov}(x_i, x_j)\text{cov}(x_j, x_j)} \tag{2.2}$$

where $\text{cov}(x_i, x_j)$ is the covariance between two random variables.

In addition, partial correlation is the correlation between two random variables, with the effect of a set of controlling random variables removed (Whittaker 1990; Lauritzen 1996; Hampson, Peterson et al. 2002). A partial correlation coefficient within a functional network measures the interaction between the time courses of two blocks, once these signals have been projected on the subspace orthogonal to the time courses of all other regions. Hence, it only considers the "direct correlation" between the two blocks of interest, without influence of other areas in the network (Marrelec, Krainik et al. 2006). By taking partial correlation instead of taking direct correlation, the inter-correlated effects within each nearby regions were removed, such that the indirect dependencies between ROI's can be filtered out.

To calculate partial correlation, the first step is to estimate the sample covariance matrix S from the data matrix $Y = (x_i); i = 1, 2, \ldots, n$. Here x_i is the time course of brain component, and there are n brain components in total. If we use $X = (x_j, x_k)$ to denote the time courses in the jth and k^{th} components, $Z = Y \backslash X$ denotes the other $n - 2$ time courses matrices. Each element of S contains the sample covariance value between two components (say j and k). If the covariance matrix of $[X, Z]$ is

$$S = \begin{pmatrix} S_{11} & S_{12} \\ S_{12}^T & S_{22} \end{pmatrix} \tag{2.3}$$

in which S_{11} is the covariance matrix of X, S_{12} is the covariance matrix of X and Z, and S_{22} is the covariance matrix of Z, then the partial correlation matrix of X, controlling for Z, could be defined formally as a normalized version of the covariance matrix, $S_{xy} = S_{11} - S_{12} S_{22}^{-1} S_{12}^T$.

As the correlation matrices were not normally distributed, so a Fisher r to z transformation was used on each element of the matrices (Fisher 1914; Liu, Liang et al. 2008).

2.5   Graph Analysis

Graph is a mathematical representation of a real-world complex system, comprised of a collection of nodes and links (or edges) between pairs of nodes. In brain network analysis, nodes usually represent brain regions, and the edges correspond to anatomical, functional or effective connections between brain regions (Friston 2011).

Analyses of FC by treating FC matrices as graph, and measure them using graph theory metrics, such as clustering coefficient, characteristic path length, local efficiency and global efficiency, summarizes the topological properties of brain networks, and provides a useful measure of how effectively information is passed and processed between different brain regions (Rubinov and Sporns 2010). Graph organizational properties may reveal disease-related abnormalities in functional brain networks among psychiatric patients from resting-state as well as task-related neuroimaging data (Lynall, Bassett et al. 2010; Wang, Metzak et al. 2010; Yu, Sui et al. 2011; Yu, Sui et al. 2011; He, Sui et al. 2012).

2.5.1   Measures of Brain Functional Networks

Topological properties reveal the characteristics of connectivity in the network. Suppose we have an undirected network G with N nodes. In weighted network, the weight between the nodes i and j is $w_{i,j}$, and the distance between the nodes i and j is the

inversed weight $\frac{1}{w_{i,j}}$. Binarized network are gained with the weights binaried with a threshold T,

$$a_{i,j} = \begin{cases} 1, if |w_{ij}| \geq T \\ 0, otherwise \end{cases} \tag{2.4}$$

The *degree* of a node K_i represents the total number (binary networks) or weights (weighted networks) of edges or connecting to a node. The degree of overall network K_{net} is the average degree of all nodes.

$$K_{net} = \frac{1}{N} \sum_{i \in G} K_i \tag{2.5}$$

For binarized networks, some others prefer to use the cost (connection density) of the network instead, which is the total number of edges in a graph, divided by the maximum possible number of edges $\frac{N(N-1)}{2}$:

$$K_{cost} = \frac{1}{N(N-1)} \sum_{i \in G} K_i \tag{2.6}$$

Then we introduce the concept of subgraph. The subgraph G_i is the set of nodes that are the direct neighbors of the node i. That is, every node in G_i could reach the node i through one edge. In binarized networks, if there are k nodes, the total possible number of edges is $\frac{k(k-1)}{2}$. For weighted networks, k is substituted with the degree of the node i, K_i.

The *absolute clustering coefficient* provides a measure of functional segregation, showing the prevalence of clustered connectivity around individual nodes (Watts and

Strogatz 1998). Locally, the clustering coefficient C_i is known as the fraction of number of existing connections (binary networks) E_i to the number of all possible edges in subgraph G_i around one node.

$$C_i = \frac{E_i}{\frac{K_i(K_i-1)}{2}} \tag{2.7}$$

For weighted networks, E_i is substituted with geometric mean of weights with each triangles (three connected nodes including node *i*),

$$E_i = \frac{1}{2}\sum_{j,h \in N} \sqrt[3]{w_{ij}w_{ih}w_{jh}} \tag{2.8}$$

Clustering coefficient of a network C_{net} is then derived by averaging the clustering coefficients of all nodes within the network.

$$C_{net} = \frac{1}{N}\sum_{i \in G} C_i \tag{2.9}$$

Another more sophisticated measures of segregation is to look into the network's *modular structure* (or community structure). Modular structure is revealed by subdividing the network into groups of nodes, with a maximally possible number of within-group links, and a minimally possible number of between-group links (Girvan and Newman 2002). The degree to which the network may be subdivided into such clearly delineated and nonoverlapping groups is quantified by a single statistic, the *modularity Q* (Newman 2004).

$$Q = \frac{1}{l}\sum_{i,j \in G}\left(w_{ij} - \frac{K_iK_j}{l}\right)\delta_{m_i,m_j} \tag{2.10}$$

where m_i is the module including node i; δ_{m_i,m_j} is an indicator function, $\delta_{m_i,m_j} = 1$ if node i and j belongs to the same node, and 0 otherwise.

The *path length* measures functional integration based on the concept of path which brain regions communicate. The shortest path length of a node pair $\min\{L_{i,j}\}$ is the smallest number (binary networks) or sum of distances (weighted networks) of edges connecting the nodes i and j. The mean shortest path length of a node L_i is the mean value of shortest path length from node i to all other nodes in the network.

$$L_i = \frac{1}{N-1}\sum_{\substack{j\in G \\ j\neq i}} \min\{L_{i,j}\} \tag{2.11}$$

Similarly, mean shortest path length of the network L_{net}, or *characteristic path length* (Watts and Strogatz 1998), L_{net} is the mean of shortest path length between all node pairs in the network.

$$L_{net} = \frac{1}{N}\sum_{i\in G} L_i \tag{2.12}$$

Characteristic path length reflects the average connectivity or overall routing efficiency of the network. When the network is disconnected (i.e., there are nodes in the network with no existing path to certain other nodes), the shortest path length is set to be infinity.

Global efficiency $E_{global,net}$ measures how efficient a network is to transfer information parallelly at a relatively low cost. It is defined as the inverse of harmonic mean of the shortest path length between each pair of nodes (Latora and Marchiori 2001; Latora and Marchiori 2003; Achard and Bullmore 2007).

$$E_{global,net} = \frac{1}{N(N-1)} \sum_{\substack{i,j \in G \\ j \neq i}} \frac{1}{\min\{L_{i,j}\}} \tag{2.13}$$

Similarly, *local efficiency* $E_{local,net}$ can be defined the same way for the subgraph G_i:

$$E_{local,i} = \frac{1}{N_{G_i}(N_{G_i}-1)} \sum_{\substack{j,k \in N_{G_i} \\ j \neq k}} \frac{1}{\min\{L_{j,k}\}} \tag{2.14}$$

$$E_{local,net} = \frac{1}{N} \sum_{i \in G} E_{local,i} \tag{2.15}$$

From the definition of subgraph, G_i itself does contain the node i. Thus, the local efficiency could be interpreted as how well the nodes in subgraph G_i exchange information when the node i is removed, revealing the tolerance of the network.

2.6 Multimodal Fusion Analysis

Functional magnetic resonance imaging (fMRI) identifies functions in human brains. As brain functions are altered in patients with mental disorders, fMRI may help finding the underlying neurophysiological abnormalities that are unique to certain diseases in patients' brains. Using fMRI, different patterns of functional activities have been found in patients during resting-state or various behavioral tests (Taylor Tavares, Clark et al. 2008; de Almeida, Versace et al. 2009; Almeida, Versace et al. 2010; Bertocci, Bebko et al. 2012; Diler, de Almeida et al. 2013).

However, compared to structural MRI, which provides information about the tissue type of the brain, the spatial resolution of fMRI images is low. Recently, collecting

more than one type (or modality) of brain data from the same individual using various non-invasive imaging techniques (i.e., MRI, DTI, electro-encephalography (EEG), MEG, etc.) has become common practice. Each brain imaging technique provides a different view of brain function or structure.

There are many attempts that combining information from functional connectivity and structural imaging data (Rykhlevskaia, Gratton et al. 2008). As in a review by (Damoiseaux and Greicius 2009), most of them utilized diffusion tensor imaging (DTI), a relatively new MRI technique that measures the diffusion of water molecules in the brain; (Le Bihan 2003), which provides anatomical connectivity in the human brain. Those studies mainly focused on a small number of connectivity, and compared functional and structural information at connectivity level instead of underlying data level.

Multimodal fusion is an effective approach for analyzing biomedical imaging data that combines multiple data types in a joint analysis (Sui, Adali et al. 2012). A key motivation for multimodal fusion is to take advantage of the cross-information provided by multiple imaging techniques, which in turn can be useful for identifying dysfunctional regions or potential biomarkers for many diseases.

A couple of multivariate fusion methods have been proposed with different optimization priorities and limitations: Some enable common as well as distinct levels of connection among modalities, such as multi-set canonical correlation analysis (mCCA) (Correa, Li et al. 2008) and partial least squares (PLS) (Chen, Reiman et al. 2009) (Lin, McIntosh et al. 2003), but their separated sources may not be sufficiently spatially sparse. For example, mCCA maximizes the inter-subject covariation across two sets of features,

and generates linked variables, one per dataset. The variables are called canonical variants (CVs), which correlate with each other only on the same indices (rows) with the corresponding correlation values that are called canonical correlation coefficients (CCC). This scheme allows for both common and distinct aspects of features, but the brain maps of CVs may look similar when the CCC are not sufficiently distinct. At the same time, some approaches perform well in spatial decomposition, such as joint ICA (jICA) (Calhoun, Adali et al. 2006) and linked ICA (Groves, Beckmann et al. 2011), which aim to maximize the independence among estimated sources combining more than two modalities, but only allow a common mixing matrix. These two methods enable detection of features common to all modalities at the cost of features which may be distinct to one or more of them, which is a situation more likely to occur when combining more than two modalities.

The mCCA+jICA framework combines mCCA and joint ICA throughout it pipeline, strikes a balance between maximize the independence among estimated sources and keeping both the common and unique features across modality. (Sui, Adali et al. 2010) first proposed this method in the 2-modal fusing framework, and (Sui, Pearlson et al. 2011) found the different features in SZ and BD from AOD-task fMRI and diffusion tensor Imaging (DTI) datasets, where the features X_1 of fMRI are extracted from beta-weight map during the stimuli, and the features X_2 of DTI are fractional anisotropy (FA) maps. (Sui, He et al. 2013) extended the framework into a more general case of n-way fusion, and applied it to resting state fMRI (beta-map of AOD task), gray matter density (GMD), and DTI (fractional anisotropy, FA). Another 3-modal study combined resting

21

state fMRI (amplitude of low-frequency fluctuation, ALFF), GMD, and DTI (FA) data to discriminiate SZ (Sui, He et al. 2013).

2.7   Datasets

2.7.1   MCIC SIRP Dataset

A total of 35 patients with chronic SZ and 35 demographically matched HC were recruited and scanned from two sites, the University of Minnesota, and the University of New Mexico, as part of the Mind Clinical Imaging Consortium (MCIC) study. Those two sites were picked out of all four sites of MCIC study as subjects' BOLD activation from these two had minimal site differences, and all subjects' behavioral data were recorded. HC were free from any Axis I disorders as assessed with the Structured Clinical Interview for DSM-IV-TR (SCID) (First, Spitzer et al. 1996). Patients met the criteria for SZ defined by the DSM-IV based on the SCID and review of the associated case files by experienced raters located with each site. All patients were stabilized on medication prior to the fMRI scan run. Handedness of subjects were determined by Edinburgh Handedness Inventory (Oldfield 1971) and the education of subjects were evaluated by Wide Range Achievement Test (3rd ed.), Reading subtest (WRAT-3RT). Demographics and clinical characteristics of subjects are presented in Table 2.1.

Table 2.1 Demographics of Subjects for MCIC dataset

	HC (n = 35)	SZ (n = 35)	p-value
Age	34.6 ± 11.6 range 18 – 60	34.3 ± 11.8 range 20 – 60	0.91

Sex (Male / Female)	27 / 8	26 / 9	0.82
Handedness (non-right hand)	3 left handed	1 left handed 3 ambidextrous	<0.0001
Parental socioeconomic status	2.4 ± 0.6	2.6 ± 1.0	0.19
Education	50.8 ± 5.0	47.7 ± 5.2	0.01
Years since diagnosis	n/a	13.1 ± 11.1	
Symtoms	n/a	Positive = 5.0 ± 2.2 negative = 7.5 ± 3.1 disorganization = 1.9 ± 2.2	

Sternberg Item Recognition Paradigm (SIRP) (Sternberg 1966) was adapted for fMRI as a block design divided into three runs. Each run contained two blocks of each of three WM load levels (Low Load: 1 digit (L1), Medium Load: 3 digits (L3), and High Load: 5 digits (L5)) presented in a pseudorandom order. As shown in Figure 2.1, each block began with a prompt that lasted for 2 seconds and displayed the word "Learn". The learning prompt was followed by the encode condition of 6 seconds, which displayed the memory set of either one, three or five digits in red font (constituting the three levels of WM load) which the subjects needed to hold on-line in WM. This was followed by a series of 14 probes each consisting of a single digit in green font, each digit lasting 1.1 seconds. Half of the probes were targets (members of the memory set) and the other half were foils. The time between each probe digit pseudo-randomly varied from 0.6 to 2.5 seconds. The probe condition lasted for 38 seconds in total. For each probe digit subjects were required to indicate whether or not the probe was a target or foil by pressing a

button with their right or left thumb (randomly assigned). There were fixation epochs between WM blocks that served as a baseline. Each run lasted 6 minutes.
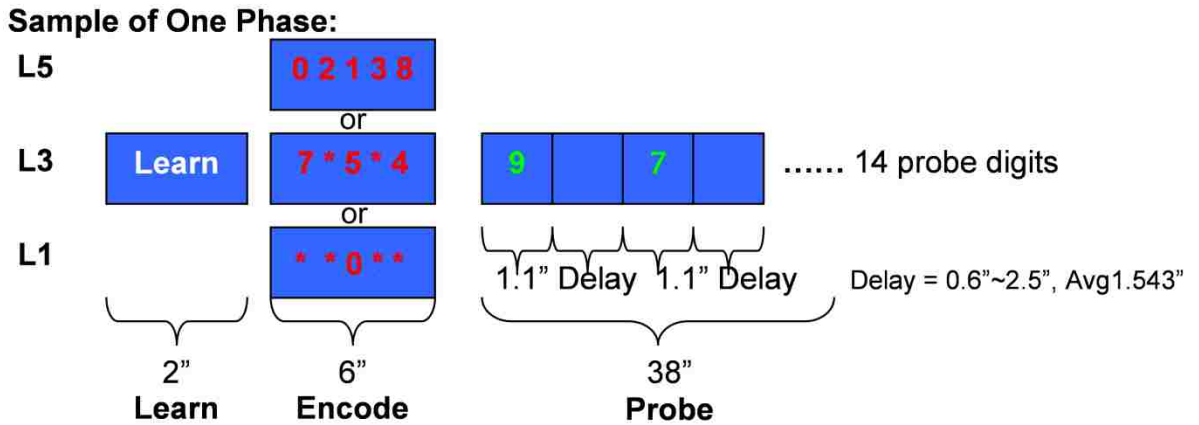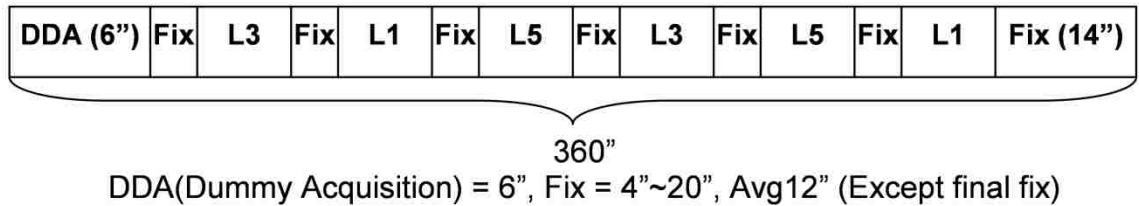
Figure 2.2 The SIRP timing and design. Top: Timing and contents of each Prompt-Encode-Probe block for each WM load level. Bottom: A sample run combining six blocks at different WM load levels in pseudo-random order.

Each subject was instructed to respond as quickly and accurately as possible. To mitigate motivational deficits subjects were given a bonus of 5 cents for each correct response, which was mailed to the participant after completion of the task.

The SIRP dataset this study utilized was also used as part of other MCIC studies (Roffman, Gollub et al. 2008; Kim, Manoach et al. 2009; Kim, Sui et al. 2010; Sui, Adali

et al. 2010; Ehrlich, Brauns et al. 2011; Ehrlich, Yendiki et al. 2011; Michael, King et al. 2011) which used different analyses from what we presented here.

Among the two sites where data were collected, the University of New Mexico was using a Siemens Sonata 1.5T scanner, and the University of Minnesota was using a Siemens Trio 3.0T scanner. The echo planar imaging sequences were utilized and the pulse sequence parameters were almost the same: orientation = AC-PC line, number of slices = 27, slice thickness = 4mm, slice gap = 1mm, TR = 2000ms, TE = 40ms (1.5T scanner) or 30ms (3T scanner), FOV = 22cm, flip angle = 90°, matrix = 64 × 64, voxel dimension = $3.4 \times 3.4 \times 4$ mm^3.

Data were preprocessed using the software package SPM5 (http://www.fil.ion.ucl.ac.uk/spm). Images were first realigned using a motion correction algorithm unbiased by local signal changes called INRIalign (Freire and Mangin 2001). The output of the realignment parameters from the SPM were kept as previous studies found functional connectivity of fMRI was sensitive to the head motion (Power, Barnes et al. 2012; Van Dijk, Sabuncu et al. 2012).

A slice-timing correction was performed on the fMRI data after realignment to account for possible errors related to the temporal variability in the acquisition of the fMRI datasets. Data were spatially normalized (Ashburner and Friston 1999) into the standard Montreal Neurological Institute space using an SPM5 echo-planar imaging (EPI) template and then spatially smoothed with a 9 × 9 × 9 mm3 full width at half-maximum Gaussian kernel. The data (originally collected at 3.4 × 3.4 × 4 mm3) was slightly subsampled to 3 × 3 × 3 mm3 (during normalization) resulting in 53 × 63 × 46

voxels. The time courses were then filtered with a Butterworth band-pass filter (0.003-0.23Hz), to reduce drift effects and noise (Fox, Snyder et al. 2005; Liu, Liang et al. 2008; Moussa, Vechlekar et al. 2011). The frequency range of the filter was based on a factor of 0.01 to 0.9 multiplied by the Nyquist frequency of TR during the scanning (2000ms, corresponding to 0.5Hz). This cutoff range kept most of useful information during the scan, and did not filter out the task frequency, where encoding and probe processes last 6 seconds (0.167Hz) and 38 seconds (0.026Hz) respectively.

2.7.2 Tulsa Resting-state Dataset

Resting-state MRI data were collected from 13 BD (Type I: $n=7$; Type II: $n=6$), 40 MDD, and 33 age and gender matched HCs at Laureate Institute for Brain Research, Tulsa, Oklahoma, USA. All patients were treatment naïve or unmedicated for at least 3 weeks (8 weeks for fluoxetine) prior to scanning. No treatment was discontinued for the purposes of the study. The study received institutional review board approval and all participants provided written informed consent. No significant age or gender effect between groups was found from ANOVA. Symptom measures, including the Montgomery-Åsberg Depression Rating Scale (MADRS) (Montgomery and Asberg 1979) and the Young Mania Rating Scale (YMRS) (Young, Biggs et al. 1978), were collected from each subject.

Table 2.2 Demographic of Subjects for Tulsa Resting-state Dataset

	BD	MDD	HC
N (Females)	13 (11)	40 (33)	33 (22)
Ages	35.15 ± 10.29	35.20 ± 9.31	33.70 ± 10.15
YMRS	6.15 ± 6.11	3.59 ± 2.33	0.16 ± 0.51
MADRS	24.92 ± 10.31	30.90 ± 6.31	0.73 ± 1.72

At the time of scanning, among the 13 BD subjects, 10 were depressed, one was in a euthymic state, and 2 were in a mixed state. All 40 MDD subjects met criteria for a current major depressive episode and either a recurrent or chronic course.

Functional MRI

During the fMRI scan, participants were instructed to keep their eyes open to not fall asleep. All images were collected on a GE Discover MR750 3-Tesla scanner with a 32-channel radio frequency coil. T2*-weighted functional images were acquired using a gradient-echo EPI sequence with TE = 27 ms, TR = 2 s, flip angle = 78°, slice thickness = 2.9 mm, field of view = 240 mm, matrix size = 96×96. The resting-state scan lasted 7.5 minutes (225 volumes) for most subjects while some subjects were scanned for 6.4 min (191 volumes).

For the fMRI data, the first seven volumes were excluded from analysis to allow for T1 equilibration. The remaining 218 or 184 volumes (depending on scan length) were included in the analysis, and FNC was computed for each subject as the temporal correlations between time course pairs. Post hoc tests showed that the relatively small difference in scanning time lengths between subjects did not significantly affect the group analysis. The SPM8 software package (http://www.fil.ion.ucl.ac.uk/spm/software/spm8) was employed to perform fMRI preprocessing. The images were first realigned using INRIalign (Freire, Roche et al. 2002), and were then spatially normalized to the standard Montreal Neurological Institute (MNI) space, resampled to 3 mm × 3 mm × 3 mm voxels using the nonlinear (affine + low frequency direct cosine transform basis functions)

registration implemented in SPM8 toolbox. Data was smoothed using a Gaussian kernel with a small full-width at half-maximum of 8 mm.

Structural MRI

For structural scans, T1 images were acquired using a gradient-echo MP-RAGE sequence with TE = 2.008 ms, TR = 5 s, flip angle = 8°, slice thickness = 0.9 mm, field of view 240 mm, matrix size = 256×256.

Structural data were preprocessed using the SPM8 software package, which was used to segment the brain into white matter (WM), gray matter (GM), and cerebral spinal fluid with unmodulated normalized parameters via the unified segmentation method (Ashburner and Friston 2005). After segmentation, the GMD images were smoothed to a full-width half maximum (FWHM) Gaussian kernel of 8 mm (White, O'Leary et al. 2001) and resliced to a matrix of $53 \times 63 \times 46$ voxels.

2.7.3 MATRICS Resting-state data

47 schizophrenia patients and 50 age-matched healthy controls were recruited as part of a multimodal schizophrenia center for biomedical research excellence (COBRE) study at the Mind Research Network (MRN) (http://cobre.mrn.org). The demographics and clinical scores of subjects are listed in Table 2.3. MCCB scores of a subject were evaluated in the same day of his/her imaging scans took place.

Table 2.3 Demographics and the correlations between MCCB composite value and specific domains, PANSS symptoms and other measures

Measure	HC	SZ	*P**	*R**
Number	50	47		

Age		36.7±12.6	35.3±12.6	0.60	0.04
Gender		20F / 30M	6F / 41M	0.01	0.17
Education		13.8±1.6	12.7±2.2	0.014	0.10
MCCB*	Composite	49.8±10.5	31.3±15.7	4.2E-09	1
	Speed of processing	51.9±9.0	35.3±13.7	1.5E-09	0.91
	Attention/Vigilance	48.3±9.9	36.0±15.1	1.4E-05	0.86
	Working memory	46.8±11.4	37.1±14.5	5.3E-04	0.83
	Verbal learning	47.4±8.9	38.0±8.6	8.4E-07	0.80
	Visual learning	49.3±9.3	36.6±12.6	1.5E-07	0.79
	Reasoning/Problem solving	54.2±9.9	46.1±11.7	5.1E-04	0.64
	Social cognition	50.8+11.1	40.5±13.0	8.3E-05	0.65
PANSS	Negative	N/A	15.1±5.4		-0.48
	Positive	N/A	15.4±5.9		-0.10

MCCB=MATRICS Consensus Cognitive Battery; PANSS= Positive and Negative Syndrome Scale. P denotes the significance value of two sample t-test performed between controls and schizophrenia patients for all measures, except gender (used chi-squared test). R* is the correlation value between MCCB composite and other measures.

Resting-state scans were a minimum of 5 minutes, 4s in duration (152 volumes). Subjects were asked to keep their eyes open during the scan and stare passively at a presented fixation cross, as this is suggested to facilitate network delineation compared to eyes-closed conditions and helps ensure that subjects are awake. The data were collected on a 3-Tesla Siemens Trio scanner with a 12-channel radio frequency coil, with single-shot full k-space echo-planar imaging (EPI) with ramp sampling correction using the inter commissural line (AC/PC) (anterior commissure/posterior commissure) as a reference. TR=2 s, TE=29 ms, flip angle = 75°, slice thickness = 3.5mm, slice gap = 1.05 mm, field of view (FOV) 240 mm, matrix size = 64×64, voxel size = 3.75×3.75×4.55 mm3.

The SPM8 software package (http://www.fil.ion.ucl.ac.uk/spm/software/spm8) was employed to perform fMRI preprocessing. The images were first realigned using INRIalign (Freire, Roche et al. 2002), and were then spatially normalized to the standard Montreal Neurological Institute (MNI) space, resampled to 3 mm × 3 mm × 3 mm voxels

using the nonlinear (affine + low frequency direct cosine transform basis functions) registration implemented in SPM8 toolbox.

Chapter 3   Altered Functional Connectivity Structures in

Schizophrenia

3.1   Introduction

3.1.1   Small-world networks structures

Small-world networks strike a balance between high levels of local clustering and short path lengths linking all nodes even though most nodes are not neighbors of one another (Watts and Strogatz 1998). This optimized property offers a structural substrate for graph analysis on functional segregation and integration of the brain (Sporns and Zwi 2004; Bassett and Bullmore 2006; Moussa, Vechlekar et al. 2011). Network metrics such as efficiency provide a vital measure of how effectively information is passed and processed between different brain regions. Analysis of network organizational properties may also reveal disease-related abnormalities in functional brain networks among patients (Stam, Jones et al. 2007; He, Chen et al. 2009), including schizophrenia (SZ) during resting state (Achard, Salvador et al. 2006; Liu, Liang et al. 2008; Yu, Sui et al. 2011) as well as task-related data such as auditory oddball (Yu, Sui et al. 2011) and verbal memory (Wang, Metzak et al. 2010). In this study, we applied the small-world network analysis towards functional magnetic resonance imaging (fMRI) data collected during a working memory (WM) task.

3.1.2   Working memory

WM is a construct that refers to maintaining and manipulating information on-line, in the mind's eye in the service of guiding behavior. It is considered to be a temporary store whose contents are continually updated, scanned and manipulated in

response to immediate processing demands (Baddeley 1992). WM deficits in SZ are consistently observed, relatively treatment-resistant and have been hypothesized to underlie many cognitive deficits and symptoms in SZ, manifested in longer reaction time and less accurate performance, especially as memory load increases (Park and Holzman 1992; Goldman-Rakic 1994; Manoach, Press et al. 1999). They are accompanied by aberrant brain activation, particularly in the dorsolateral prefrontal cortex (DLPFC) (Manoach, Press et al. 1999; Manoach 2003; Brown, McCarthy et al. 2009). The relation of working memory load or demand to DLPFC activation can be described as an inverted-U shaped function with activation increasing with increasing demand to the point that capacity is reached, at which point activation declines. In schizophrenia, this point is reached at a lower level of demand, and this hypothetical curve is shifted to the left, reflecting lower WM capacity (Callicott, Mattay et al. 2003; Manoach 2003; Karlsgodt, Glahn et al. 2007). In addition to DLPFC, WM performance is associated with activation in a network of brain regions (Saykin, Gur et al. 1991; Petrides, Alivisatos et al. 1993; McCarthy, Blamire et al. 1994; Cohen, Braver et al. 1996), as well as deactivation in the default mode network (DMN) (Hampson, Driesen et al. 2006). Deficient WM in SZ is associated with aberrant activation in these networks (Sawaguchi and Goldman-Rakic 1991; Salvador, Martinez et al. 2008; Camchong, Macdonald et al. 2009; Potkin, Turner et al. 2009; Kang, Sponheim et al. 2011).

Several studies utilizing graph analysis have investigated changes in functional network properties during WM tasks. For example, small-world structure has been reported in simultaneous MEG and EEG (MEEG) at different bands (Palva, Monto et al. 2010). Analyses of EEG data demonstrate that optimal patterns are decreased or absent in

SZ (Micheloyannis, Pachou et al. 2006; Pachou, Vourkas et al. 2008). Bassett and colleagues (Bassett, Bullmore et al. 2009) reported that task performance correlated with global cost efficiency of the MEG beta-band network. An fMRI study in healthy subjects also showed that small-world network connectivity decreases as a function of increasing WM load (Ginestet and Simmons 2010). These studies have utilized the n-back paradigm (Owen, McMillan et al. 2005), which requires the temporal tagging and updating of information on each trial, and therefore has a very steep difficulty slope with increasing demand (i.e., 1 to 3 back) making it difficult to vary the load and stay within the capacity of SZ. As the Sternberg Item Recognition Paradigm (SIRP) (Sternberg 1966) emphasizes the maintenance over the manipulation of information, the difficulty slope is less steep, allowing the parametric manipulation of load while staying within the WM capacity of SZ (Potkin, Turner et al. 2009). In a previous report on fMRI data collected during the SIRP (Kim, Manoach et al. 2009), group independent component analysis (ICA) showed significant abnormalities in SZ relative to HC in both negatively task-correlated brain regions (DMN), and positively task-correlated areas (DLPFC). To our knowledge, no studies have evaluated network alterations in task-related brain regions in SZ during performance of a WM task with varying load.

The goal of this study is to investigate the topological properties in small-world networks derived from a data-driven (ICA defined) examination of task-elicited brain activity for both SZ and HC during the SIRP at three levels of WM load. We hypothesized that the functional network of task-related brain regions would change according to WM load in all subjects, and that SZ will show less efficient small-world network structures when compared to HC.

3.2   Methods

In this study, the MCIC SIRP Dataset was used.

3.2.1   Selection of Regions of Interest

The GIFT toolbox (http://icatb.sourceforge.net) was used to perform group spatial independent component analysis with infomax algorithm (Bell and Sejnowski 1995). Time courses of three runs for each subject were temporally concatenated during the group ICA. The component number was set to be 26 as estimated by a modified minimum description length (MDL) criterion (Li, Adali et al. 2007).

Regressions were performed against the stimuli for each component, to get the weights (beta values) on each of the regressors. There were 12 regressors for each run, corresponding to two encodes and two probes for each of the three WM loads. To find the more task-related components, one sample t-tests were performed on the 12 beta values assessed from the regression. The components were sorted based on the p-value of t-test: the lower the p-value of the beta weights, the more task-related the component. For each of the 12 regressors, we listed the 5 components with the lowest p-values (10^{-5} – 10^{-27}) in order to identify the most frequently occurring components among all regressors. Three common components were found as most task-related, i.e., Component 19, 14 and 24, as shown in Figure 3.1.
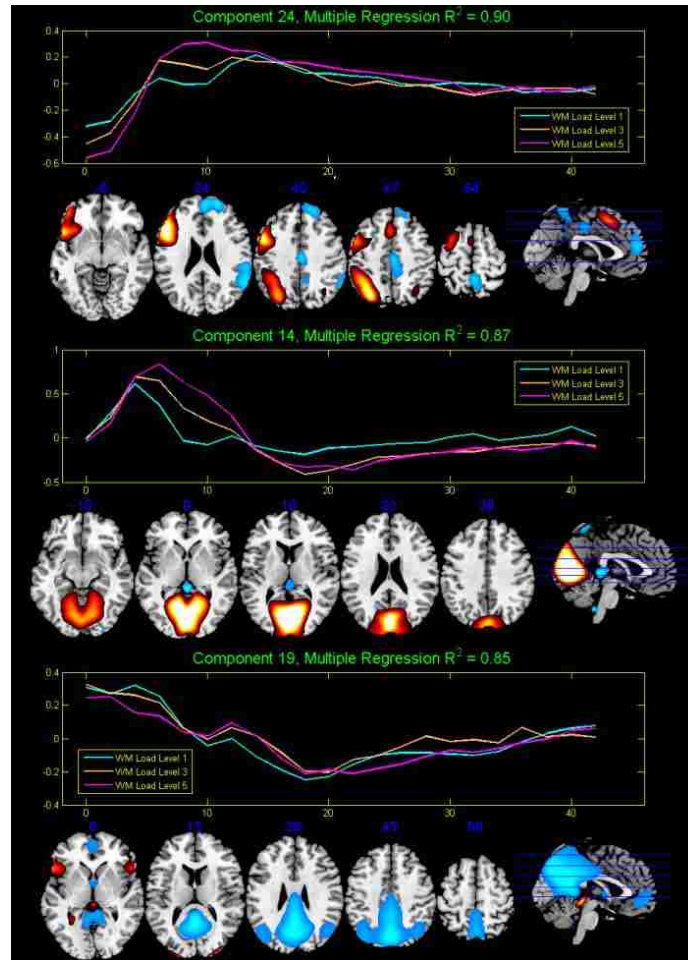
Figure 3.1 The Three selected components and their averaged time courses from Group ICA.

Specifically, component 24 overlapped the left DLPFC, consistent with demonstrated neural substrates of verbal WM tasks; component 14 was located in the bilateral occipital lobe, which is involved in visual perception; and component 19 overlapped regions found in the default mode network (Buckner, Andrews-Hanna et al. 2008) including the posterior cingulate, precuneus, and cuneus. The three components were selected as regions of interest on which the small world network was implemented. Components 24 and 14 were positively correlated with presentation of the task stimuli, while component 19 was negatively correlated.

35

The mask of regions of interest (ROIs) was generated by thresholding the spatial maps of the 3 selected components with $|z| > 2.0$. ROI was then divided into 105 spatially adjacent $3 \times 3 \times 3$-voxel sized blocks. Every block was then subsampled by averaging together, that is, the preprocessed BOLD signal of all voxels within a given spatial block were averaged into one time course, resulting 105 spatial blocks which were used to compute partial correlation below. The finial mask is shown in Figure 3.2.
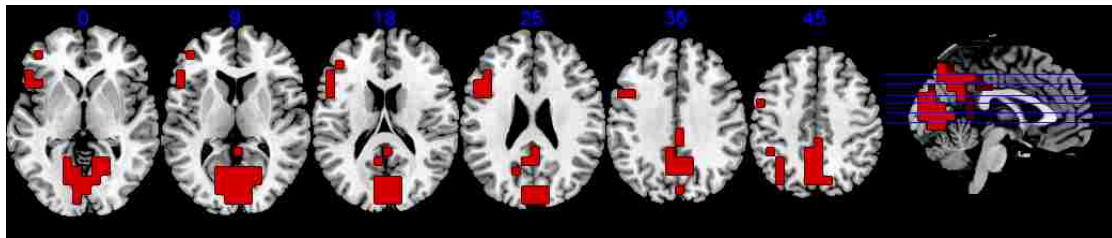
Figure 3.2 The spatial mask applied to build network.

3.2.2 Dividing the Time Courses According To WM Load

Time courses were grouped according to WM load levels (1, 3, 5-digit). The time courses of source data were truncated into blocks based on the onset time of design matrix. Each block consisted of one encode and one probe epoch, while the learn prompt was discarded. The time courses of each six blocks with the same WM load level were then concatenated, so that the BOLD signals in each subject were separated according to different WM load levels instead of task runs. This results in three time series for each subject, corresponding to each of the 1, 3 or 5-digit condition in SIRP.

3.2.3 Partial correlation matrices

To measure the functional connection strength between brain regions, partial correlation was adopted to construct the connectivity matrices of the networks. This approach has been used in previous small-world brain networks studies like (Liu, Liang et al. 2008; Yu, Sui et al. 2011; Yu, Sui et al. 2011). To denote the interaction between each ROI at a specific WM load level, three networks corresponding to each load level were built for each subject. Due to the 105 spatial blocks in the ROI, each partial correlation matrix in this study was a 105 by 105 symmetric matrix, in which each off-diagonal element z_{ij} was the correlation coefficient between time courses in corresponding i^{th} and j^{th} block after filtering out the contribution of activations from all other 103 brain regions in ROI.

As the partial correlation matrices were not normally distributed, so a Fisher r to z transformation was used on each element of the matrices (Fisher 1914; Liu, Liang et al. 2008).

3.2.4 Constructing Brain Network

In many recent studies on brain networks, edge weights are often binarized. Binary networks are generally simpler to characterize since the null model used in statistical comparisons is more easily defined. This is achieved by specifying a weight threshold and discarding weak and non-significant edges (Rubinov and Sporns 2010). In order to find unweighted undirected networks, we binarized the elements with a threshold T,

$$e_{ij} = \begin{cases} 1, if \left| z_{ij} \right| \geq T \\ 0, otherwise \end{cases} \tag{3.1}$$

where e_{ij} is the new weight value and z_{ij} is the old weight value in the unthresholded network.

The selection of threshold T will be discussed in following sections. The diagonal elements of the adjacency matrices are set to be 0 as there is no edge from a node to itself.

3.2.5 Small-world properties

Mathematically, small-world networks have similar characteristic path length but higher absolute clustering coefficients comparing to random networks (Watts and Strogatz 1998), that is,

$$\gamma = \frac{C_{net,small-world}}{C_{net,random}} > 1 \tag{3.2}$$

$$\lambda = \frac{L_{net,small-world}}{L_{net,random}} \approx 1 \tag{3.3}$$

The small-worldness is defined as

$$\sigma = \frac{\gamma}{\lambda} \tag{3.4}$$

which is larger than 1 for small-world network (Achard, Salvador et al. 2006; He, Chen et al. 2007; Humphries and Gurney 2008).

The measures on clustering coefficients and characteristic path length of random networks with similar degree distribution should be obtained for comparison when

computing the small-worldness. Previous studies have shown that the theoretical values

of these two measures are:

$$C_{net,random} = \frac{K_{net}}{N} \tag{3.5}$$

$$L_{net,random} \approx \frac{\ln(N)}{\ln(K_{net})} \tag{3.6}$$

where K_{net} and N are the degree and total number of nodes in the existing network

(Achard, Salvador et al. 2006). However, some studies have suggested that building

random networks with equal (or at least equal) degree sequences as the real small-world

networks may not provide valid statistical comparisons (Stam, Jones et al. 2007). This is

because theoretical random networks have Gaussian degree distributions which differ

from the distributions of real networks being compared against. Therefore, to obtain a

more valid comparison for each network to be measured, we built 25 random networks

using Markov-chain algorithm starting from its degree distribution (Maslov and Sneppen

2002; Milo, Shen-Orr et al. 2002; Sporns and Zwi 2004). The small-worldness value for

each network is then derived by averaging the 25 σ values. This method has been used in

previous studies (Liu, Liang et al. 2008; Liao, Zhang et al. 2010; Yu, Sui et al. 2011).

3.2.6 Thresholding the Networks in Small-World Regime

To make the networks comparable, the thresholding condition for all networks

must be uniform. The threshold values should be within a certain range to keep the

network under the optimized small-world structure, same as previous small-world

network studies (Liu, Liang et al. 2008; Liao, Zhang et al. 2010; Yu, Sui et al. 2011).

First, the maximum threshold should ensure that every network is fully connected, that is,

all nodes in a network could be accessible via one or multiple steps from any other nodes in the same network, or no infinite shortest path length for all nodes. At the same time, the minimum threshold must make sure that all networks hold small-world properties. Specifically, every thresholded network must have a small-worldness value of larger than one (Achard and Bullmore 2007).

It is obvious that different threshold values will have a major impact on the topological properties of the thresholded networks. Because between-subject variations, and the variations in weights for each edge within the networks are both large, binarizing all networks with a uniform threshold may not be a good choice. However, leaving a same degree value for each network may keep similar structures along all subjects, and will be easier to perform comparisons between SZ and HC. A degree range was found between 19.9 and 35.0 (equivalent to cost from 0.191 to 0.337), which satisfies fully connected small-world network condition for all subjects in each of the three memory loads. Within this range, sixteen degrees values, from 19.9 to 34.9 (equivalent to cost from 0.191 to 0.336), with an increment of 1.0, were taken for multiple observations.

3.2.7 Graphical and Statistical Analysis

At each of 16 degree values, an observation of network measures including clustering coefficient (C_{net}), characteristic path length (L_{net}), local efficiency ($E_{local,net}$) and global efficiency ($E_{global,net}$), was calculated for every binarized network. Site effects on individual network measures were corrected for proceeding analysis by conducting one-way analysis of variance (ANOVA). The averages of network measures were estimated over 16 observations per subject to show the overall changes across WM loads. To assess for differential effects of WM load on functional connectivity in SZ

versus HC, we conducted two-way ANOVA to test the main effects of WM load x group interaction. In addition, we used two-sample t-tests to further determine group differences in functional network properties at each WM load level. Similar two sample t-test were also utilized to compare the measures in HC at WM load level 5 and those in SZ at level 3, since previous studies (Callicott, Bertolino et al. 2000; Manoach, Gollub et al. 2000; Perlstein, Carter et al. 2001) have found that WM performance and prefrontal activation in HC at high WM load match those in SZ at medium WM load. Right-tailed (or left-tailed) one sample t-tests were performed on the contrasts of measures between WM loads for each group, to test the increases (or decreases) of measures as WM load level increases. During statistical tests, the averaged network measures across 16 observations were checked first. If significance exists, network measures at each observation were further looked into. False discovery rate (FDR) correction (Benjamini and Hochberg 1995) was used on p-values gained from t-tests made on 16 individual observations, to control for multiple comparisons.

To evaluate how the network properties affect the actual WM performance, we used Pearson's correlation coefficients to investigate the relationships between small-world network measures (i.e., clustering coefficients, characteristic path length, local efficiency and global efficiency) and WM behavior data (i.e. averaged reaction time of each load, which denotes the duration between subject seeing the number and pushing the button at the probe epoch). The Pearson's correlation coefficients were also adopted to check if there are any effects on network measures from subjects' demographic information (age, education, and handedness), the SZ's clinical characteristics (the Scale for the Assessment of Negative Symptoms (SANS) (Andreasen 1984) and the Scale for

41

the Assessment of Positive Symptoms (SAPS) (Andreasen 1984), and head motion during the scanning.

3.3 Results

3.3.1 Behavioral Results

Reaction times for each subject were averaged on correct trials only. Subjects showed a reasonably high percentage of correct responses (mean accuracy $\geq$ 95% for all WM loads). Both groups showed decreased accuracy and increased reaction time as WM load increased. Two-way ANOVA test indicated group and load effect (F = 20.11, p = 1.2×10-5 for group effect, and for F = 41.91, p < 0.0001 load effect) on RT, and group effect (F = 17.72, p < 0.0001) on accuracy. No interaction between group and load was found in both RT and accuracy.

3.3.2 Network Measures at Each WM Load

Two-way ANOVAs on averaged network measures showed significant group by load interaction in averaged C_{net} and $E_{local,net}$ (p < 0.05). Among individual observations, marginally significant group by load interactions (p < 0.1, FDR corrected) were found for C_{net} and $E_{local,net}$ at most of the observations.

For averaged network measures across 16 degree points at single WM load, the t-test indicated group differences (p < 0.05) at WM load level 3 on all four measures, clustering coefficient C_{net}, characteristic path length L_{net}, local efficiency $E_{local,net}$ and global efficiency $E_{global,net}$. No significant group differences were found at WM load levels 1 or 5.
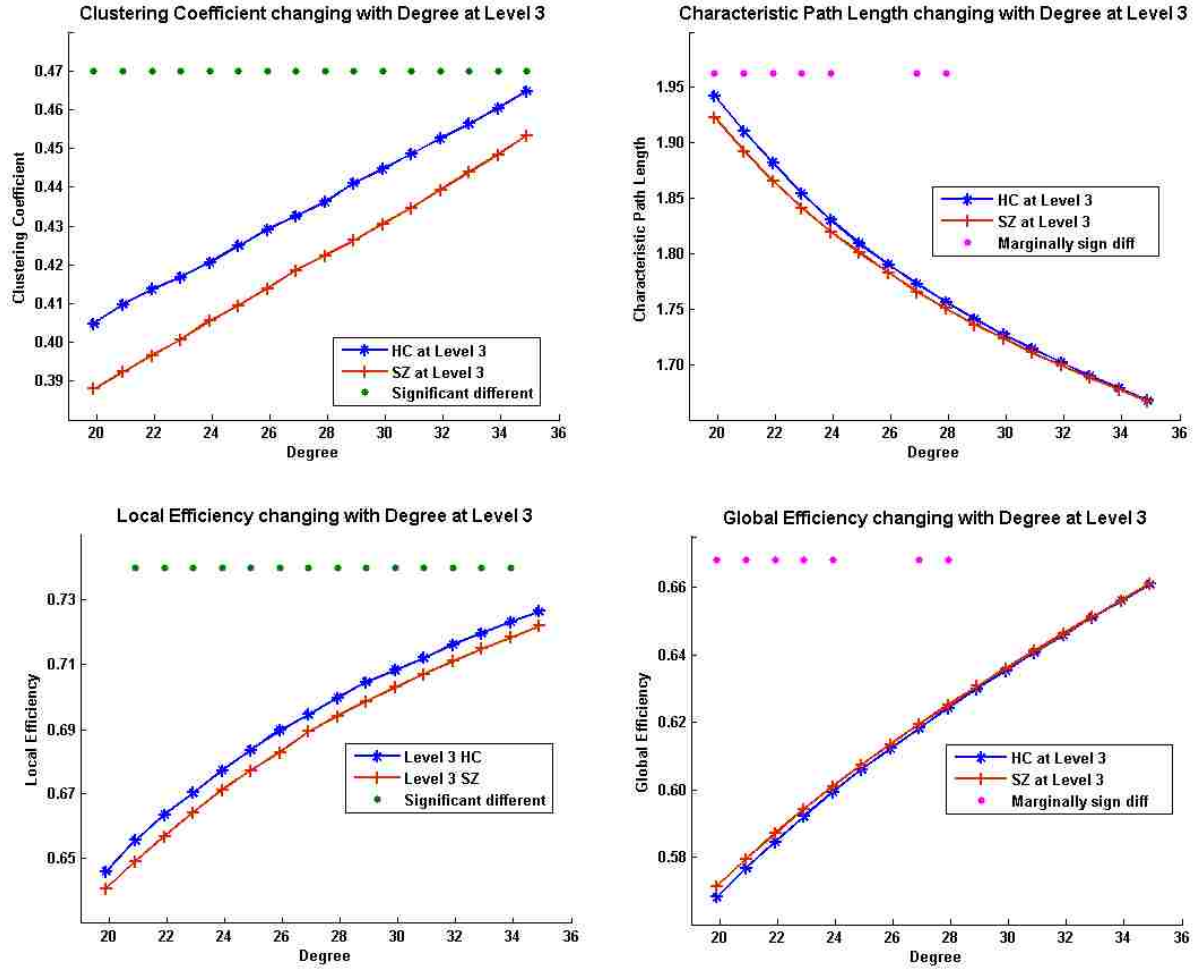
Figure 3.3 Group comparison on network measures at medium load. Network measures on individual observations as a function of degree between groups on WM load level 3. Green dots above indicate significant group difference (p < 0.05, FDR corrected) and pink dots above indicate marginally group difference (p < 0.1, FDR corrected) between HC and SZ at that observation.

Next, we examined individual observations at each degree value K_{net} in the small-world regime within WM load level 3 (Figure 3.3). Throughout 16 observations, two sample t-tests showed all C_{net} and most of $E_{local,net}$ had significant group differences (p < 0.05, FDR corrected). Some L_{net} and $E_{global,net}$ had group differences that approached but did not achieve statistical significance (p < 0.1, FDR corrected). When degree K_{net} increases (i.e., more edges being added into the network), C_{net}, $E_{local,net}$,

43

and $E_{global,net}$ also increase whereas L_{net} decreases. In all observations at WM load level 3, networks in SZ had lower $C_{net}, L_{net}, E_{local,net}$ and higher $E_{global,net}$ than HC.
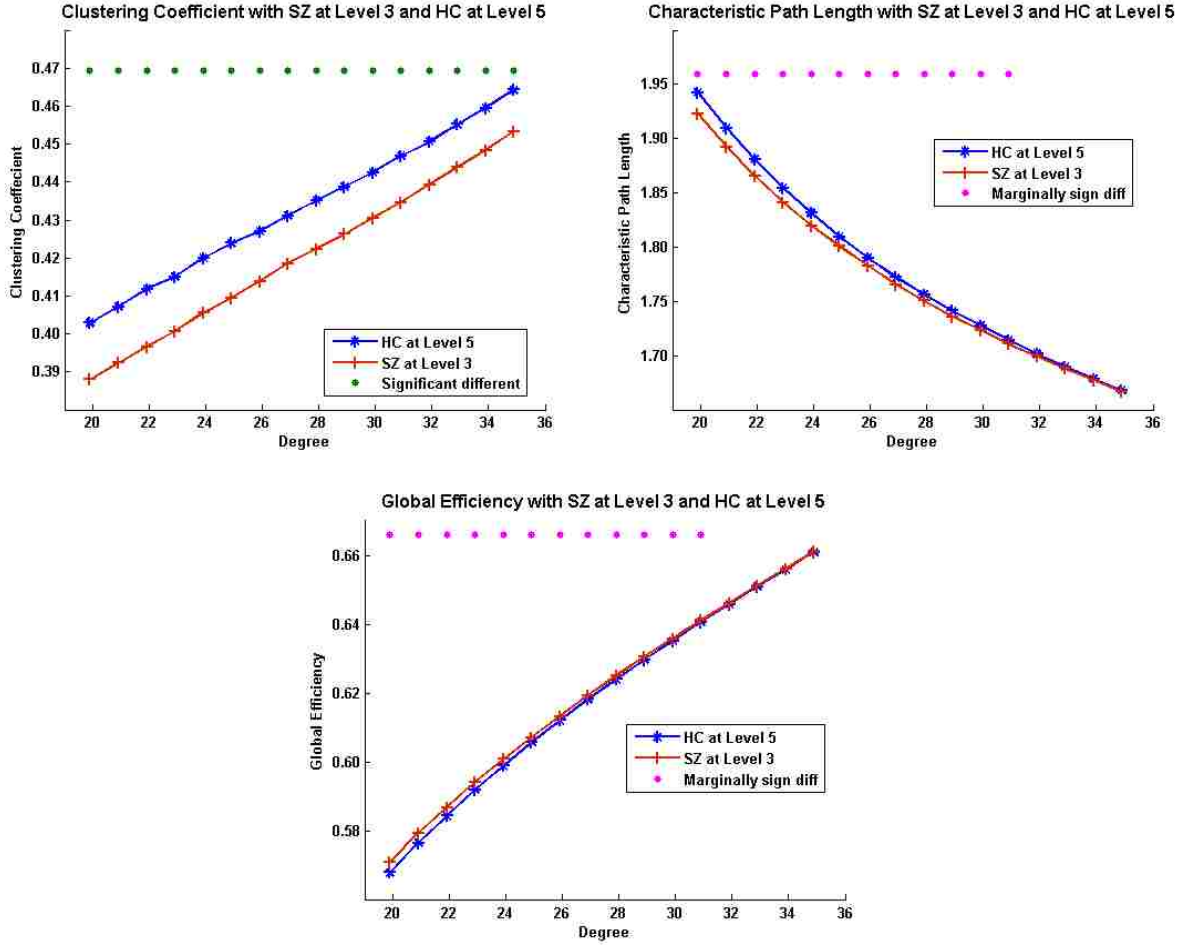
Figure 3.4. Network measures between SZ at high load and HC at medium load. Green dots above indicate significant group difference (p < 0.05, FDR corrected) and pink dots above indicate marginally group difference (p < 0.1, FDR corrected) between HC and SZ at that observation.

In contrasting WM loads between SZ at level 3 and HC at level 5, we still found significant group differences (p < 0.05) in averaged C_{net}, L_{net}, and $E_{global,net}$. Among individual observations, significant group differences (p < 0.05, FDR corrected) existed in C_{net} at all observations, and marginal significant group differences (p < 0.1, FDR corrected) in L_{net} and $E_{global,net}$ at most of the observations (Figure 3.4).

44

3.3.3 Network Measures Change at Different WM Loads

When WM load increases, changes in network measures showed different patterns in each group. Figure 3.5 showed a general trend of averaged network measures change across different WM loads.

In HC, there were no significant changes in network measures between different WM loads in HC. Network measures in SZ, however, revealed significant changes across three WM loads. All four averaged measures in patients had no significant different between WM load level 1 and 5, but altered significantly ($p < 0.05$) in level 3. In individual observations, C_{net}, and $E_{local,net}$ in all observations in SZ showed significant decreases ($p < 0.05$, FDR corrected) from WM load level 1 to level 3, and significant increases ($p < 0.05$, FDR corrected) from WM load level 3 to level 5. At the same time, L_{net} and $E_{global,net}$ in SZ showed marginal significant changes ($p < 0.1$, FDR corrected) from WM load level 1 to level 3 in some (5 out of 16) observations, and marginal significant changes ($p < 0.1$, FDR corrected) from WM load level 3 to level 5 in most (14 out of 16) observations.
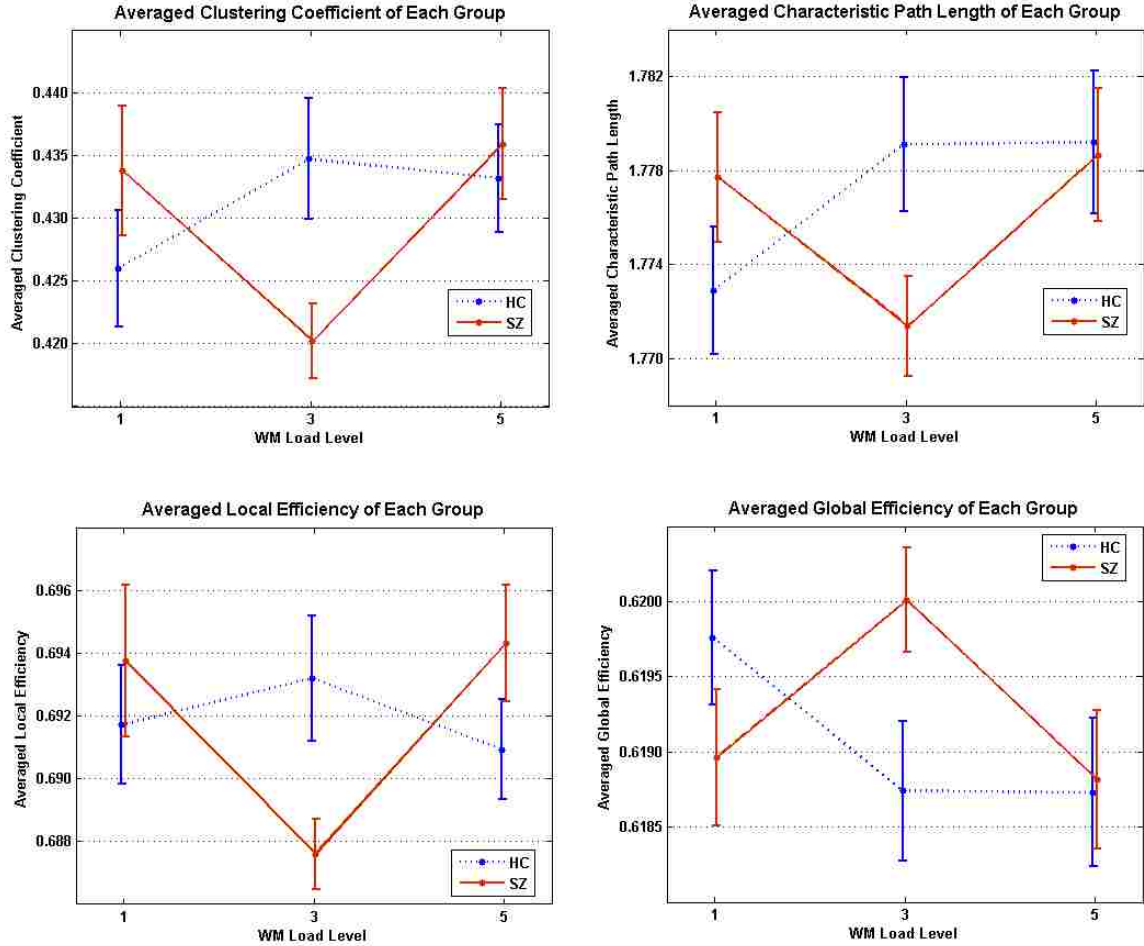
Figure 3.5 Averaged network measures changes across three load levels in HC and SZ. Solid lines between WM load levels indicate significant increases/decreases (p < 0.05), and dotted lines indicate no significant changes when WM load levels increases.

3.3.4 Correlation between Network Measures and Behavioral Data

Significant negative correlations (p < 0.05) were found between reaction time and averaged network measures C_{net} and $E_{local,net}$ for all subjects at WM load level 3. Patterns are shown in Figure 3.6. No correlations were found in other WM loads.
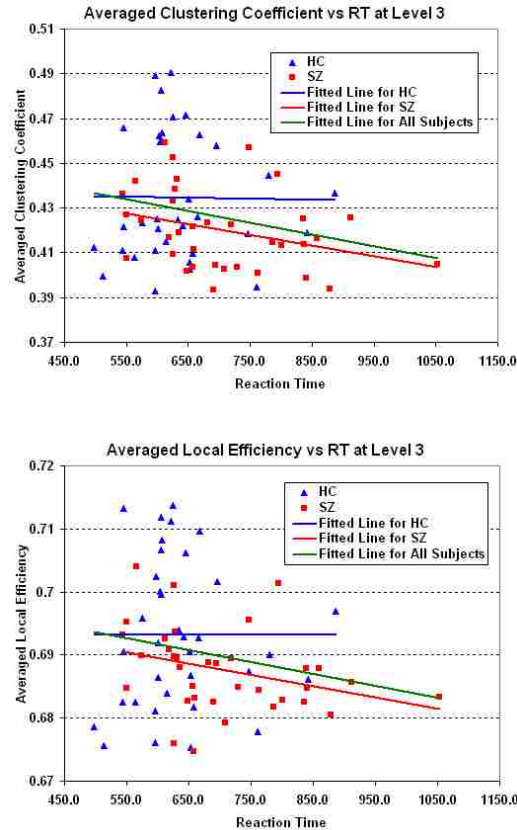
Figure 3.6 Scatter Plots of averaged clustering coefficients and local efficiency against RT at at medium load. Scatter plots with trend lines showing averaged **C$_{net}$** and **E$_{local,net}$** as function of reaction time in all subjects and each group. Significant negative correlation (p < 0.05) was found between reaction time and averaged **C$_{net}$** and **E$_{local,net}$** for all subjects (green line).

In individual observations, lower C_{net} and $E_{local,net}$ were also predicative of longer reaction times at medium WM load level. All 16 observations of C_{net} and most (11 out of 16) observations $E_{local,net}$ showed significant correlations (p < 0.05, FDR corrected).

Within each group, there were no associations of the measures with reaction time in HC. In SZ, the correlations at more than half (9 out of 16) of observations approached but did not achieve statistical significance (p < 0.1, FDR corrected).

3.3.5 Effects from Demographics, Clinical Characteristics and Head Motion

No statistically significant effects (p < 0.05) were found on network measures from either demographics in both groups or clinical characteristics data in SZ.

On each of the six parameters of head motion (translation and rotation on each axis) outputs of the SPM realignment parameters, no statistically significant group differences (p < 0.05) showed between HC and SZ. Four measurements of head motion (mean motion, maximum motion, mean rotation, and number of movements) during the entire scanning process were further calculated using the translation and rotation parameters from the rigid body correction (Jenkinson, Bannister et al. 2002; Van Dijk, Sabuncu et al. 2012). Significant group differences (p < 0.05) were found in mean motion, mean rotation, and number of movements. However, there is no statistically significant correlation between any head motion measurements and network measures.

3.4 Discussion

In this fMRI study, topological and efficiency properties of WM-related networks were examined for both HC and SZ groups. First, group ICA was performed to detect task-related networks. Then partial correlation was used to generate adjacency matrices on 105 WM-related regions for each subject per WM load level. The networks were thresholded within the small-world regime. Statistical tests on network measures taken at 16 different degrees showed significant altered topology and efficiency in SZ at medium WM load. The pattern of altered network measures in SZ at medium WM load is similar to findings in (Potkin, Turner et al. 2009; Kim, Tura et al. 2010), which showed altered DLPFC activation in SZ at medium WM load during a similar SIRP performance. The

48

subjects' demographics, clinical characteristics and head motion during scanning had no significant effects on network measures.

The findings indicate that network measures differed significantly in SZ at the medium WM load level during the SIRP performance. For both topological and efficiency measures, we found that most group differences were between SZ at WM load level 3 and healthy control at either level 3 or level 5. Clustering coefficients, characteristic path lengths and local efficiency were lower for people with SZ while global efficiency was higher for that group.

Topologically, clustering coefficients equivalent to the fraction of the node's neighbors that are also connected with each other (Watts and Strogatz 1998), which reveals the abilities for specialized processing to occur within densely interconnected groups of regions in brain (Rubinov and Sporns 2010). Lower clustering coefficients in SZ for intermediate working memory loads indicate that the networks had fewer local functional interconnections, and thus were less efficient for local information transfer. Functional dysconnectivity found in SZ here is also consistent with the facts found in (Manoach, Gollub et al. 2000), which confirmed that SZ activated fewer DLPFC voxels in common than HC, even when task performance was matched with HC.

Local efficiency reflects the fault tolerance of the network system, or the efficiency of communication between the first neighbors of a node when it is removed (Latora and Marchiori 2001). Brain networks with high clustering and high local efficiency are robust in local information processing even if some neurons are inefficient or damaged (Tang, Zhao et al. 2008). The low local efficiency and low clustering in SZ at

WM load level 3 we found in the current study suggests that the network of task-related brain regions in SZ had lower fault tolerance (i.e., more vulnerable) locally than HC. The findings on reduced local efficiency and clustering are also consistent with prior fMRI and EEG studies on functional brain networks in SZ (Micheloyannis, Pachou et al. 2006; Bluhm, Miller et al. 2007; Liu, Liang et al. 2008; Rubinov, Knock et al. 2009; Lynall, Bassett et al. 2010; Wang, Metzak et al. 2010).

In general, subjects with longer reaction time also had lower clustering coefficient and local efficiency at WM load level 3, as seen in the negative correlation between reaction time and those two measures. The less clustered structure and lower efficiency of task-related networks in SZ may affect the performance to accomplish the task.

In brain networks, the identified paths show potential routes of information flow between pairs of brain regions (Rubinov and Sporns 2010). Characteristic path length is a measurement on the extent of average connectivity or overall routing efficiency of the network. Global efficiency in graph system is the efficiency of a parallel system, where all the nodes in the network exchange information concurrently (Latora and Marchiori 2001). Networks with shorter characteristic path length and high global efficiency are of significance in minimizing noise, shortening signaling delay and increasing synchrony (Kaiser and Hilgetag 2004). Shorter path lengths between nodes have also been shown to promote effective interactions across different cortical regions (Bassett and Bullmore 2006; Achard and Bullmore 2007). Among SZ, the networks related to intermediate WM loads had shorter path lengths and higher global efficiency than those in HC. Because of abnormalities within brain regions like DLPFC, SZ may need to compensate for this impairment by involving more brain regions concurrently so as to achieve comparable

WM performance, resulting shorter path lengths and higher global efficiency. The phenomena that SZ shows reduced clustering but globally efficient and robust were also found in previous network studies (Alexander-Bloch, Gogtay et al. 2010). (Lynall, Bassett et al. 2010) suggested that reduced local dominance will generally be offset by greater network robustness in SZ. In contrast, activations in HC subjects at WM medium load levels concentrated more on certain brain areas, even at the cost of low global efficiency within the network.

In a previous WM study on SZ which utilized the same version of the SIRP (Potkin, Turner et al. 2009), Potkin et al. also found that the medium WM load was most responsible for significant group differences in the DLPFC activation. They attributed these differences to the "inefficiency" of this brain region that might not be directly caused by increases in WM load. A multivariate analysis using Partial Least Squares on the same data (Kim, Tura et al. 2010), Kim et al. showed that other areas in frontal lobe, pre and post central gyrus, and the angular gyrus showed a similar pattern for the probe condition, while the visual cortex showed a pattern of greater activation in the SZ subjects in the encoding of the medium load WM condition rather than during the probe epoch. (Kim, Manoach et al. 2009) used ICA on a SIRP dataset of which this was a subset, and identified a frontal/parietal network which showed more activation in SZ subjects in the moderate load conditions as well. This small-world network analysis did not distinguish encode from probe responses in determining the network edges, but considered the correlations among the 105 brain regions at each WM load. Although encoding and maintaining information involve different psychological processes, they are both affected by load and are needed to perform a WM task. Many previous studies on

WM combine them, for example, N-back paradigm (Owen, McMillan et al. 2005), looks into the two psychological processes in subjects simultaneously. Brain connectivity associated with both encode and probe (a.k.a. retrieval) conditions have also been combined in previous SIRP studies (Karlsgodt, Glahn et al. 2007; White, Schmidt et al. 2011). The combination of encode and probe still identified the moderate WM load level as the condition in which the network measures in SZ were different from those in HC.

Depending on the level of demands on working memory, different physiological responses showed up in each group to accomplish the task. In HC, we found no significant changes across different WM load. Although previous studies in WM like (Manoach, Press et al. 1999; Callicott, Bertolino et al. 2000; Manoach, Gollub et al. 2000) have shown increased BOLD activities as WM load increases within subjects' capacities, the topology and efficiency of functional networks in HC remain stable.

In contrast, the small-world network measures in SZ showed a different pattern of responses with increasing WM loads, consistent with the inverted-U function relating fMRI signal to WM load (Callicott, Mattay et al. 1999; Manoach 2003). There were significant differences in small-world network measures across different WM load levels among patients. The fact that local clustering coefficient and local efficiency in SZ during WM load level 1 were close to those in HC at WM load level 3, indicated that more effort may have been used by patients to perform the low difficulty task (Callicott, Mattay et al. 2003). As WM load level increased from low to medium, the clustering coefficients and local efficiency dropped significantly, but path length reduced and global efficiency rose. This implies that connectivity tends to be more spread across the brain regions included in analysis, or that more voxels in brain regions for SZ were utilized concurrently to

perform the task, as discussed above. When tasked with the medium WM load, functional brain networks adapt to the increased WM demands by increasing global integration and efficiency (Bassett, Meyer-Lindenberg et al. 2006; Bassett, Bullmore et al. 2009; van den Heuvel, Stam et al. 2009; Fornito, Yoon et al. 2011). However, when the difficulty level increased further from medium to high, the clustering coefficients and local efficiency returned to values comparable to those in the low difficulty condition. These changes suggest that the highest memory load may have approached SZ's WM capacity, and the patients will be no longer able to adequately perform more difficult tasks (Manoach 2003; Kim, Manoach et al. 2009; Potkin, Turner et al. 2009).

In this study, we focused on the small world network of task-related regions. In order to avoid certain bias, we also tried another approach by using components of the whole brain that includes non-task-related regions, in which group ICA is performed on the same data, generating 80 components. After eliminating artifactual components (by visual inspection) which contain obvious skull edge effects or ventricles, 39 components were chosen, each as one node, to build the connectivity network using the same method mentioned above. The trends we observed were consistent with the main results discussed above, but with weaker between-group differences. Since the selected components included both task-related and non-task-related ICs, results suggested that the non-task-related brain regions contributed less to the WM task, but may add more individual variation to the network.

There are several methodological issues that should be considered in this study. First, we used group ICA to find the task-related region, and divided the region into 105 contiguous voxel clusters, corresponding to nodes in the brain networks. Although cluster

size and the randomness generated from group ICA may impact network structures, we have averaged the results of group ICA from multiple runs so as to mitigate against this possibility. Secondly, we used partial correlation on BOLD signals between brain regions to construct brain networks, which may be affected by the operation of truncating and reordering the time courses to separate WM loads. There are other methods that may be worth trying in future studies. Pearson's correlation and partial correlation of time series between different brain regions are commonly used in fMRI networks (Liu, Liang et al. 2008; Wang, Metzak et al. 2010; Kang, Sponheim et al. 2011; Moussa, Vechlekar et al. 2011; Yu, Sui et al. 2011; Yu, Sui et al. 2011). However, a recent study (Fornito, Yoon et al. 2011) built task-related functional networks from the correlations of beta values derived from regression against stimuli. Also, the networks we analyzed are undirected and binarized. Future studies may perform a weighted network analysis which could supply more information as has been done in two recent studies (van den Heuvel and Hulshoff Pol 2010; Wang, Douw et al. 2010). Another concern is that patients had received antipsychotic treatment, but the detailed medication history was not available for all subjects recruited in this study. This raises the potential confound that antipsychotics may contribute to the differences in graph parameters among patients.

In conclusion, we examined the differences between healthy controls (HC) and people with schizophrenia (SZ) on topological properties of small-world networks that were derived from fMRI data acquired during working memory performance. Brain networks were constructed for each subject based on the functional connectivity between brain regions constrained to components of task-related brain areas for each WM load level. The constructed brain networks were thresholded to derive small-world networks

54

with a series of constant number of edges for all subjects. Next, topological and efficiency measures for brain networks in both groups were generated. Results showed that topologies and efficiencies of functional networks in HC were stable as WM load increases, while network measures in SZ altered significantly at medium WM load. The network measures implied brain connectivity in SZ was more diffuse and less strongly linked locally in functional network at intermediate level of WM when compared to HC. The differential local and global patterns of connectivity and efficiency for people with SZ across levels of WM load indicate that patients are inefficient and variable in response to WM load increase, comparing to stable highly clustered network topologies in HC. Sophisticated graph network measures provide a means of characterizing the effects of dysfunctional neural circuitry and variations in impaired connectivity across levels of dysconnectivity working memory demands in SZ (Manoach, Press et al. 1999; Manoach, Gollub et al. 2000; Callicott, Mattay et al. 2003; Potkin, Turner et al. 2009). The present findings also suggest that graph theoretic descriptions of neural connectivity may help isolate the conditions under which neural contributions to working memory deficits are most evident in the disorder.

Chapter 4   Functional Network Connectivity to Differentiate Bipolar and Major Depression

4.1   Introduction

4.1.1   Bipolar and Major Depressive Disorder

Bipolar disorder (BD) and major depressive disorder (MDD, or unipolar depression) rank among the most debilitating illnesses worldwide (Murray, Lopez et al. 1996). Both BD and MDD are similarly characterized by depressive episodes, making it difficult to differentiate between the two disorders during the depressed phase (Judd, Akiskal et al. 2002; Judd, Akiskal et al. 2003). BD patients are often misdiagnosed as MDD (Hirschfeld, Lewis et al. 2003; Hirschfeld and Vornik 2005), leading to inappropriate and longer medication trials, a poorer prognosis, and greater health care expenses (Kupfer 2005; Dudek, Siwek et al. 2013). Objective neuroimaging markers that distinguish BD from MDD may significantly improve diagnostic accuracy, especially in the early phases of the illness (Strakowski, Adler et al. 2012), and may thereby facilitate optimal clinical and functional outcome for individuals suffering from either disorder (Cardoso de Almeida and Phillips 2013). For example, functional magnetic resonance imaging (fMRI) may prove helpful for identifying neurophysiological abnormalities that distinguish BD from MDD. Different patterns of functional activities have been found in BD versus MDD during resting-state or task-based fMRI studies (Taylor Tavares, Clark et al. 2008; de Almeida, Versace et al. 2009; Almeida, Versace et al. 2010; Bertocci, Bebko et al. 2012; Diler, de Almeida et al. 2013; Cerullo, Eliassen et al. 2014).

56

4.1.2 Motivation

Analyses of FC by computing graph theory metrics, such as clustering coefficient, characteristic path length, local efficiency and global efficiency, further assess the topological properties of brain graphs, and provides a useful measure of how effectively information is passed and processed between different brain regions (Rubinov and Sporns, 2010). Graph organizational properties may reveal disease-related abnormalities in functional brain networks among psychiatric patients from resting-state as well as task-related neuroimaging data (He et al., 2012; Lynall et al., 2010; Wang et al., 2010; Yu et al., 2011a; Yu et al., 2011b). However, no previous study has compared the FNC properties between BD and MDD.

The goal of the present study was to investigate the different FNC patterns in BD and MDD patients during the resting-state. We compared connectivity strengths (single-edge weights) and other graph measures of FNC between the two groups. Characterizing how FNC structure differs in the fMRI data obtained from BD versus MDD samples may increase our understanding of the organization of functional brain networks in these disorders, and may provide potential diagnostic biomarkers to allow for the differentiation of BD from MDD.

4.2 Methods

In this study, preprocessed fMRI data on BD, MDD and HC from the Tulsa Resting-state Dataset was used.

4.2.1 Group ICA and post-processing on functional data

Group ICA was performed on the fMRI data using GIFT software (http://mialab.mrn.org/software/gift) (Calhoun and Adali 2012). Individual fMRI images

were decomposed via principal component analysis (PCA), with the first 100 components selected for dimension reduction (Allen, Erhardt et al. 2011; Erhardt, Rachakonda et al. 2011; Yu, Sui et al. 2011). The infomax algorithm (Bell and Sejnowski 1995) was repeated 10 times using ICASSO (http://www.cis.hut.fi/projects/ica/icasso) to improve the reliability of the decomposition, result in 75 group independent components. Time courses (TCs) and spatial independent components (ICs) of individuals were then back-reconstructed (Calhoun, Adali et al. 2001; Erhardt, Rachakonda et al. 2011).

Similar to the IC selection procedures described in (Allen, Erhardt et al. 2011; Damaraju, Allen et al. 2014), we generated a one-sample t-test map for each spatial map across all subjects, and thresholded the map to obtain regions of peak activation clusters for each IC. The mean power spectra of the corresponding TCs from each IC were also calculated. The intrinsic connectivity networks (ICNs) were identified if they exhibited peak activations in gray matter, and also showed low spatial overlap with known vascular, ventricular, motion, edges, and susceptibility artifacts according to the thresholded t-test maps. We additionally ensured that the mean spectral powers of ICNs were dominated by low-frequency fluctuations (Cordes, Haughton et al. 2000). Forty-eight ICs were characterized as ICNs, while 27 ICs were attributed to physiological, movement related, or imaging artifacts. As remaining noise effects like heart beat and respiration, especially head motion artifact has been reported on connectivity analysis (Power, Barnes et al. 2012; Van Dijk, Sabuncu et al. 2012; Yan, Craddock et al. 2013), related TCs underwent additional post-processing to remove them (Allen, Damaraju et al. 2014), including 1) detrending linear, quadratic, and cubic trends, 2) multiple regression

of the 6 realignment parameters and their temporal derivatives, 3) removal of detected outliers (despiking along each TC), and 4) low-pass filtering with a cutoff of 0.15 Hz.

4.2.2 FNC Analysis

For each subject, an FNC matrix was calculated using the absolute values of Pearson's correlation between TCs of each pair of 48 ICNs. P-values of corresponding correlation coefficients also were obtained for further analysis. The FNC matrices were then normalized into z-scores using Fisher r-to-z transformation, in order to induce normality on the correlation coefficients. One 48×48 symmetric FNC matrix was obtained for each subject, with entry of element (i, j) corresponding to the strength (or weight) of connectivity between ICNs i and j. The network connectivity strength (Lynall, Bassett et al. 2010) was specified as absolute z-scores. FC-of-interest were then selected based on p-values obtained from Pearson's correlation with corresponding $p < 0.05$ (2-tailed, uncorrected) in more than 80% of subjects in any one of three groups. An identical overall FC-of-interest pattern was maintained across all subjects for comparison. With non-FC-of-interest entries set to zero, 398 significant connectivity strengths (sparsity at $398 \div 1128 = 35.3\%$) in each FNC matrix were retained for further testing. This sparsity value falls within a range that is not only biologically plausible (Sporns 2011), but also proved to keep graph structure reliable (Dennis, Jahanshad et al. 2012). Two types of analysis were performed on the FNC matrices: a connectivity analysis and a graph analysis.

4.2.3 Connectivity analysis

Connectivity analysis was performed on the elements of FNC metrics (i.e. strengths of the FC between ICN pairs). ANOVA across groups was performed

simultaneously on each FC strength to assess the significance of group effects. Two-sample t-tests were then applied to assess the significance of pair-wise group differences in connectivity for contrasts in which $p < 0.05$ from ANOVA. Please refer to supplemental material S3 for detailed background on the statistical tests. The false discovery rate (FDR) correction (Benjamini and Hochberg 1995) for multiple testing was applied to the p-values obtained from the statistical tests made on 398 individual FC strengths. Pearson's correlations were used to evaluate relationships between the symptom rating scale scores (MADRS in both BD and MDD subjects) and FC strengths that differed between groups.

4.2.4 Graph analysis

In graph-theory based analyses, FNC were normalized (FC strengths were linearly rescaled into [0, 1] with a uniform factor in all FC strengths across all subjects) and treated as weighted graphs. In the graphs, ICNs correspond to nodes, and the weights of edges linking nodes-pairs are the FC strengths. Within each graph, three nodal metrics including strength, clustering coefficients, and local efficiency were estimated at the functional-network-level (micro-level) for each of 48 nodes. At the same time, four graph metrics including averaged clustering coefficients, characteristic path lengths, global efficiency and averaged local efficiency were evaluated for each brain graph as a whole at the macro-level. The brain connectivity toolbox (http://sites.google.com/site/bctnet/) was utilized for the graph metrics computation. Detailed definitions of and formula for these graph metrics can be found in (Rubinov and Sporns 2010). On nodal graph metrics, significance of group effects were first computed using ANOVA. Nodes with $p < 0.05$ underwent post-hoc t-tests to examine the significance of contrasts between group pairs.

The p-values from statistical tests made on 48 individual nodal metrics were corrected using FDR. On global brain graph measures, statistical significance of both group effects and pair-wise group contrasts were tested using ANOVA and t-tests respectively. Correlation between symptom rating scale scores (MADRS in both BD and MDD groups) and graph metrics that showed group differences were evaluated. The BrainNet Viewer toolbox (http://www.nitrc.org/projects/bnv/) was used for visualization (Xia, Wang et al. 2013).

4.3 Results

4.3.1 Group ICA and FNC

Figure 4.1a displays the spatial maps of 48 ICNs identified from group level ICA. Based on their anatomical and presumed functional properties, 48 ICNs are arranged into groups of auditory (AUD), somatomotor (SM), visual (VIS), cognitive control (CC; putatively referring to the planning, monitoring, and adapting one's behavior), default-mode (DM), and cerebellar (CB) components. ICNs were similar to those observed in previous high model order ICA decompositions (Kiviniemi, Starck et al. 2009; Abou-Elseoud, Starck et al. 2010; Allen, Erhardt et al. 2011; Allen, Damaraju et al. 2014; Sui, Huster et al. 2014). Figure 4.1b shows the averaged FNC in each group, FNC was averaged over all subjects and inverse Fisher transformed ($r = tanh(z)$) back to correlation coefficient for display, facilitating comparisons with previous studies. Overall, BDs showed stronger FC strengths, while strengths in MDDs were slightly weaker.
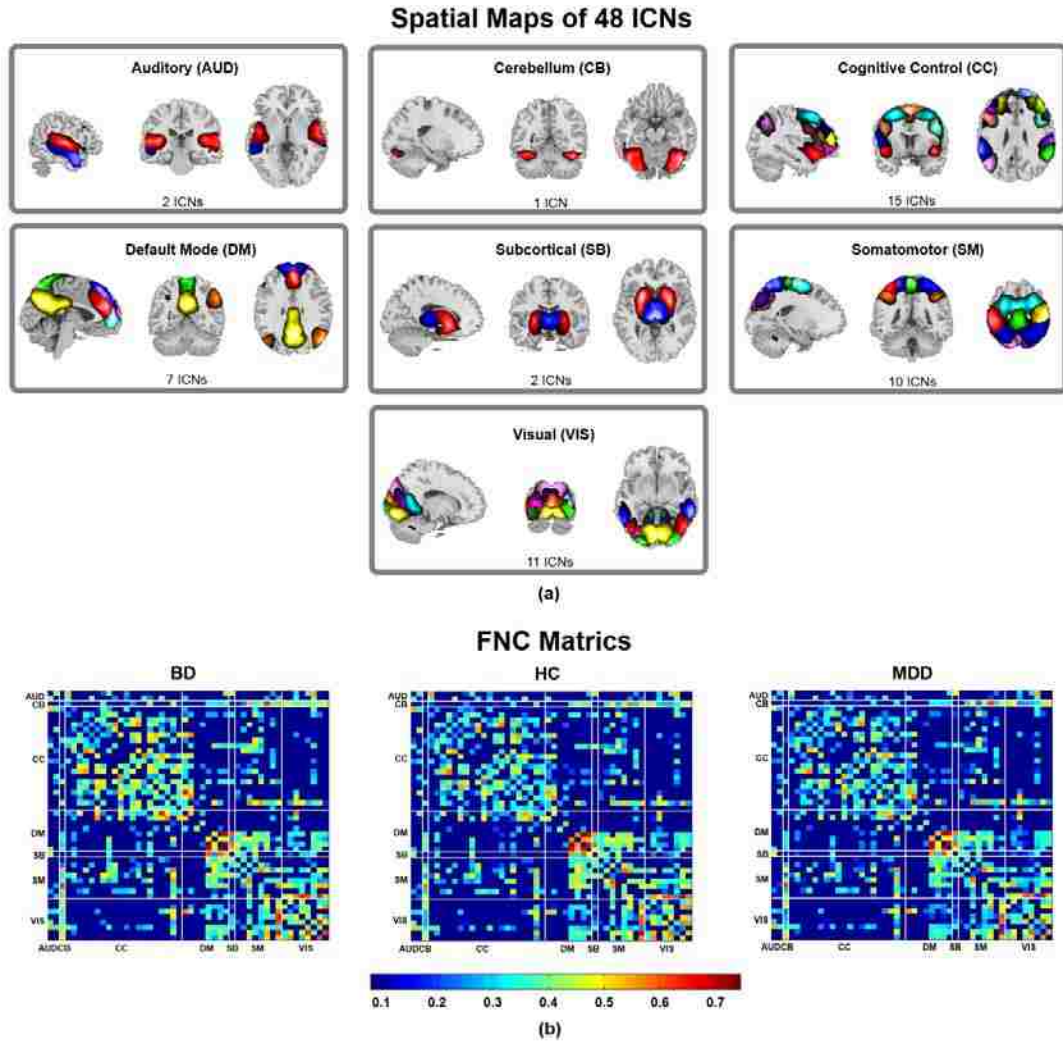
Figure 4.1 (a) Spatial maps of 48 ICNs and (b) the FNC (correlation matrix) in each group. ICNs are divided into groups and arranged based on their anatomical and functional properties. FC strengths are averaged over all subjects in each group. (AUD: auditory; SM: somatomotor; VIS: visual; CC: cognitive control; DM: default mode; CB: cerebellar)

From ANOVA, strong group effects were found in two FC strengths after FDR correction, as displayed in Figure 4.2: FC strengths between inferior frontal and anterior cingulate cortex (ICN59 – ICN61, $p = 4.50 \times 10^{-4}$), and between left inferior parietal lobule and precentral gyrus (ICN3 – ICN41, $p = 4.46 \times 10^{-4}$). However, both FC only passed FDR at $q = 0.1$, but did not achieve statistical significance after correction at $q =$

0.05. Based on group-pair comparison of FC strengths, two sample t-tests revealed that six FC strengths were either strongly or significantly differentiating between BD and MDD, and another FC strength differed between MDD and HC.

Compared to MDD, BD showed significantly stronger FC strengths within dorsolateral prefrontal (DLPFC) and ventrolateral prefrontal (VLPFC) areas (2 FC strengths, ICN14 – ICN32 p = 1.82×10^{-4}, and ICN6 – ICN32, p = 4.77×10^{-4}, both FDR corrected), between left postcentral and cuneus (ICN17 – ICN46, p = 2.84×10^{-4}, FDR corrected), as well as inferior frontal/ DLPFC to anterior cingulate cortex (ACC) (ICN59 – ICN61, p=3.24×10^{-4}, FDR corrected). Two more FC displayed higher strengths in BD than MDD, including lingual/cuneus to superior temporal (ICN22 – ICN25, p = 9.16×10^{-4}) and medial frontal and superior frontal regions (ICN32 – ICN75, p = 9.82×10^{-4}), which approached but did not achieve significance after correction (passed FDR at q = 0.1 only, but did not at q = 0.05).

Compared to HCs, weaker FC strengths were found in MDD from left inferior parietal lobule to precentral gyrus (ICN3 – ICN41, p = 1.30×10^{-4}). However, this difference in FC strengths was reduced to a non-significant trend after correction for multiple testing.

4.3.2   Graph analysis on FNC

A summary of ICNs (nodes) with significant group difference and group effects on nodal graph measures are listed in Table 4.1 and highlighted in Figure 4.3.
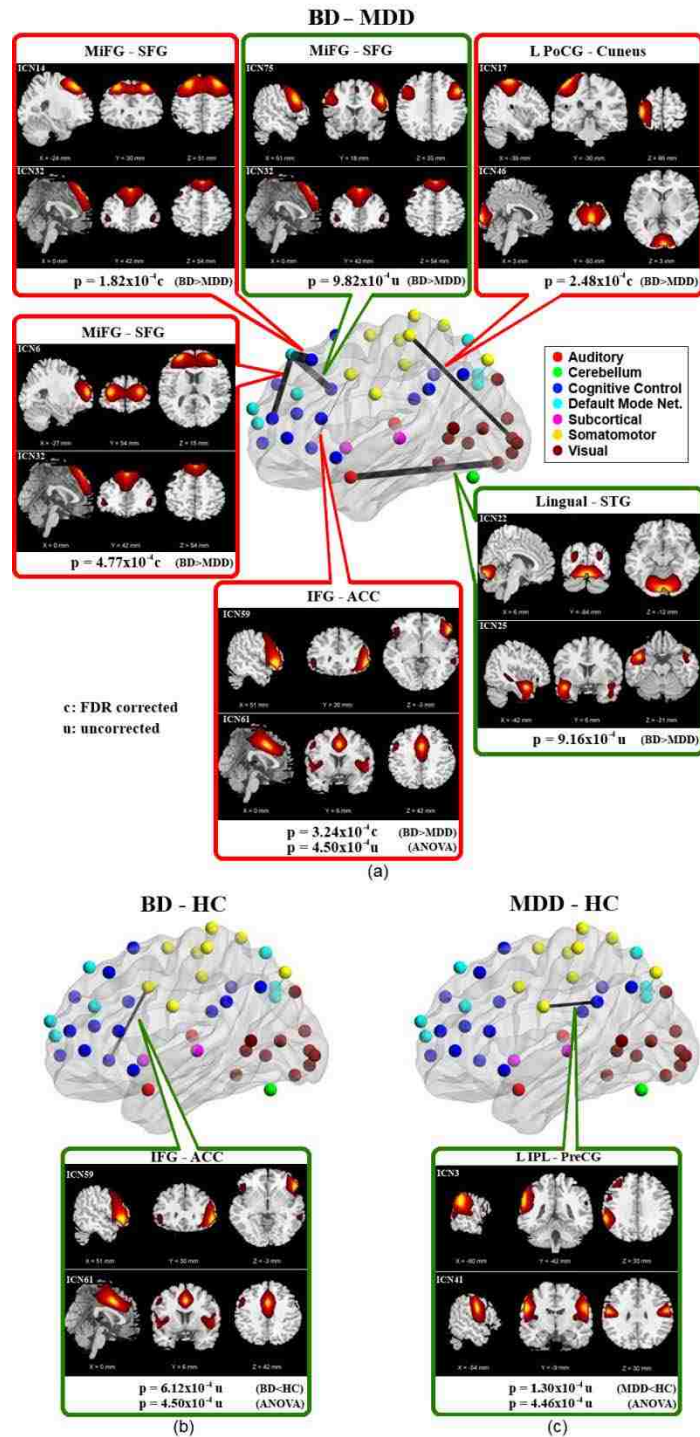
Figure 4.2 The FC strengths that differentiated (a) BD to MDD, (b) BD to HC, and (c) MDD to HC with two-sample t-tests (p < 0.001). Width of FC strengths in the brain map indicates the averaged strength difference between groups. The FC strengths in red frames showed significant group differences between BD and MDD (p < 0.05, FDR corrected), while others approached significance but did not survive multiple comparisons.

64

As shown in Figure 4.3a, significant group effects from ANOVA existed in nodal strength of ICN67 after FDR correction. The t-tests show five networks, including ICNs lie in DLPFC, VLPFC, ACC and inferior parietal area, were significantly higher (p < 0.05, FDR corrected) in nodal strengths in BD than MDD. No significant differences are found between patients and controls.

Figure 4.3b displays the networks with significant group effects and group difference in clustering coefficients. Five ICNs showing significant group effect (p < 0.05, FDR corrected) from ANOVA, which were mostly concentrated in prefrontal regions. In t-tests, three ICNs indicated stronger clustering in BD than HC after FDR correction. A total of fourteen ICNs distinguished BD from MDD, which lie in frontal, ACC, posterior cingulate cortex (PCC), superior temporal, and parahippocampal areas.

For local efficiency, significant group effect (p < 0.05, FDR corrected) on local efficiency was found in ICN67 again from ANOVA test. Seventeen ICNs demonstrated significantly (p < 0.05, FDR corrected) higher values in BD comparing to MDD after correction, including ICNs in pre- and mid-frontal, ACC, PCC, superior temporal, cuneus and parahippocampal areas (Figure 4.3c).
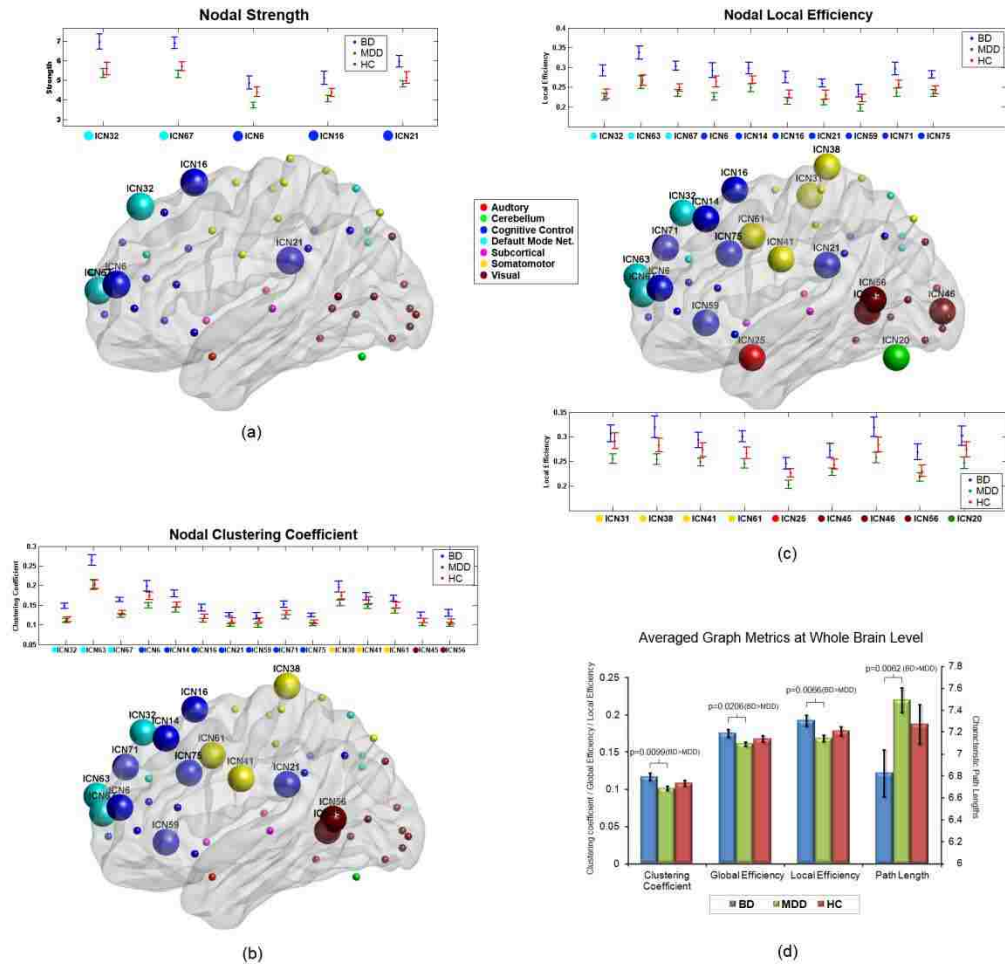
Figure 4.3 The measures of (a) nodal strength, (b) nodal clustering coefficient, (c) nodal local efficiency, and (d) averaged graph measures at whole brain level. For the nodal measures, only ICNs that showing significant group difference or group effect (p < 0.05, FDR corrected) are shown in the error bar plots, and highlighted in the brain maps.

For ANOVA on global brain graph metrics, local efficiency showed significant group effect (p = 0.0376), while p-values of clustering coefficient (p = 0.0513), characteristic path lengths (p = 0.0568) and global efficiency (p = 0.0901) were also small but only marginally significant. Between group pairs, despite the fact that no significant group differences were revealed for the graph metrics between patients and HC, all four global brain graph metrics showed differences between BD and MDD (Figure 4.3d). Compared to MDD, BD showed significantly higher values in clustering

66

coefficient (p = 0.0099), global efficiency (p = 0.0206) and local efficiency (p = 0.0066), as well as significantly shorter characteristic path lengths (p = 0.0062) across the whole brain, indicating the higher efficiency in topology structure of BD.

Table 4.1 ICNs with Group Differences / Group Effect in Nodal Metrics

ICN	Peak Coord (mm)	Nodal Strength		Nodal Clustering Coefficient			Nodal Local Efficiency	
		P_{BD-MDD}	P_{ANOVA}	P_{BD-MDD}	P_{BD-HC}	P_{ANOVA}	P_{BD-MDD}	P_{ANOVA}
Auditory								
Parahippocampal (ICN25)	-42,6,-21						0.0116	
Cognitive Control								
DLPFC/ACC (ICN6)	-27,54,15	0.0011		0.0005		0.0030	0.0010	
DLPFC (ICN14)	-24,30,51			0.0011		0.0028	0.0011	
DLPFC (ICN16)	0,15,66	0.0038		0.0016			0.0009	
IPL (ICN21)	63,-33,27	0.0008		0.0001		0.0047	0.0005	
MFG (ICN59)	51,30,-3			0.0096			0.0183	
DLPFC (ICN71)	30,51,36			<0.0001			0.0060	
DLPFC (ICN75)	51,18,33			0.0034			0.0060	
Default Mode								
DLPFC/VLPFC (ICN32)	0,42,54	0.0009		0.0001	0.0030	0.0013	0.0004	
SFG (ICN63)	15,66,21			0.0084	0.0023		0.0162	
SFG/ACC (ICN67)	0,63,12	0.0001	0.0005	0.0128	0.0009	0.0002	0.0001	0.0004
Cerebellum								
Cerebellum (ICN20)	-39,-69,-21						0.0193	
Somatomotor								
R PoCG (ICN31)	45,-24,63						0.0121	
MFG (ICN38)	0,-33,78			0.0064			0.0055	
PreCG (ICN41)	-54,9,30			0.0139			0.0087	
ACC (ICN61)	0,6,42			0.0185			0.0039	
Visual								
PCC/ Parahippocampal (ICN45)	-6,-54,3			0.0047			0.0078	
Cuneus (ICN46)	3,-93,3						0.0069	
STG (ICN56)	-57,-57,9			0.0026			0.0058	

4.3.3 Correlation with Symptom Scores

No significant correlation with symptom scores was found in individual FC strengths and global network measures.

Table 4.2 Significant Correlations between Nodal Metrics and Symptom Scores

ICN	Peak Coord (mm)	Nodal Strength		Nodal Clustering Coefficient		Nodal Local Efficiency	
		YMRS (BD)	MADRS (BD+MDD)	YMRS (BD)	MADRS (BD+MDD)	YMRS (BD)	MADRS (BD+MDD)
Auditory							
Parahippocampal (ICN25)	-42,6,-21						r = -0.3605 p = 0.0080
Cognitive Control							
DLPFC (ICN16)	0,15,66	r = 0.6518 p = 0.0158	r = -0.3009 p = 0.0286	r = 0.6397 p = 0.0185	r = -0.2971 p = 0.0307	r = 0.6280 p = 0.0215	r = -0.3184 p = 0.0202
IPL (ICN21)	63,-33,27				r = -0.2949 p = 0.0321		r = -0.2750 p = 0.0462
DLPFC (ICN71)	30,51,36				r = -0.2833 p = 0.0398		r = -0.2920 p = 0.0339
Somatomotor							
R PoCG (ICN31)	45,-24,63						r = -0.2753 p = 0.0460
ACC (ICN61)	0,6,42				r = -0.2919 p = 0.0339		r = -0.3605 p = 0.0080

In contrast, the nodal graph measures of the ICNs that located in the DLPFC, ACC, inferior parietal, and parahippocampal cortex regions were negatively correlated (p < 0.05, uncorrected) with MADRS scores in both the BD and MDD groups (Table 4.2). Figure 4.4 shows a typical network (ICN16) with the overall trends between nodal strength and symptom scores. In the patients with higher MADRS scores the overall nodal connectivity strength, nodal clustering coefficient and nodal local efficient of the ICNs were lower in these brain networks.
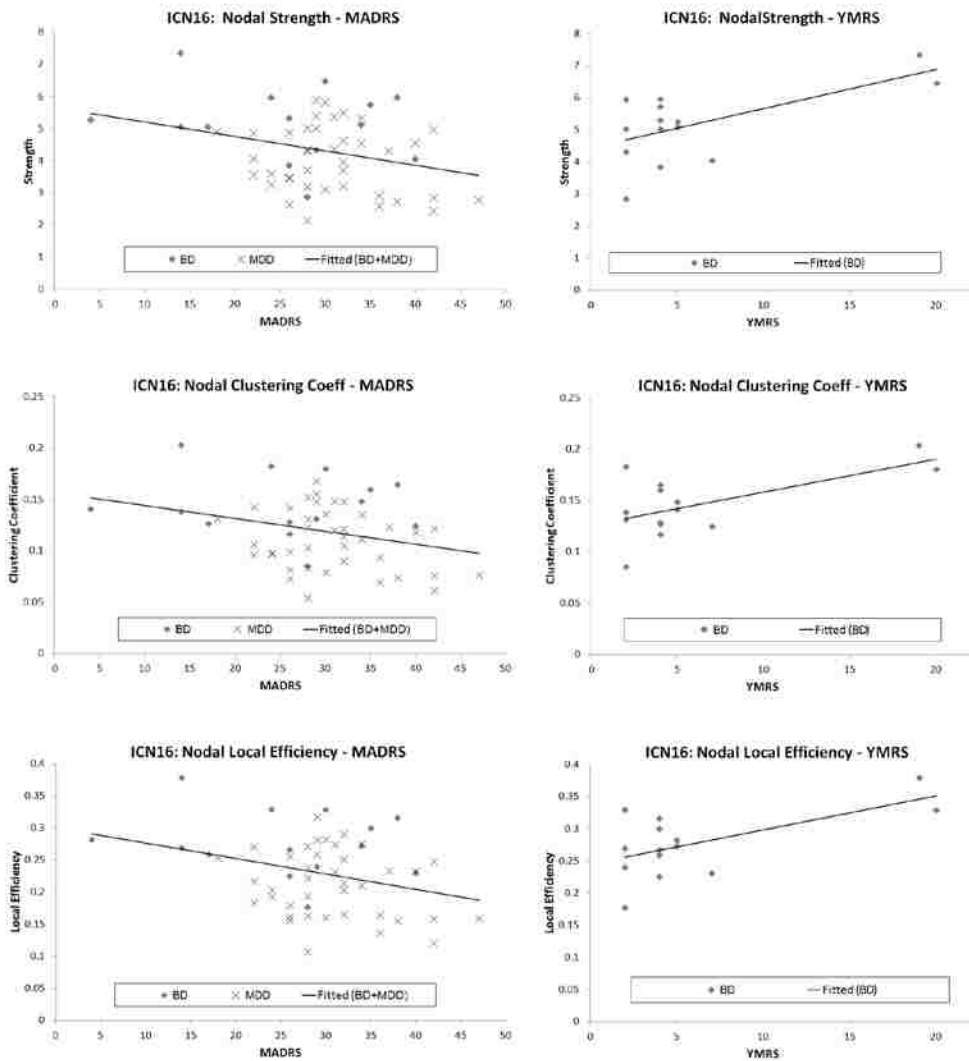
Figure 4.4 Significant correlation between nodal graph measures (nodal strength, clustering coefficient, and local efficiency) and symptom scores (MADRS in both BD/MDD patients and YMRS in BD) at a typical ICN in DLPFC (ICN16).

4.4   Discussion

In this study, we used ICA, a data-driven method to separate resting-state fMRI data into ICNs, and built the whole brain functional graph, in which the FNC strengths and its graph measures were computed. We observed that, compared to the MDD group, the FNC of the BD group exhibited higher FC strengths and also was characterized by

more efficient topological structures based on measures obtained using graph theory at the functional-network-level in prefrontal cortex as well as at the whole-brain-level. In particular, our findings revealed that the FC strengths and corresponding graph structures which differentiate BD and MDD were mainly located in prefrontal networks including the DLPFC and VLPFC as well as ACC, which is consistent with findings in (Jie, Zhu et al. 2015). Greater depressive symptom severity correlated with less interconnected structure in prefrontal cortical areas in the patients from both the BD and MDD groups. Although the correlations did not remain significant after correction for multiple comparisons, the trend indicates the potential linkage between altered FC patterns in those ICNs and clinical symptom scores.

Several ICNs implicated in the pathophysiology of mood disorders (e.g., involving functional interactions between prefrontal, anterior cingulate, parahippocampus, cuneus, temporal, parietal, and occipital cortices) were significantly different in FC between the BD and MDD groups. Pair-wise comparisons show that relative to the MDD group, the BD group had significantly stronger FNC strengths within the prefrontal cortex, between the prefrontal cortex and anterior cingulate cortices, cuneus and temporal regions. The prefrontal regions, including the orbitofrontal cortex (OFC), ACC, dorsomedial prefrontal cortex (DMPFC), DLPFC and VLPFC, have been most consistently implicated in cognitive control processes (Sui, Pearlson et al. 2015), including decision-making and emotion regulation (Phillips, Ladouceur et al. 2008; Kupfer, Frank et al. 2012). Specifically, the ACC and other medial prefrontal areas play major roles in processing emotion and in automatic or implicit regulation of emotion, whereas lateral prefrontal cortical systems like the DLPFC and VLPFC are implicated in

cognitive control and voluntary or effortful regulation of emotion (Drevets 2001; Phillips, Ladouceur et al. 2008). The DLPFC and VLPFC constitute of the limbic-cortical-striatal-pallidal-thalamic circuit system that has been hypothesized to be dysfunctional in mood disorders based on neuroimaging studies (Drevets 2000; Price and Drevets 2012). Another study employing effective connectivity analyses (Stein, Wiedholz et al. 2007) to examine neural activity in response to fearful and angry faces in healthy subjects found an information-processing path from OFC to DLPFC. Recently, ACC and medial PFC regions have been recognized as part of a neural subcircuit involved in a process with recursive self-focused thinking that leads to negative mood, i.e. rumination (Cooney, Joormann et al. 2010), which may associate with both BD and MDD (Johnson, McKenzie et al. 2008). Furthermore, it has been reported consistently that the DLPFC and VLPFC are not functioning efficiently towards negative emotions in BD (Brotman, Kassem et al. 2007; Pavuluri, O'Connor et al. 2007; Pavuluri, O'Connor et al. 2008). These findings are consistent with our results on FNC and symptoms, where significant negative correlations were found between depressive symptom scores and the level of interconnected structure in prefrontal areas in both BD and MDD patients.

The networks of strongest connectivity in the BD group were present in the DLPFC and VLPFC (i.e. ICN6, ICN14, ICN16, and ICN32). The increased FNC indicates possible stronger phase coherence in these ICNs in BD than MDD patients. As reported in electroencephalogram (EEG) studies (Varela, Lachaux et al. 2001; Spencer, Nestor et al. 2004), phase synchrony has been related to the integrity of the circuits between two brain regions, that is, if two brain regions are locked in phase with each other, their functioning is closely connected. The significantly different FC strengths and

71

local graph measures in the prefrontal ICNs, as well as those in the ACC, PCC, superior temporal, and parahippocampal areas that consist of the fronto-limbic circuitry between BD and MDD, which implicate the underlying cognitive and mood control schemes are distinct from each other.

Similar findings have been reported by other studies. A low frequency resting-state fMRI study revealed higher correlations between left and right VPFC in BD (Chepenik, Raffo et al. 2010). Another ICA-defined FNC analysis reported the BD group shows increased connectivity in emotion evaluation regions such as bilateral medial PFC, and in "affective working memory network" including the DLPFC and VLPFC, during an affective working memory task (Passarotti, Ellis et al. 2012). Abnormal medial PFC connectivity between ICA components were also found during resting-state in the BD group (Ongur, Lundy et al. 2010; Calhoun, Sui et al. 2011; Sui, Pearlson et al. 2011). Decreased blood flow and metabolism in the DMPFC and DLPFC in MDD group have been reported in multiple studies (Baxter, Schwartz et al. 1989; Bench, Friston et al. 1992; Drevets 2000). Compared to BD, (Taylor Tavares, Clark et al. 2008) found the MDD group failed to recruit the VLPFC and DMPFC during behavioral reversal learning task that required subjects to ignore misleading negative feedback.

Topologically, clustering coefficients are equivalent to the fraction of the node's neighbors that are also connected with each other (Watts and Strogatz 1998). This metric reveals the capacity for specialized processing to occur within densely interconnected brain region groups (Rubinov and Sporns 2010). Local efficiency reflects the fault tolerance of the graph system, or the efficiency of communication between the first neighbors of a node when it is removed (Latora and Marchiori 2001). The significantly

higher clustering coefficients in the BD group relative to the MDD and HC groups indicate that the ICNs in default-mode nodes including the DLPFC, superior frontal gyrus (SFG) and ACC exhibit stronger local functional interconnections, and thus potentially showed greater efficiency for local information transfer in those regions in the BD group relative to the other groups. Abnormal function in default-mode networks have been documented in a previous study (Ongur, Lundy et al. 2010), suggesting abnormal functional organization of neural circuits within BD. At the same time, lower local efficiency in these brain areas suggest that the MDD participants had lower fault tolerance (i.e., more vulnerable) locally compared to BD. However, lower efficiency in frontal cortex may relate to more depressive symptoms, as several networks showed a negative correlation between MADRS and nodal graph measures like strength, clustering coefficient and local efficiency.

The graph metrics at the whole brain level are the averaged metrics across all nodes. Although only a few local ICNs that have significant differences between BD and MDD, which are mostly in prefrontal regions, the averaged metrics shows the same trend. This indicates those graphs are the most influential to the overall brain graph in our study.

With respect to global measures, compared to MDD, FNC in BD had higher global efficiency and shorter characteristic path length. The identified paths show potential routes of information flow between pairs of brain regions (Rubinov and Sporns 2010). Characteristic path length is a measurement of the extent of average connectivity or the overall routing efficiency of the graph. Shorter path lengths between nodes have also been shown to promote effective interactions across different cortical regions (Achard and Bullmore 2007). Global efficiency of a graph system is the efficiency of the

73

parallel system, where all the nodes in the graph exchange information concurrently (Abou-Elseoud, Starck et al. 2010). According to explanations from (Kaiser and Hilgetag 2004), ICNs in BD, which have shorter characteristic path length and high global efficiency, are of significance in minimizing noise, shortening signaling delay and increasing synchrony.

Although our study emphasized the identification of differences between BD and MDD, it worth noting that among those comparisons from both FC strengths and graph measures, the most significant group differences occurred between the BD and MDD groups, with weaker contrasts between each mood disorder groups relative to the HC group. Regarding the contrasts between the MDD and HC groups, although the trend of reduced FNC in many brain regions in MDD is consistent with previous literature (Anand, Li et al. 2005; Anand, Li et al. 2005; Veer, Beckmann et al. 2010; Wang, Hermens et al. 2012; Zhu, Wang et al. 2012), the group differences reported here were not significant after correction for multiple comparisons. Possibly the high order (number of ICs) ICA model we applied to the whole brain analysis reduced statistical sensitivity by requiring corrections for a relatively large number of comparisons. Notably, a similar result was reported in another study on resting-state FC differences between MDD and HC (Craddock, Holtzheimer et al. 2009), where no statistical group difference was evident after applying corrections for multiple testing. As shown from the bar plots of graph measures in both whole-brain-level and functional-network-level in various ICNs, BD and MDD were far from each other, with HC in the middle. This overall trend showing HC in between BD and MDD were also found in studies on BOLD responses to positive and negative stimuli (Diler, de Almeida et al. 2013; Grotegerd, Stuhrmann et al. 2014).

Note that there was a modest variation in the scanning duration across subjects (191 or 225 volumes) although each scan length was similarly represented within each diagnostic group and the mean scan length did not differ significantly across groups. We included all time points available during computation of the temporal correlations. An alternative method is to involve truncation of the longer time courses to match the duration of the shorter ones (keeping only 184 time points for all subjects). However, this step may result in the loss of information. Nevertheless, we retested FNC built from first 184 time points in all subjects, the group differences still exist in most measures with p-value changed, with several FC strengths and nodal measures failed to pass FDR correction at q = 0.05. In addition, we also checked the correlations between the scan durations and reported FNC measures (FC strengths and graph measures) that demonstrated group differences. No significant correlation was found, indicating the relatively small difference in scanning duration did not have a major effect on our results.

Several experimental and methodological issues in our study design merit comment. The major limitation was the small sample size, especially in the BD group. To reduce the potential confound of medication, our study was limited to subjects who were treatment-naïve or unmedicated for at least three weeks, which constrained the patient pool. Nevertheless, most recent neuroimaging studies reviewed in (Cardoso de Almeida and Phillips 2013) also included sample sizes ranging from 10 to 30 subjects per patient group. It would be helpful to increase statistical power by including more subjects in future studies. In order to maximize the sample size, we included two BD subjects in mixed states and one in a euthymic state, which may have increased the variability of the fMRI data. Consequently, we performed a post hoc analysis to compare the depressed

MDD patients versus only the 10 depressed BD subjects, and results were essentially the same as those reported in the original analysis: the group differences still existed although the p-values increased nominally. Further studies may address this limitation by recruiting more specific and clinically matched subjects. Another methodological limitation is that we characterized FNC as the correlation between ICN TCs, rather than use non-linear metrics, such as mutual information, or coherence. While the use of correlation restricts the detection of nonlinear dependencies and the resolution phase of and spectral relationships, this approach is preferred for its straightforward interpretation and tractability. Nevertheless different connectivity computation methods may be applied in future studies of FNC to gain additional information.

In conclusion, our results show distinct functional network connectivity underlying BD and MDD during resting-states. Overall brain graphs were more topologically efficient in BD than in MDD. The FC strengths and FNC graph metrics that differentiate BD and MDD existed predominantly in prefrontal networks including DLPFC, VLPFC and ACC, which play roles in cognitive control of emotional processing and in other aspects of emotional and visceromotor modulation. These findings raise the possibility that distinct mood control schemes exist between these mood disordered subgroups, which ultimately may be used to guide future studies aimed at differentiating MDD and BD on the basis of biomarkers.

Chapter 5   Interrelated Features in both FNC and Low Frequency

Fluctuations Associated With Cognitive Deficits in Schizophrenia

5.1   Introduction

The cognitive deficits of schizophrenia are largely resistant to current treatment and tend to be a life-long burden of the illness. The MATRICS consensus cognitive battery (MCCB) "provides a reliable and valid assessment of cognition across a comprehensive set of cognitive domains for schizophrenia" (Green, Nuechterlein et al. 2004). The MCCB includes 10 neurophysiologic tests clustered in 7 cognitive domains (Green, Kern et al. 2004): speed of processing, attention/vigilance, working memory, verbal learning, visual learning, reasoning/problem solving, and social cognition.

Despite its widespread use, the neural networks underlying MCCB performance in schizophrenia have been examined in only a few single-modality brain imaging studies (Rissling, Makeig et al. 2010; August, Kiwanuka et al. 2011; Tregellas, Smucny et al. 2014). Only one study has examined MCCB correlates of fused neuroimaging data (MEG and DTI) using joint independent component analysis (Stephen, Coffman et al. 2013). A posterior visual processing network was related to reduced MEG amplitude, reduced FA and poorer MCCB composite scores in schizophrenia, suggesting the advantage of this fusion technique. Currently, National Institute of Mental Health (NIMH) emphasizes the importance of "target engagement" in clinical trials (Sui, He et al. 2013). Understanding the brain network organization related to MCCB performance may allow imaging

assessments to be engaged early in clinical trials; hence accelerates the development of new therapeutic approaches to enhance cognition. However, in resting-state fMRI, both the functional connectivity and spatial alterations specifically associated with MCCB have not been examined. Therefore we aim to use two functional measures including functional network connectivity (FNC) and fractional amplitude of low frequency fluctuations (fALFF) to examine the functional correlates of MCCB with resting-state fMRI and to find the potential functional biomarkers of cognitive dysfunction in schizophrenia.

5.2   Methods

In this study, preprocessed fMRI dataset on SZ and HC from the MATRICS Resting-state Dataset was used.
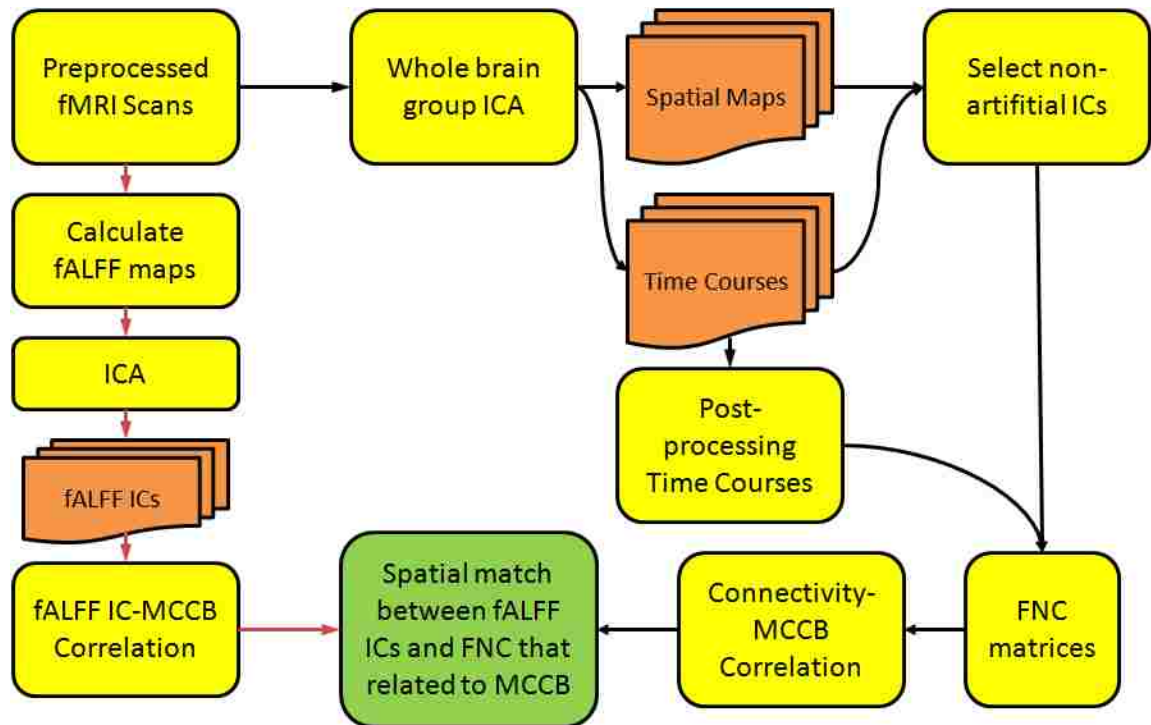
Figure 5.1 Flowchart to obtain the functional correlates of MCCB with fALFF and FNC. Amplitude of low frequency fluctuations (fALFF, left) and functional network connectivity (FNC, right) were

calculated and correlated with MCCB respectively. Finally, the spatial maps of fALFF and FNC with high MCCB correlations were overlay for comparison and visualization.

The flowchart of this analysis is shown in Figure 5.1. Two analyses to explore the functional measures correlated with MCCB were performed in parallel, and finally they were spatially matched to see if there are consistent and replicable interrelationships between MCCB and the abnormalities seen in both fractional amplitude of low frequency fluctuations (fALFF) (Zou, Zhu et al. 2008; Sui, He et al. 2013) and functional network connectivity (FNC) maps (Calhoun and Adali 2012).

First, the fALFF maps were computed based on the time courses of each voxel. Prior to computing ALFF, the original 4D fMRI data sets were divided by their global mean (over time and space) to normalize differences in scan intensity units. To eliminate remaining noise sources, the fMRI data underwent additional post-processing. We further regressed out 6 motion realignment parameters, white matter and CSF in de-noising, the mean framewise displacements showed no significant group difference (meanFD, mean of root of mean square frame-to-frame head motions assuming 50 mm head radius (Allen, Erhardt et al. 2011); HC: 0.224±0.12mm, SZ: 0.227±0.12mm, p = 0.91). Finally, data were spatially smoothed with a Gaussian kernel with full width at half max (FWHM) of $8{\times}8{\times}8$ mm^3. We extracted the voxel-wise fractional ALFF (fALFF) to generate a map for each subject as in (Zou, Zhu et al. 2008; Erhardt, Allen et al. 2011; Calhoun and Allen 2013; Sui, He et al. 2013). The fALFF calculation consisted of computing the fast Fourier transform on post-processed time series of each voxel, taking the square root of the power spectrum to obtain amplitude, and averaging amplitude in [0.01, 0.1] Hz (Calhoun and Allen 2013). The fALFF maps were then decomposed in to 8 independent sources by

independent component analysis (ICA) using infomax algorithm (Bell and Sejnowski 1995). The Pearson correlation between MCCB composite scores and loading profile of each independent component (IC) were estimated for all subjects as well as subjects in each group, and IC showing the highest correlation was selected.

Second, the whole brain fMRI images were decomposed into 100 functional networks. Group ICA was performed on preprocessed resting-state fMRI data using the GIFT software (http://mialab.mrn.org/software/gift) (Calhoun and Adali 2012). Individual fMRI images were decomposed via principal component analysis (PCA), with the first 120 components selected for dimension reduction. The infomax algorithm (Bell and Sejnowski 1995) was then repeated 10 times, estimating 100 group independent components via ICASSO (http://www.cis.hut.fi/projects/ica/icasso) to improve the reliability of the decomposition. Time courses and spatial ICs of individuals were then back-reconstructed (Erhardt, Rachakonda et al. 2011). Since ICs may include artifacts and noises, all ICs were manually selected for further study. The ICs selected for further FNC analysis are called intrinsic connectivity networks (ICNs), theoretically exhibited peak activations in gray matter, low spatial overlap with known vascular, ventricular, motion, and susceptibility artifacts (Cordes, Haughton et al. 2000). Fifty-two non-artificial networks were characterized as ICNs, as opposed to physiological, movement related, or imaging artifacts. ICN related time courses underwent additional post-processing to remove remaining noise sources, including 1) linear, quadratic, and cubic terms for detrending, 2) multiple regression of the 6 realignment parameters and their temporal derivatives, 3) removal of detected outliers, and 4) band-pass filtering with a cutoff of [0.01, 0.1] Hz. The FNC maps were then calculated as correlation matrices

across post-processed time courses of 52 ICNs. There is one 52×52 symmetric FNC matrix for each subject, with entry of element (i, j) corresponding to the strength of connectivity between ICN i and j. The connectivity-wise strengths correlations with MCCB were calculated for all subjects and subjects in each group respectively. The FNC with most significant connectivity strength-MCCB correlations were found out and shown in Figure 5.2.
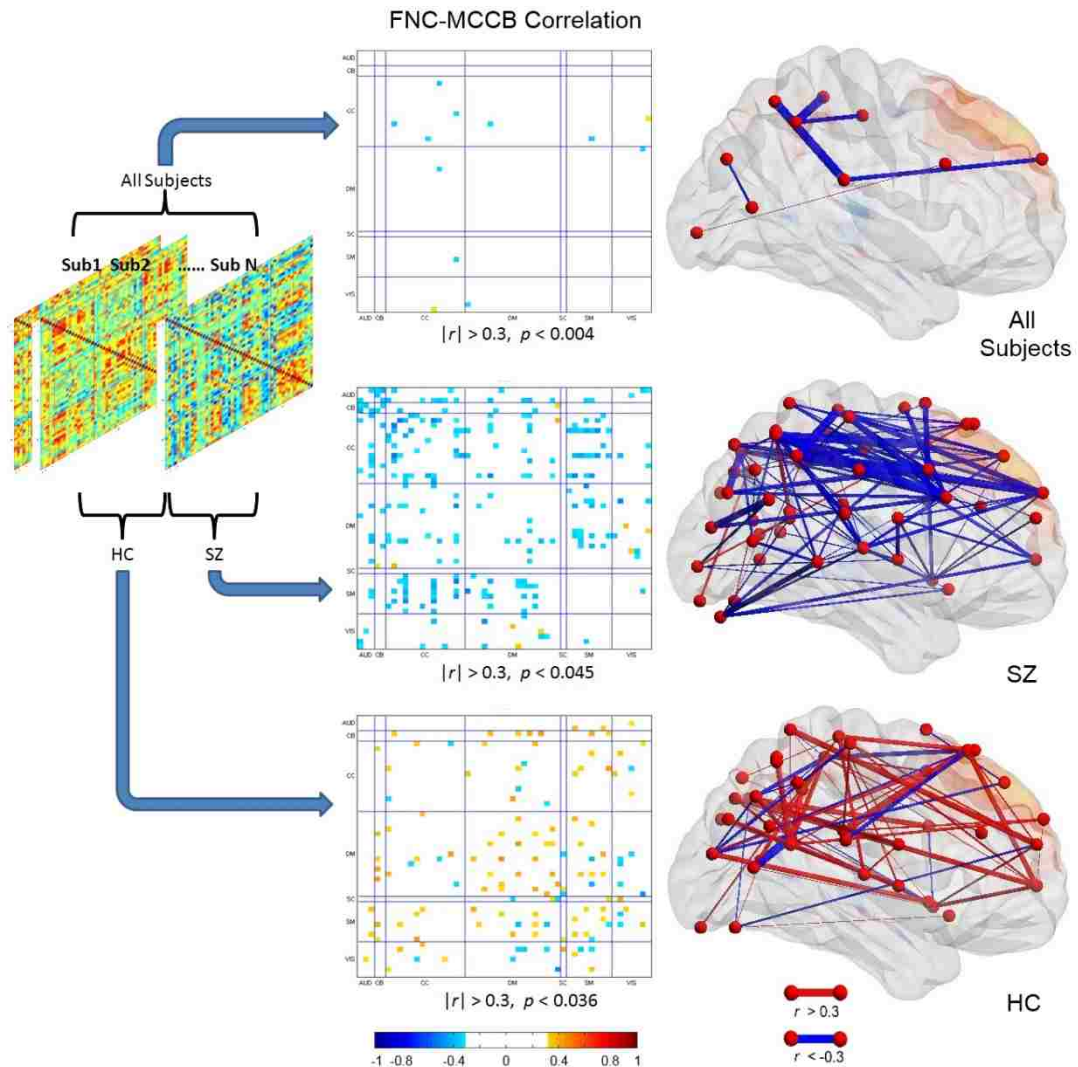
Figure 5.2 Correlating functional network connectivity (FNC) strengths with MCCB. The FNCs that shown in red correspond to positive correlation and those shown in blue refer to negative correlation.

Finally, to compare the relationship between MCCB-correlated fALFF and FNC, the ICNs connected with significant strength-MCCB correlation were spatially overlay with the z-map of fALFF IC of interest selected in the first step. The BrainNet Viewer toolbox (http://www.nitrc.org/projects/bnv/) was used for visualization (Xia, Wang et al. 2013).

5.3 Results

In fALFF analysis, among 8 ICs derived from ICA, one IC had significant correlation with MCCB composite scores for all subjects ($r = 0.25$, p=0.016) and for SZ group ($r = 0.36$, $p = 0.014$). Specifically, subjects with higher MCCB scores indicated higher ALFF values in their brain areas including dorsolateral prefrontal cortex (DLPFC), superior frontal gyrus (SFG), inferior parietal lobe (IPL), and inferior frontal gyrus (IFG). At the same time, higher MCCB scores also associated lower ALFF values in left superior temporal gyrus (STG), middle temporal gyrus (MTG), thalamus, and striatum. No IC correlated with MCCB was found in HC group.

As shown in Figure 5.2, six FNC strengths showed significant correlation ($|r| > 0.3$) with MCCB composite scores in all subjects. Higher MCCB scores were correlated with stronger FNC between IFG and lingual, while related with weaker strengths in other five FNC, including FNCs that were connected with IPL, supplemental motor area (SMA), SFG and MTG. IPL was a hub with the most FNC strengths associated with MCCB. Detailed ICN maps are displayed in Figure 5.3.
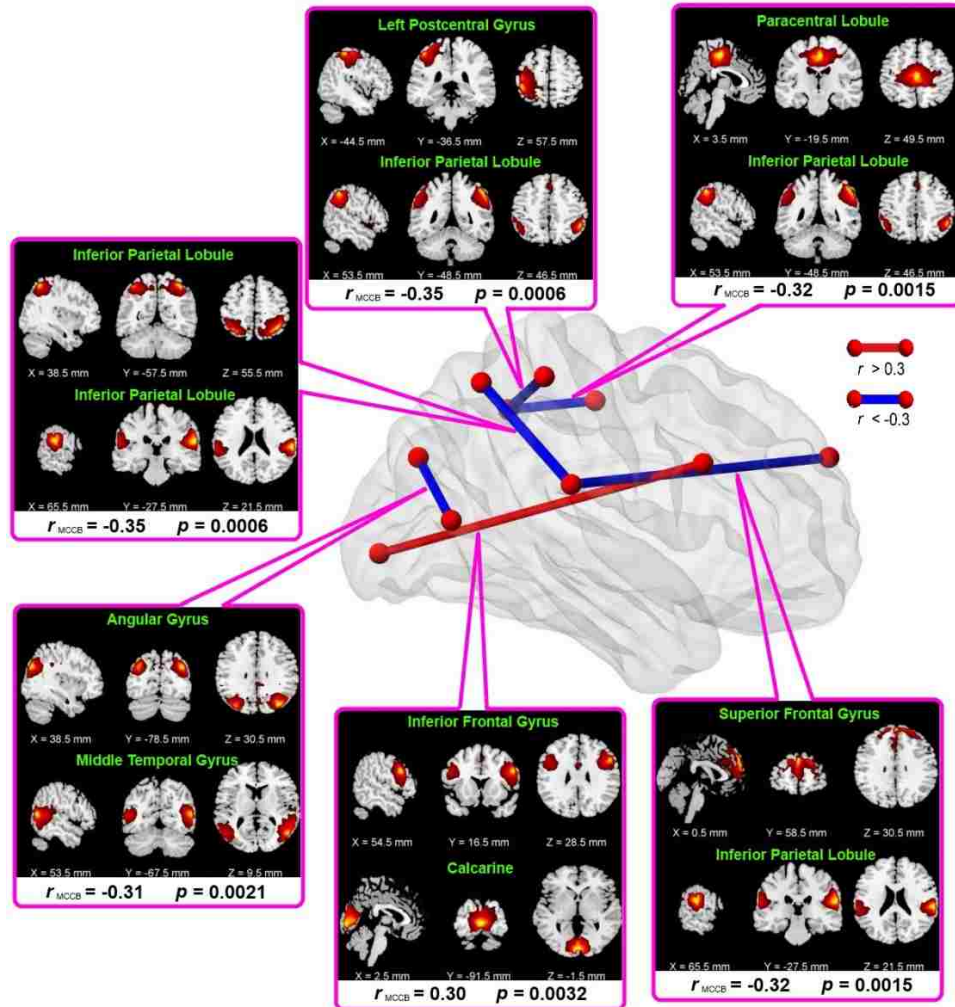
Figure 5.3 Six FNC strengths that showed significant correlation (|r| > 0.3, p < 0.004) with MCCB composite scores in all subjects. The FNCs that shown in red correspond to positive correlation and those shown in blue refer to negative correlation.

We also looked into the FNC strength-MCCB correlation in each group. The same threshold ($|r| > 0.3$) was used for comparison (Figure 5.2). There were 66 FNCs in HC and 121 FNCs in SZ with $|r| > 0.3$. The MCCB-correlations in two groups were showing in different connectivity, and with opposite trends: most FNC strengths were positively correlated with MCCB in HC, while more FNC strengths were negatively correlated with MCCB in SZ.

The overlapped MCCB-correlated FNC on fALFF 3D maps are displayed in Figure 5.4. Interestingly, the FNC strengths with significant correlations with MCCB were in well agreement with the activated regions with highest |z| values in fALFF IC: the high MCCB-correlated fALFF map and FNC overlaps in brain regions like prefrontal area, MTG and IPL.
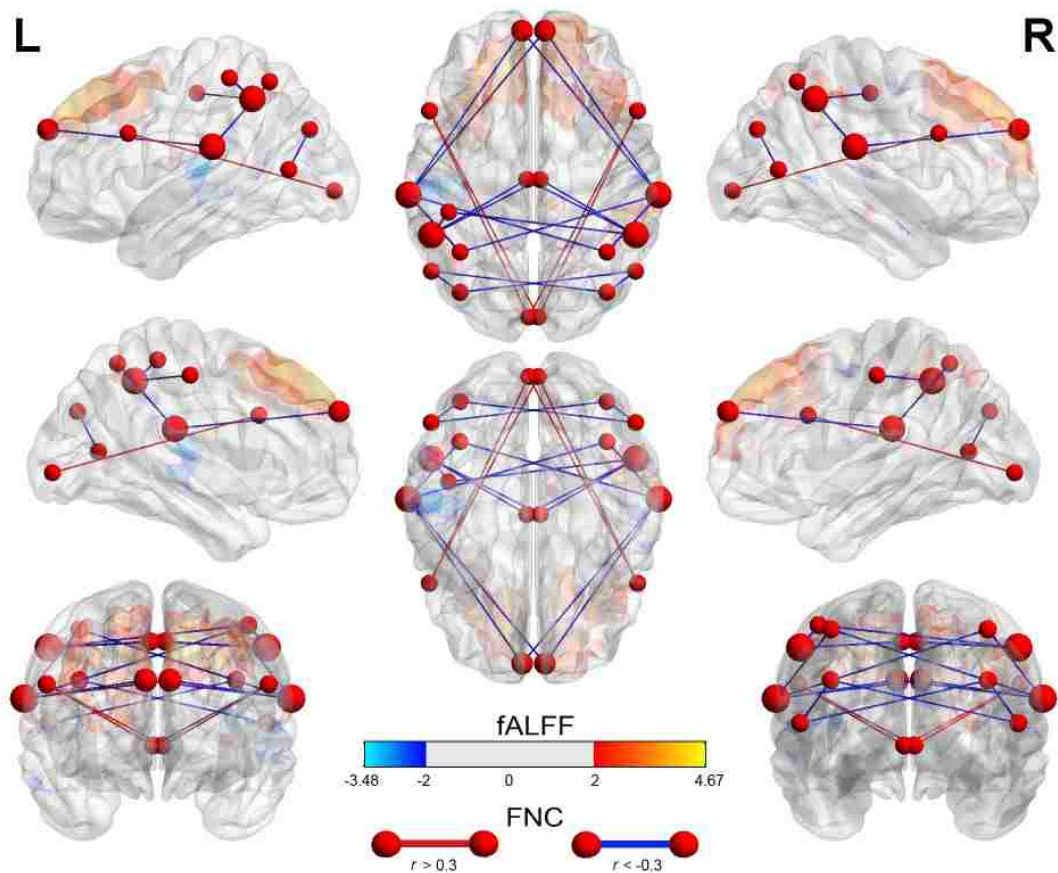
Figure 5.4 Overlapping MCCB-correlated FNC on 3D map of MCCB-correlated fALFF IC. The spatial map of fALFF was thresholded at $|z|>2$, with both positive (red regions) and the negative (blue regions) z-values. The FNCs that shown in red correspond to positive correlation and those shown in blue refer to negative correlation. Nodes represent the peak value location of ICN in each hemisphere (if an ICN is bilaterally distributed, two nodes will be shown symmetrically).

5.4   Discussion

ALFF values correspond to intensity of regional spontaneous brain activity; while FNC describe the temporal coherence among brain regions even they are not anatomically connected. Prefrontal cortex appears in both MCCB-correlated ALFF and FNC. This region has long been demonstrated important for execution, decision making, and working memory (Stuss and Benson 1984; Sui, Adali et al. 2009; He, Sui et al. 2012), which are key components of evaluating the cognitive deficit (Elliott 2003).The brain regions including prefrontal cortex, striatum and thalamus form a cortical-striato-thalamic loop described in (Parent and Hazrati 1995; Kegeles 2006). In specific, the striatum, which is made up of the caudate and the putamen, receives its inputs from the cortex, thalamus, hippocampus, and amygdala; then projects its output structures to thalamus; the thalamus finally projects back to the cortex, thereby completing a closed circuit (Alexander, DeLong et al. 1986; Simpson, Kellendonk et al. 2010). MCCB-correlated ALFF IC affirmed the activity in this cortical-striato-thalamic circuits affect the cognitive performance.

IPL was another hub for both MCCB-correlated ALFF and FNC. Higher fALFF values in subjects with better cognitive performance supports previous findings on IPL including angular gyrus (AG), which have been shown strong involvement in semantic processing (Binder, Desai et al. 2009), social cognition (Green, Bearden et al. 2012) or theory-of-mind (Spreng, Mar et al. 2009). The stronger FNC strengths from IPL in cognitive deficits subjects indicate the activation in IPL in those subjects is less intense, and more efforts from other brain regions may be needed to collaborate with IPL in cognitive processes.

It is worth noting that FNC strengths showed different trends with MCCB in two groups. In HC, where most high FNC-MCCB correlations were positive, indicating better cognitive performance under stronger FNC strengths. While in SZ, other FNCs showed negatively correlation with MCCB. This phenomenon may lead to FNC strengths less sensitive to MCCB when pooling all subjects together. As altered FNC structures has been reported in prior resting-state fMRI studies (Yu, Sui et al. 2011; Yu, Sui et al. 2013), more analysis could be done to look into the impact of altered FNC topology properties on cognition impairment in future works.

5.5   Conclusions

This study is the first attempt to combine two approaches to investigate functional neuroimaging correlates of MCCB in schizophrenia, and both methods resulted in consistent findings. Our results support the view that functional deficits in distributed cortico-striato-thalamic circuits and inferior parietal lobe may account for several aspects of cognitive impairment in schizophrenia, placing the nature of the cognitive symptom in a new light.

Chapter 6   Multimodal fusion with N-way mCCA+jICA Framework

6.1   Theoretical Development

In mCCA+jICA framework, we assume an n-modal set X_k as a linear mixture of M_k sources given by S_k, with a non-singular mixing matrix A_k for each modality k, that is:

$$X_k = A_k S_k, k = 1,2, \dots, n \tag{6.1}$$

Typically, the number of data points per subject L_k in X_k is much larger than subject number N. For each modality k, X_k is a $N \times L_k$ feature matrix, and S_k is a $M_k \times L_k$ matrix. The underlying sources S_k are distinct within each dataset. The columns of A_i and A_j have higher correlation only on their corresponding indices, with modality $i, j \in \{1,2, \dots, n\}, i \neq j$. Due to the high dimensionality and high noise levels in the brain imaging data, order selection is critical to avoid over-fitting the data.

6.1.1   Number of Components

A modified minimum description length (MDL) criterion described in (Li, Adali et al. 2007) is adopted to estimate the number of independent components for each modality. MDL uses a sub-sampling scheme to obtain a set of effectively independently identical distributed (i.i.d.) samples from the dependent data samples, and then applies information-theoretic criteria (ITC) formulas to the effectively i.i.d. sample set. To maximally retains the joint information while to keep that the decomposed sources are independent from each other, the final component number for joint ICA is set as $M = \max(\widetilde{M_1}, \widetilde{M_2}, \dots, \widetilde{M_k})$.

Dimension reduction is first performed on each X_k using singular value decomposition (SVD) to determine the signal subspace given by

$$Y_k = X_k E_k \tag{6.2}$$

where Y_k is in size of $N \times M$ and E_k contains eigenvectors corresponding to top M eigenvalues.

6.1.2 Multi-set Canonical Correlation Analysis

Multi-set CCA is then performed on Y_k, generating the canonical variates D_k by maximizing the sum of squares of all correlation values in its corresponding columns as adopted in (Li, Adali et al. 2009). The canonical correlations can be obtained by optimizing a number of cost functions proposed in (Kettenri.Jr 1971), e.g., maximizing the sum of squared correlations (SSQCOR) among the canonical variates. Consider the canonical variates D_k, where each is a linear combination of the dataset Y_k given as

$$D_k = Y_k w_k \tag{6.3}$$

where w_k are the canonical coefficient vectors. The multi-set CCA procedure based on sum of squares cost can be summarized as:

Stage 1:

$$\left\{ w_1^{(1)}, w_2^{(1)}, \dots, w_n^{(1)} \right\} = \arg\ \max_w \left\{ \sum_{k,l}^{n} \left(r_{k,l}^{(1)} \right)^2 \right\} \tag{6.4}$$

Stage 2:   Loop i from 2 to M

$$\left\{ \boldsymbol{w}_1^{(i)}, \boldsymbol{w}_2^{(i)}, \ldots, \boldsymbol{w}_n^{(i)} \right\} = \arg \max_w \left\{ \Sigma_{k,l}^n \left(r_{k,l}^{(i)} \right)^2 \right\}, \text{s.t. } \boldsymbol{w}_k^{(i)} \perp \left\{ \boldsymbol{w}_k^{(1)}, \boldsymbol{w}_k^{(2)}, \ldots, \boldsymbol{w}_k^{(i-1)} \right\}$$

(6.5)

End loop

where $\boldsymbol{w}_k^{(i)}, i = 1,2, \ldots M$ is the ith column of the $\boldsymbol{w}$ matrices, $M \leq \min(\text{rank}(\boldsymbol{Y}_k))$. $r_{k,l}^{(i)} = \text{corr}\left(\boldsymbol{D}_k^{(i)}, \boldsymbol{D}_l^{(i)} \right), (k, l = 1,2, \ldots, n; \ k \neq l)$ is the column-wise correlation across modality.

Stage 1 is solved by calculating the partial derivative function of the SSQCOR cost with respect to each $\boldsymbol{w}_k^{(1)}$ and equating it to zero to find the stationary point. Because the SSQCOR cost is a quadratic function of $\boldsymbol{w}_k^{(1)}$, the partial derivative is a linear function of $\boldsymbol{w}_k^{(1)}$, the closed form solution can be derived. Starting from an initial point, each $\boldsymbol{w}_k^{(1)}$ vector is updated and consequently guarantee an increase in the cost function and a sweep through all the $\boldsymbol{w}_k^{(1)}$ constitute one step of the iterative maximization procedure. The iterations are stopped when the cost convergence criterion is met, and the resulting $\boldsymbol{w}_k^{(1)}$ vectors are taken as the optimal solution. Loops in Stage 2 are solved in a similar manner with the cost function replaced by a Lagrangian incorporating the orthogonality constraints on the canonical coefficient vectors.

Based on the above optimization, we simultaneously obtain $\boldsymbol{D}_k, k = 1,2, \ldots, n$ in all modalities, which satisfy

$$E\{\boldsymbol{D}_k^T \boldsymbol{D}_k\} = \boldsymbol{I}$$

(6.6)

$$E\{\boldsymbol{D}_k^T \boldsymbol{D}_l\} \approx diag\left(r_{k,l}^{(1)}, r_{k,l}^{(2)}, \dots, r_{k,l}^{(M)}\right); k, l = 1, 2, \dots, n; k \neq l \qquad (6.7)$$

where $r_{k,l}^{(1)}, r_{k,l}^{(2)}, \dots, r_{k,l}^{(M)}$ are the so-called canonical correlation coefficients. Thus mCCA as a preprocessing step aligns the components by a data projection that jointly maximizes the N-way correlations.

Based on the linear mixture model, we consequently get the associated maps $\boldsymbol{C}_k$ via $\boldsymbol{X}_k = \boldsymbol{D}_k \boldsymbol{C}_k, \boldsymbol{C}_k = pinv(\boldsymbol{D}_k)\boldsymbol{X}_k$. However, multi-set CCA may achieve complete source separation in $\boldsymbol{C}_k$ only when $r_{ij}^1, r_{ij}^2, \dots, r_{ij}^M$ are sufficiently distinct (Li, Adali et al. 2009). However, this constraint is not always easily satisfied, especially when the number of components M is large (e.g. > 10) or the canonical correlation coefficients are very close in values. In most real brain data, the multimodal connection among components are not very high and could be similar in value (Sui, Pearlson et al. 2011), mCCA output $\boldsymbol{C}_k$ will typically be a set of sources that are not fully separated.

6.1.3 Joint Independent Component Analysis

ICA is a blind source separation method which has been widely used in many fields such as signal and image processing (Comon 1994; Hyverinen, Karhunen et al. 2001). In an ICA model, the observed data are treated as a linear combination of unknown independent sources, and the aim is to decompose the observed data and extract the sources through maximizing the independence among them. As the potential common correlation values among $r_1, r_2, \dots, r_M$, applying individual ICA within each dataset respectively may introduce ambiguity in feature matching via cross-correlation (Sui, Zhang et al. 2010). Therefore, further applying joint-ICA (jICA) on the concatenated

maps across modalities $C = [C_1, C_2, \ldots, C_n]$ decomposes the mixtures transformed to an orthogonal space. Joint-ICA is a joint analysis obtained by forming an overall data input via stacking the data from different modalities together.

$$[S_1, S_2, \ldots, S_n] = W[C_1, C_2, \ldots, C_n] \tag{6.8}$$

After applying ICA algorithm, the data from each modality C_k will be represented by joint independent source $S = [S_1, S_2, \ldots, S_n]$ with a same estimated demixing matrix W. Each the row of S_k is placed adjacent to form a total combined row with length of the total number of voxels in all features (Calhoun, Adali et al. 2006). The independence among transformed components is maximized by reducing the statistical dependencies among them. ICA as a central tool for BSS has been studied extensively and we utilized Infomax (Bell and Sejnowski 1995). This algorithm is well known for its stability and reliability when the underlying sources are mostly super-Gaussian, and the underlying brain imaging sources are expected to be sparse, leading to heavy-tailed distributions (James and Hesse 2005).

The overall mixing profiles A_k linked via correlation can be expressed from the combination of mixing matrices from mCCA and jICA:

$$A_k = D_k W^{-1} \tag{6.9}$$

Putting together, the overall linear procedure in Eq. 6.1 can be written as

$$X_k = (D_k W^{-1}) S_k \tag{6.10}$$

6.2   Simulation

According to the priority of the optimization and the analysis schemes, the existing multivariate fusion models can be reclassified into 3 main categories which are good at:

1) Separating sources precisely and discovering the common mixing profiles.

2) Finding flexible connections among modalities

3) Enabling both flexible modal connection and high-quality source separation.

We select one representative method from each optimization strategy to contrast them in a simulation, namely, joint ICA, multi-set CCA and mCCA + jICA. For fair comparison, all 3 methods are blind, using same features as input, thus it would be helpful to show why the findings generated by one method may not be obtained by another.

6.2.1   Simulated Dataset

We choose $k = 3$ for simulation. For each modality, eight sources were generated to simulate images or one-dimensional signals, with different data points per source $L_1 = 128 \times 128 = 16384$, $L_2 = 1 \times 5000 = 5000$, and $L_3 = 120 \times 120 = 14400$ respectively, ground true sources are S_1 (in dimension of 8×16384), S_2 (in dimension of 8×5000) and S_3 (in dimension of 8×14400). The vector lengths, or the number of data points L_k were deliberately designed to be different across modality k as is case for real data.
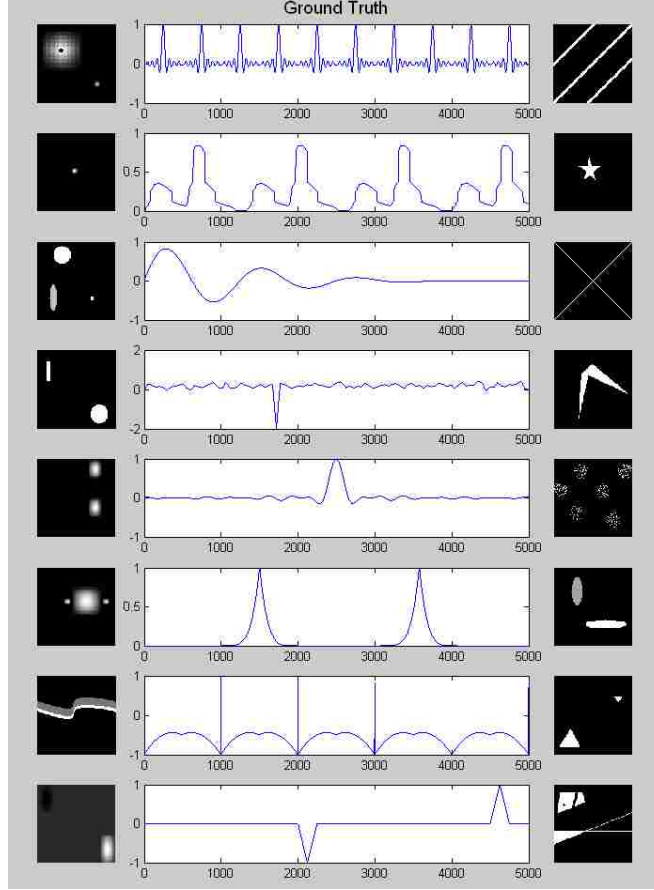
Figure 6.1 Ground truth of eight sources in three modalities

The mixing matrices for each feature on $N = 80$ subject, A_1, A_2 and A_3 (each in dimension of 80×8) were constructed with diverse correlation between their corresponding columns. The column-wise correlation values are as follows:

$$A_1 - A_2 = [0.77, 0.51, 0.25, 0.44, 0.42, 0.10, 0.18, 0.16],$$

$$A_2 - A_3 = [0.69, 0.36, 0.20, 0.30, 0.12, 0.05, 0.03, 0.16],$$

$$A_1 - A_3 = [0.77, 0.41, 0.14, 0.39, 0.14, 0.12\ 0.09, 0.03].$$

Eighty noisy mixtures were generated for each feature under each of the 11 noisy conditions via $X_k = I_k + N_k = A_k S_k + N_k; k = 1,2,3$ where I_k is the true mixed signal and N_k is random Gaussian noise. The corresponding mean peak signal-to-noise ratios (PSNR) are selected in range of $[- 1 \ 20]$ dB. The PSNR is a most commonly used measure of image quality after corruption or recovery. The jth mixture (simulated signal of subject j) in modality k at every noisy condition is defined as

$$PSNR(k,j) = 10\log_{10}\left[\frac{\max_{i\in[1,L_k]}(I_k(i))^2}{\frac{1}{L_k}\sum_1^{L_k}(X_k(i)-I_k(i))^2}\right]; j = 1,2,\dots 80; k = 1,2,3 \qquad (6.11)$$

According to (Thomos et al., 2006), a typical PSNR value for acceptable image quality is about 30 dB. Our PSNR range for simulation is lower than this for worse noise situation, as the lower the value, the more degraded the image.

6.2.2 Evaluation of mCCA + jICA Estimation

Three joint BSS models: jICA, mCCA, and mCCA + jICA were implemented on simulated datasets respectively under every PSNR for 5 runs. The decomposed components are paired with the true sources via cross-correlation automatically within each feature. We adopted three metrics to estimate the joint BSS performance:

1) the average correlation of the estimated components with the true source S;

2) the average correlation of the estimated mixing profiles with the true mixing profile A;

3) the mean square error of the estimated column-wise correlations between A_1 and A_2, A_2 and A_3, and A_1 and A_3 compared to the true value.

In reality, the component number is unknown. To test the robustness of our model, we also varied the source numbers to be estimated on the same mixed signals X_k under 11 increasing noise conditions. For each model, the estimated numbers were set to be either less ($M = 6$), or more ($M = 10$ and 12) than the number of true sources ($M = 8$). To evaluate the performance, we picked the best matched 6 components from true sources when estimated numbers were set to be 6, or the best matched 8 components from BSS results when estimated numbers were larger than 8. Correlations were calculated between the selected components and their corresponding true values.
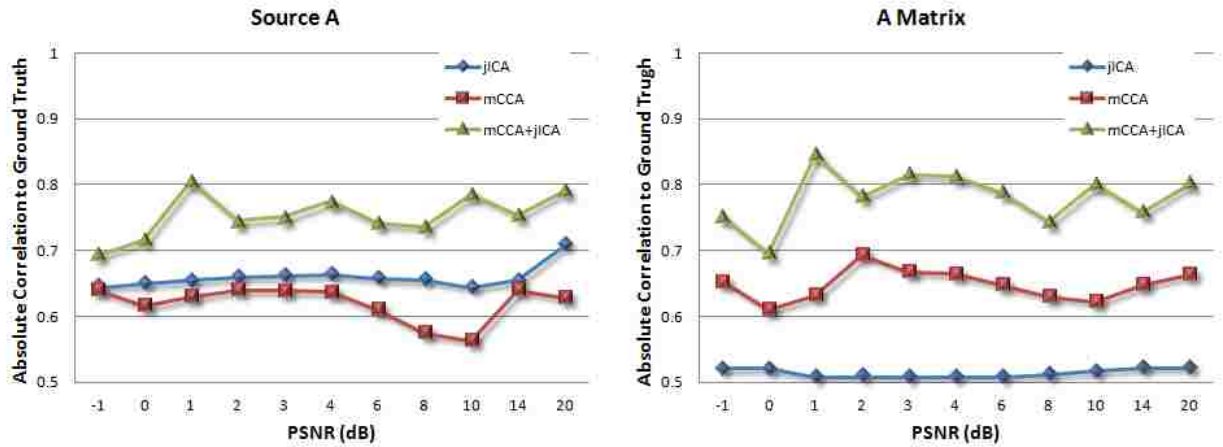
Figure 6.2 Source (S) estimation accuracy and mixing matrix (A) estimation accuracy in different noisy levels measured by peak signal-to-noise ratio (PSNR)

Figure 6.2 to 6.3 compares the first two performance metrics for different noise levels (Fig. 6.2, averaged across all components) and varying source distributions (Fig. 6.3, averaged across 11 noise levels). It is evident that mCCA + jICA is quite robust to noise and its BSS performance was consistently the best in all noise conditions. Consequently, joint ICA was the second best in source estimation and mCCA was the

95

second best in mixing matrix estimation; Note that when PSNR $= -1$ dB, i.e., noise exceeds signal, all three methods have an estimation accuracy higher than 0.5.
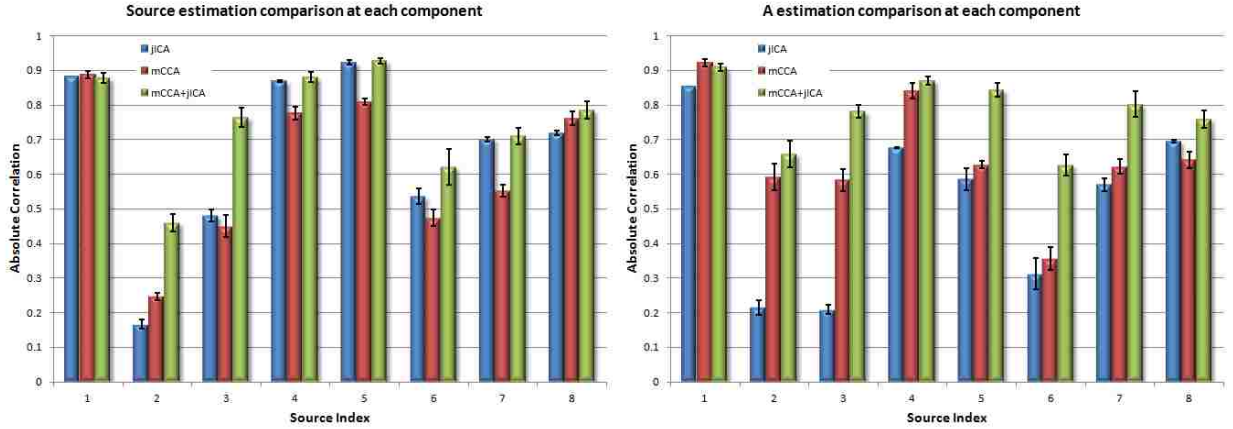
Figure 6.3 Source estimation (S) accuracy and mixing matrix (A) estimation accuracy were compared in different source distributions

Figure 6.4 compared the modal-connection estimation, where the true $A_1 - A_2$, $A_2 - A_3$ and $A_1 - A_3$ correlation were given by yellow bars for every source, while the mean square error and its standard derivation of the link estimation were plotted in red for mCCA and in green for mCCA + jICA. Note that both high (0.79) and low (0.07) correlation values exist in modal connections, representing shared or distinct factors among modalities. mCCA + jICA out performed mCCA again especially for sources whose have low $A_i - A_j$ correlation values that are close to many others, e.g. the $A_1 - A_2$ and $A_1 - A_3$ correlation of source 6.
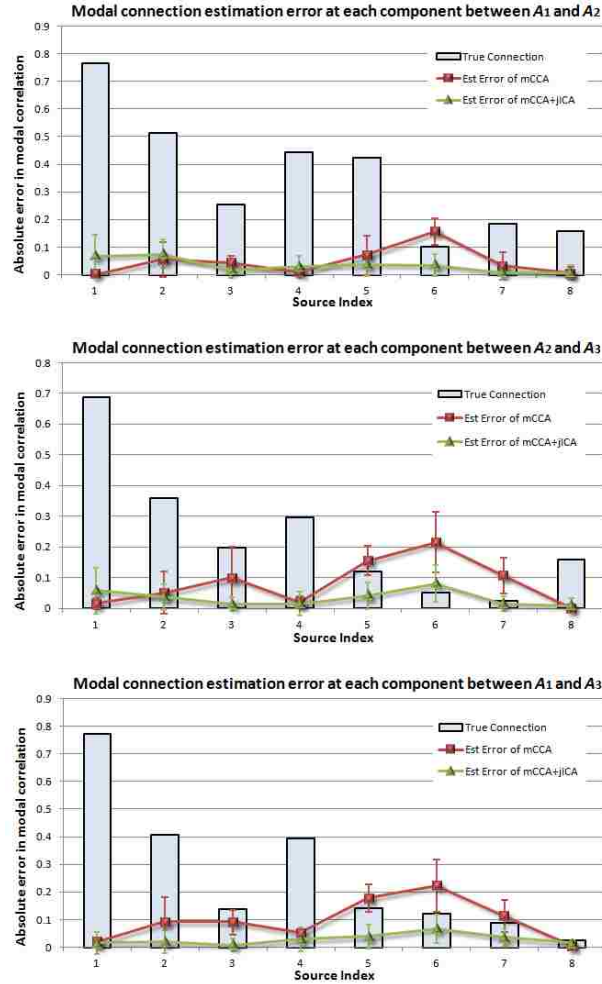
Figure 6.4 Comparison of the modal-connection estimation. The true $A_1 - A_2$, $A_2 - A_3$ and $A_1 - A_3$ correlation were given by blue bars for every source, while the mean square error and its standard derivation of the link estimation were plotted in red for mCCA and in green for mCCA + jICA.

The performance comparison using different estimation of component numbers is listed in Table 6.1, where each correlation value was averaged across selected components for corresponding modality and method. The blue bold values indicate the best performance among three methods. It is clear that mCCA + jICA showed highest or close to highest correlations among three methods in most cases.

Table 6.1 Decomposition performance comparison using different component numbers

No. of comps	Models	Sources			Mixing Matrices		
		S_1	S_2	S_3	A_1	A_2	A_3
8	mCCA + jICA	**0.788**	**0.671**	**0.802**	**0.839**	**0.683**	**0.823**
(true	jICA	0.674	0.589	0.717	0.567	0.403	0.574
value)	mCCA	0.570	0.626	0.664	0.620	0.654	0.671
	mCCA + jICA	**0.846**	**0.643**	**0.795**	**0.874**	0.654	**0.796**
6	jICA	0.736	0.567	0.691	0.550	0.351	0.546
	mCCA	0.707	0.612	0.681	0.777	**0.659**	0.653
	mCCA + jICA	**0.804**	0.697	0.840	**0.799**	**0.635**	**0.781**
10	jICA	0.802	**0.699**	**0.843**	0.764	0.48	0.705
	mCCA	0.625	0.679	0.712	0.607	0.622	0.64
	mCCA + jICA	0.801	**0.700**	0.865	**0.773**	0.545	0.795
12	jICA	**0.826**	0.645	**0.908**	0.760	0.404	**0.803**
	mCCA	0.624	0.697	0.711	0.582	**0.579**	0.616

6.2.3 Evaluation of Compact from Component Number

To test the impact of different component numbers M_k from each modality, another simulation assumes the data from different modalities have M_1, M_2, and M_3 respectively, and tests using various number of M if the "mCCA + jICA" can achieve better performance. For evaluation, we calculate the estimation accuracy of min (M, M_i) number of components that are most similar to ground truth. The estimation accuracy includes mean source correlation with ground truth and mean mixing matrix correlation with ground truth. The sources and mixing matrices used here are the same with above.

Two runs of simulations, which randomly select 4, 6, and 8 sources (Run 1), or 6, 8, and 4 sources (Run 2) from S_1 (in dimension of 8 × 16384), S_2 (in dimension of 8 × 5000) and S_3 (in dimension of 8 × 14400) respectively and their corresponding loadings from A_1, A_2 and A_3. The numbers of M ranges from 4 to 14. The results are listed in Table 6.2 and 6.3.

Table 6.2 Run 1: randomly select 4, 6, and 8 sources from S_1, S_2, and S_3 respectively

No. of comps	Models	Source			Loading		
		S_1 ($M_1 = 4$)	S_2 ($M_2 = 6$)	S_3 ($M_3 = 8$)	A_1 ($M_1 = 4$)	A_2 ($M_2 = 6$)	A_3 ($M_3 = 8$)
4	mCCA+jICA	0.756	0.655	**0.826**	**0.801**	0.673	**0.846**
	jICA	**0.848**	0.685	0.788	0.618	0.314	0.616
	mCCA	0.644	**0.702**	0.586	0.694	**0.783**	0.622
6	mCCA+jICA	0.913	0.638	**0.828**	**0.852**	0.541	**0.853**
	jICA	**0.913**	0.557	0.801	0.673	0.270	0.639
	mCCA	0.707	**0.678**	0.607	0.623	**0.663**	0.657
8	mCCA+jICA	0.908	**0.707**	**0.847**	**0.783**	**0.612**	**0.827**
	jICA	**0.951**	0.593	0.807	0.656	0.318	0.710
	mCCA	0.743	0.692	0.568	0.506	0.597	0.598
10	mCCA+jICA	0.935	**0.749**	0.864	**0.806**	0.569	**0.826**
	jICA	**0.943**	0.681	**0.893**	0.707	0.304	0.770
	mCCA	0.753	0.724	0.569	0.449	**0.632**	0.530
12	mCCA+jICA	**0.928**	**0.771**	0.871	**0.852**	0.578	**0.806**
	jICA	0.956	0.758	**0.937**	0.772	**0.625**	0.800
	mCCA	0.787	0.733	0.575	0.425	0.565	0.481
14	mCCA+jICA	**0.954**	**0.801**	0.881	**0.878**	**0.632**	0.847
	jICA	0.949	0.790	**0.951**	0.847	0.613	**0.882**
	mCCA	0.773	0.742	0.606	0.456	0.537	0.466

Table 6.3 Run 2: randomly select 6, 8, and 4 sources from S_1, S_2, and S_3 respectively

No. of comps	Models	Source			Loading		
		S_1 ($M_1 = 6$)	S_2 ($M_2 = 8$)	S_3 ($M_3 = 4$)	A_1 ($M_1 = 6$)	A_2 ($M_2 = 8$)	A_3 ($M_3 = 4$)
4	mCCA+jICA	**0.896**	0.708	**0.806**	**0.902**	0.760	**0.768**
	jICA	0.885	0.635	0.664	0.770	0.381	0.358
	mCCA	0.690	**0.733**	0.727	0.753	**0.824**	0.640
6	mCCA+jICA	0.860	0.660	0.868	**0.848**	0.648	**0.784**
	jICA	**0.916**	0.565	**0.905**	0.779	0.350	0.598
	mCCA	0.538	**0.678**	0.797	0.572	**0.723**	0.754
8	mCCA+jICA	**0.929**	**0.670**	**0.939**	**0.907**	**0.668**	**0.837**
	jICA	0.917	0.564	0.896	0.844	0.383	0.638
	mCCA	0.608	0.618	0.811	0.585	0.619	0.687
10	mCCA+jICA	**0.928**	**0.703**	**0.949**	**0.905**	**0.628**	**0.826**
	jICA	0.920	0.675	0.919	0.850	0.470	0.737
	mCCA	0.668	0.644	0.910	0.568	0.596	0.679
12	mCCA+jICA	0.924	0.778	**0.951**	0.898	**0.677**	**0.802**
	jICA	**0.945**	**0.806**	0.917	**0.933**	0.633	0.749
	mCCA	0.675	0.653	0.889	0.544	0.531	0.661
14	mCCA+jICA	0.925	**0.818**	**0.953**	0.932	**0.736**	**0.831**
	jICA	**0.944**	0.812	0.903	**0.975**	0.709	0.728
	mCCA	0.896	0.708	0.806	0.902	0.760	0.768

In both cases, mCCA + jICA works either best or close to the best among 3 methods when $M \geq \max(M_1, M_2, M_3)$, and using a high order of component number in joint separation does not hurt the separation, instead, the estimation accuracy tends to increase with M. Therefore we choose $M \geq \max(M_1, M_2, M_3)$ in our application.

Chapter 7   Search for Multimodal Neuroimaging Biomarkers with

FNC and SMRI in Bipolar and Major Depressive Disorders

7.1   Introduction

During neurodevelopment the formation of gyral folding patterns within the cerebral cortex is thought to reflect the anatomical connections between distinct cortical areas, which in turn relate to cerebral function (Van Essen and Dierker 2007; Poldrack 2010). This relationship between brain structure and function has been supported by previous neuroimaging studies (Greicius, Supekar et al. 2009; van den Heuvel, Mandl et al. 2009; Mars, Jbabdi et al. 2011). However, the relationship between altered brain function and structure in mood disorders remains unclear. Generally, each neuroimaging modality provides a certain perspective on brain function or structure. However, data fusion through a joint analysis not only capitalizes on the strengths of each imaging modality, but also reveals underlying inter-relationships, potentially providing a more comprehensive understanding of brain deficits in psychiatric disorders (Calhoun, Adali et al. 2006; Sui, Adali et al. 2012; Calhoun and Sui 2016). To date, few studies of BD and MDD have assessed multimodal brain imaging data collected from the same subject sample. A conventional multimodal practice is firstly to analyze each modality separately, and then to compare at the results level (Rigucci, Serafini et al. 2010). However, such an approach cannot capture directly the joint information available in multimodal imaging data (Sui, Adali et al. 2012; Calhoun and Sui 2016). In a classification analysis on BD and MDD, Jie et al (Jie, Zhu et al. 2015) utilized a machine learning model to select multimodal diagnostic discriminating features from combined

fMRI and structural MRI (sMRI) data. Nevertheless, the joint function-structure changes that span across fMRI and sMRI in BD and MDD have not been characterized previously.

In this study, we utilized the resting-state FNC generated from our prior study as characteristics of fMRI. At the same time, gray matter densities (GMD) from the same subject samples were acquired using sMRI. In order to identify the co-altered networks across modalities, we assume that 1) whole brain FNC is a linear mixture of sources in the form of multiple sub-networks (Park, Kim et al. 2014), 2) whole brain GMD can also be linearly separated into a number of sources as spatial independent components (Xu, Groth et al. 2009), and 3) disorder incurred functional and structural brain changes are correlated across the source factors of modalities. A joint analysis was applied to FNC and GMD using a data fusion approach called multi-set canonical correlation analysis + joint independent component analysis (mCCA+jICA) (Sui, Adali et al. 2010; Sui, He et al. 2013). We expected that the analysis which incorporates FNC and brain structure would reveal changes specific to BD or MDD, and that the abnormalities defined using this approach ultimately may served as potential diagnostic biomarkers with the potential to discriminate these two mood disorders.

7.2   Methods

In this study, preprocessed fMRI and sMRI data on BD, MDD and HC from the Tulsa Resting-state Dataset will be used. More subjects with the same scanning protocol are expected to available from our collaborators. FNC maps will be generated in the same way as the study in Chapter 4.

7.2.1 mCCA+jICA

The overall procedure of mCCA+jICA framework is illustrated in Figure 7.1. To ensure the range of input data compatible across modalities, both FNC and GMD will be normalized into z-score before the mCCA+jICA pipeline. In this study, the component number M was set to be 8 estimated using a modified MDL method (Li, Adali et al. 2007).
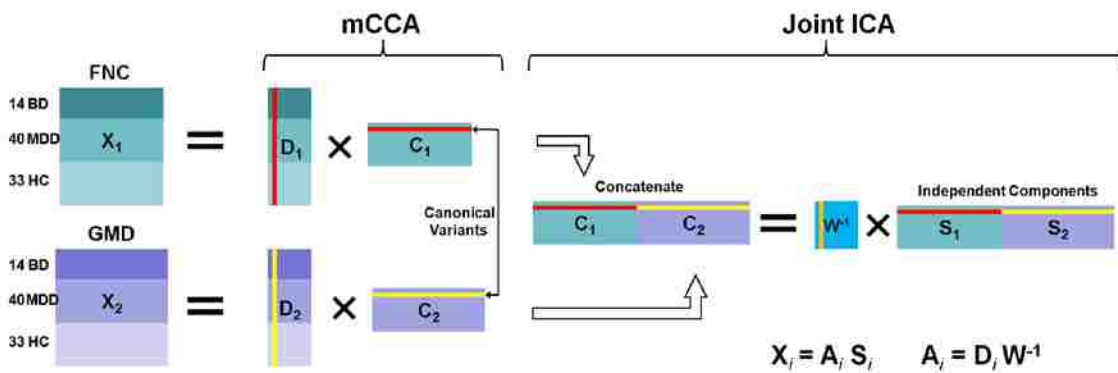
Figure 7.1 Two-way "mCCA + jICA" fusion strategy for FC map and GMD.

7.2.2 Statistical testing on group abnormalities

To reduce the age and gender effects, we regressed out the subjects' age and gender as covariates from mixing profiles A_k, and performed statistical tests on residuals A_k'. Analysis of variance (ANOVA) and two-sample t–tests were performed on mixing coefficients A_k' of each IC for each modality k, to reveal the components that have significant group difference among subjects. Any component of the same index that showed significant group difference in both modalities was considered a modality-common (or joint) group-discriminative IC. In contrast, any group difference of one component that occurred in a single modality was considered a modality-specific group-discriminative IC. These ICs were termed joint or distinct abnormalities respectively. The

false discovery rate (FDR) correction (Benjamini and Hochberg 1995) for multiple testing was applied to the p-values obtained from the statistical tests.

7.2.3   Identifying Community Structures and Hubs

ICs of FNC correspond to the connectivity weights of multiple edge-sharing sub-networks within the brain (Park, Kim et al. 2014). To better capture the characteristics of the sub-networks that showed a group difference, those FNC components were further analyzed using graph theory. Modular community structure has been repeatedly demonstrated in resting state functional brain connectivity networks. The brain regions that are functionally associated and subserve similar roles may be divided into a same module during the modular analysis. In particular, the brain nodes that are highly connected with other regions in the same module are called hubs (Rubinov and Sporns 2010).

To assess the modular community structures and hubs, the connectivity weights of FNC subnetworks were first rescaled into [-1, 1]. A fine-tuned Louvain algorithm (Reichardt and Bornholdt 2006; Ronhovde and Nussinov 2009) from the brain connectivity toolbox was adopted to discover the optimal community structure of the FNC subnetworks, which divide the graph into non-overlapping groups of nodes (modules) in a way that maximizes the number of within-group edges, and minimizes the number of between-group edges.

Highly connected node within a module q could be identified by measuring of intra-module connectivity. Intra-module connectivity of node i, k_i^q is given by the sum of connectivity strengths S_{ik} with all other nodes in module q:

$$k_i^q = \sum_{k \in q} S_{ik} \tag{7.1}$$

The z-score (Guimera and Amaral 2005)of node i is defined as

$$z_i = \frac{k_i^q - \bar{k}_q}{\sigma_q} \tag{7.2}$$

where $\bar{k}_q$ and σ_q are the mean and standard deviation of k_k^q for all nodes in module q. Nodes with higher z-scores are more strongly connected to the other nodes in the same module. In this study, we define a node with $z_i > 1.0$ as a hub (Yu, Plis et al. 2011). The BrainNet Viewer toolbox (http://www.nitrc.org/projects/bnv/) was used for visualizing FNC subnetworks (Xia, Wang et al. 2013).

7.2.4 Classifications Based on the Features Selected

For the identified group-discriminative components, we further tested their potential use for disease classification (Figure 7.2). For each modality, we normalized (subtracted by mean then divided by standard deviation) each IC with significant group difference into z-values, which then were thresholded (FNC at $|z| > 2.0$, and GMD at $|z| > 3.0$) to generate a mask from each modality. The masks of the same modality then were combined and applied to the raw input data of each modality, which served as the input used to further classify 3 BD, MDD, and HC based on uni-modal and multi-modal features.
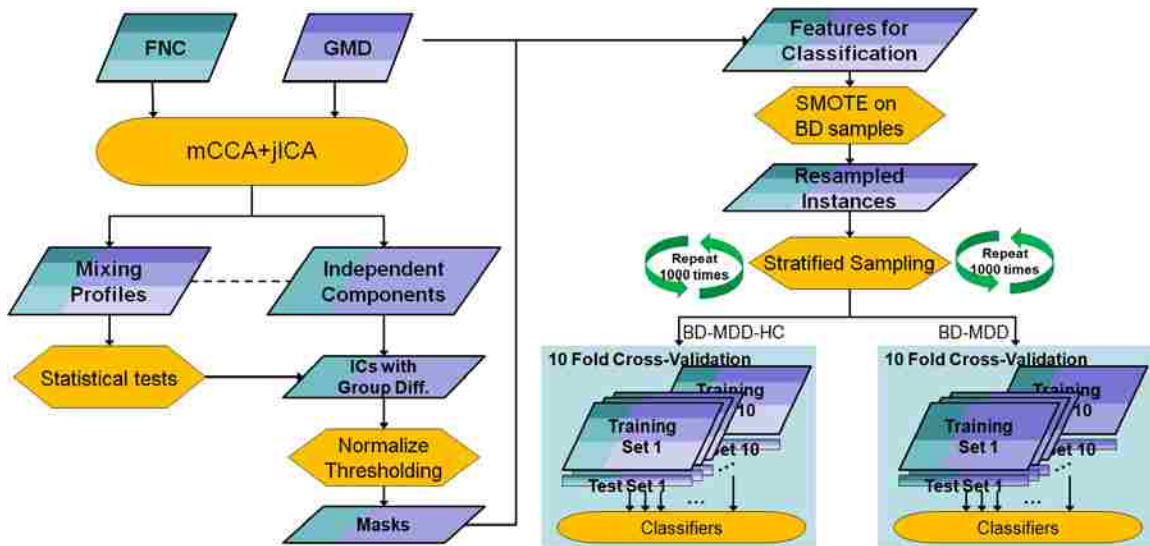
Figure 7.2 Flowchart of disease classification with components derived from multimodal fusion.

For comparison, we evaluated classifiers based on the features from the individual modality (FNC or GMD only), as well as combined features from both modalities (FNC+GMD). Classifiers were built and tested on the Weka 3.6 platform (http://www.cs.waikato.ac.nz/ml/weka/)(Witten, Frank et al. 2011). In order to balance the sample numbers in each group, the instances of BD group were resampled using a Synthetic Minority Oversampling TEchnique (SMOTE) (Chawla, Bowyer et al. 2002) to generate 39 BD samples. Each sample was assigned a class label based on its corresponding diagnostic group (BD, MDD or HC). We then trained four different classifiers: 1) Sequential Minimal Optimization for Support Vector Machine (SMO) (Keerthi, Shevade et al. 2001), 2) Naïve Bayes (John 1995), 3) Random Forest (Breiman 2001), and 4) K-nearest neighbors (kNN) (Aha, Kibler et al. 1991) where $k = 5$. To ensure stable performance of each classifier, stratified ten-fold cross validation was repeated 1000 times, yielding 10000 testing accuracy rates. For every ten-fold cross validation run, the samples were assigned into 10 groups randomly. In Iteration (Fold)

106

$(k = 1,2, ..., 10)$, group k was left out as testing cases towards the classifier model that was trained on other nine groups. Since distinguishing BD and MDD is a major clinical challenge, the classification process was applied to distinguish all 3 groups as well as the BD and MDD groups only.

7.3   Results

7.3.1   Group Difference on Mixing Profiles

One joint group-discriminative IC (IC5) and one modality-specific group-discriminative IC (GMD-IC2) were detected, as shown in Figure 7.3, based on the statistical tests of the mixing coefficients derived from mCCA+jICA.
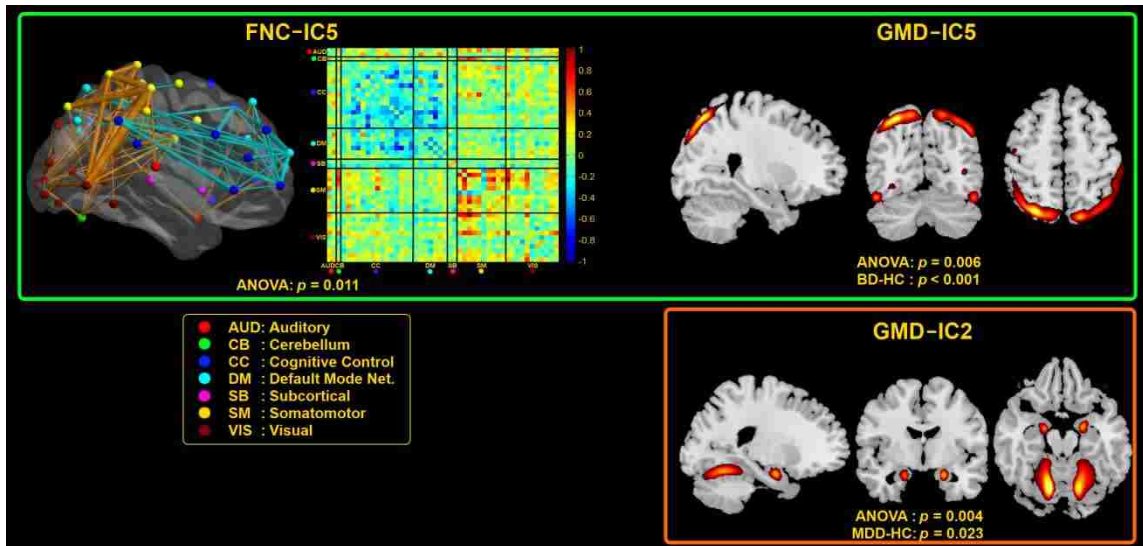
Figure 7.3 Components that showing significant group effects. IC5 demonstrated significant group differences in both FNC (top left) and GMD (top right). IC2 showed a significant group difference in GMD only (bottom). In FNC-IC5, the nodes correspond to intrinsic connectivity networks (ICNs), and the links are edges of the subnetwork between node-pairs. Thickness of links represent to connectivity weights of the subnetwork. Only the top 10% weighted links are displayed for clearer visualization. Orange links indicate the weights are positively correlated with the mixing profile of FNC-IC5, while green links indicate the weights are negatively correlated with mixing profile of FNC-IC5.

ANOVA on IC5 revealed significant group difference in both FNC ($p = 0.011$, FDR corrected) and GMD ($p = 0.006$, FDR corrected). In FNC-IC5, the subnetwork comprised of reduced functional connectivity magnitude (less correlated BOLD activity) in the superior parietal lobe (SPL), precentral gyrus (PreCG), postcentral gyrus(PoCG), middle temporal gyrus(MTG) and middle occipital gyrus(MOG) and cerebellum, but increased connectivity magnitude within regions associated with the superior frontal gyrus (SFG), precuneus, middle frontal gyrus (MFG), inferior parietal lobe (IPL), and limbic subcortical networks. GMD-IC5 corresponds to gray matter density in the SPL and MOG. A significant group difference was also found in GMD-IC5 between BD and HC in t-test ($p < 0.001$, FDR corrected, BD < HC). At the same time, pair-wise t-test indicated difference in FNC-IC5 between BD and HC ($p = 0.027$, uncorrected, BD < HC) and in GMD-IC5 between BD and MDD ($p = 0.014$, uncorrected, BD < MDD). However, these two p-values did not remain significant after correction for multiple testing (FDR). The correlation of mixing profiles between FNC and GMD was $r = 0.23$, indicating the changes within this component found in FNC and GMD are related across patients with BD.

IC2 showed a significant group difference in GMD only ($p = 0.004$, FDR corrected), which included cerebellum, amygdala and hippocampus. Both MDD and BD showed lower GMD than HC in this component, as shown in Figure 7.3 (MDD-HC: $p = 0.023$, FDR corrected; BD-HC: $p = 0.037$, uncorrected).

7.3.2 Community Structures and Hubs of FNC Component

In the FNC component that showed significant group difference (IC5), three non-overlapping modules were identified by fine-tuned Louvain algorithm, including two

major community modules with nodes that are strongly interconnected together and a module that include nodes relatively isolated to others, as shown in Figure 7.4. Specifically, Module 1 contains 20 nodes intensively connected within default-mode (SFG and precuneus), cognitive control (MFG and IPL), and limbic subcortical networks. Module 2 comprised of 18 nodes, mostly in somatomotor networks (SPL, PreCG and PoCG), cerebellum, and visual networks (MTG and MOG). The remaining 10 nodes that are less closely connected were separated into Module 3.
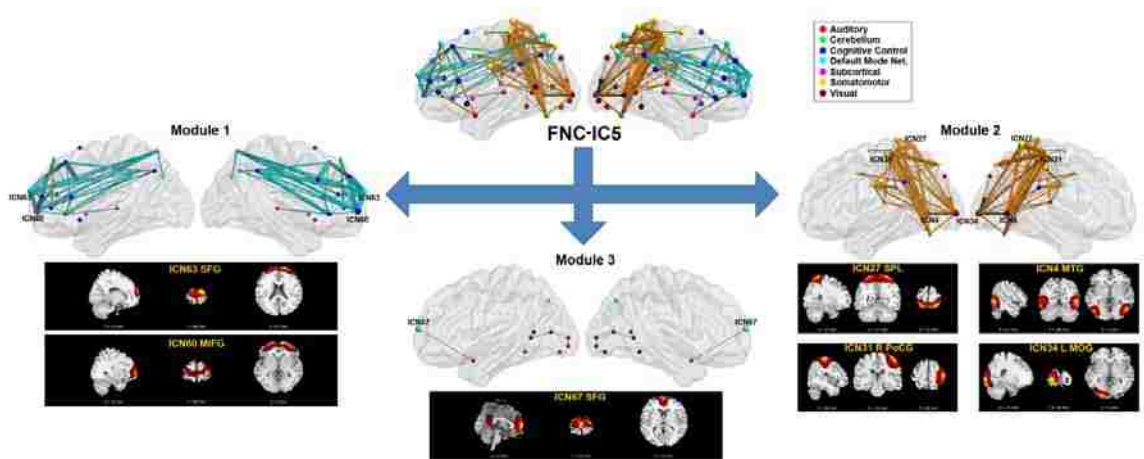
Figure 7.4 Modules and hub nodes in FNC-IC5. Forty-eight ICNs in the subnetwork FNC-IC5 can be divided into three modules. Hubs nodes in each module are enlarged and labeled. There were two hubs in Module 1, four hubs in Module 2, and one hub in Module 3. Only top 10% weighted links are displayed for better visualizing purposes. Orange links indicate the weights are positively correlated with the mixing profile of FNC-IC5, while green links indicate the weight are negatively correlated with mixing profile of FNC-IC5.

It noteworthy that the connectivity weight of the subnetwork in Modules 1 and 2 were opposite in valence (orange for positive and cyan for negative weights in Figure 7.4), indicating subjects with higher connectivity strength magnitudes in one module have lower FC magnitudes in the other. Moreover, the mixing profile of FNC-IC5 in the BD group was lower than in the HC group, which suggested that the BD group manifest a more densely interconnected Module 1 but less interconnected Module 2 comparing to

HC in this subnetwork. Interestingly, this dual modular parcellation corresponded to two major areas organized from a recent resting-state FC study (Stoddard, Gotts et al. 2016), which was based on a different approach of clustering voxel-wise connectivity.

Seven hubs were identified in the modular structure of FNC-IC5, including two hubs (MFG and SFG) in Module 1, four hubs (MTG, SPL, right PoCG, and left MOG) in Module 2, and one hub (SFG) in Module 3. These seven hubs are highlighted as larger nodes in Figure 7.4, indicating these brain regions play important roles in the altered FNC structure, and link to the abnormal GMD in BD.

7.3.3 Classifications
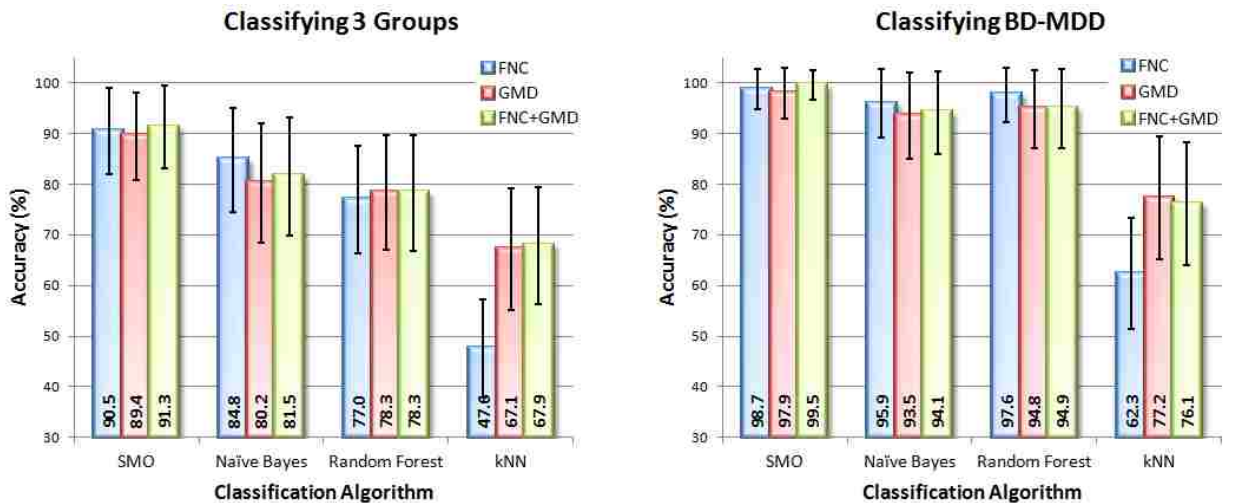
Figure 7.5 Performance of classification algorithms that discriminating 3 groups (left) and BD vs. MDD (right), depicted as mean and standard deviation of accuracy from each of four classifiers trained with features extracted from fusion analysis.

The average and standard deviation of 1000 accuracy rates of both 3-group and BD-MDD classification are shown in Figure 7.5. SMO performed best among 4 algorithms tested: averaged accuracy reached 91.3±8.1% for 3-group classification and 99.5±2.9% for distinguishing between BD and MDD using features from both modalities.

For each of 4 algorithms, we also compared results of classifier trained using either unimodal or multimodal features. Overall, training with multimodal features achieved best or close to best accuracy with all algorithms.

7.4   Discussion

In this study, we conducted fusion analysis on functional and structural MRI data by applying mCCA+jICA framework to whole brain FNC and GMD. We aimed to identify abnormalities spanning across multiple imaging modalities and to evaluate the feasibility accuracy of these biomarkers to distinguish BD and MDD. Both modal-specific and modal-common components were identified. Further analysis on the group-discriminating FNC component revealed community structure and hubs, which conceivably may be associated with the mechanisms that are distinct to each disorder.

7.4.1   Functional and Structural Co-alterations in BD

IC5 showed significant group differences in both FNC and GMD, and t-tests found abnormalities are mostly in BD. From the spatial maps, IC5 in both modalities highlighted parietal and occipital lobes. Generally, the parietal lobe is commonly considered to be involved in processing tactile and proprioceptive information, language comprehension, speech, writing, and aspects of spatial orientation and perception. At the same time, the occipital lobe includes regions that are involved in visual perception and processing (Nolte 2009). Several sMRI studies showed significant reductions gray matter density and volume in BD subjects versus controls in the parietal lobe (Doris, Belton et al. 2004; Lyoo, Kim et al. 2004; Frazier, Breeze et al. 2005; Lyoo, Sung et al. 2006) and the occipital lobe (Doris, Belton et al. 2004; Lochhead, Parsey et al. 2004; Lyoo, Sung et al. 2006). Our results of GMD-IC5 thus appear consistent with these findings.

Earlier studies proposed the cortical thinning in sensory association cortices may be related to impairments in visual spatial neuropsychological function within BD subjects (Sweeney, Kmiec et al. 2000; Ferrier, Chowdhury et al. 2004). As a joint-discriminative IC in our study, IC5 confirmed that the reduced GMD in the parietal and occipital cortices were related with the alterations in cerebral function in the BD group. According to graph theory, the hub nodes of a module interact actively with other brain components, facilitate functional integration, and participate in module organization (Rubinov and Sporns 2010). The four hubs of Module 2, including two hubs in the parietal lobe, one in the temporal lobe, and one in the occipital lobe, were spatially distribute across different somatomotor and visual areas, indicating the abnormalities may have widespread effects in the function of sensory association cortices. Based on analysis of FNC-IC5, the parietal, occipital, temporal, and cerebellar fusiform areas were categorized into Module 2 with reduced connectivity in BD, demonstrating the direct correspondence of structural and functional deficits in this disorder.

In Module 1, the two hubs along with majority of implicated nodes were located within the prefrontal cortex. The prefrontal regions, including the orbitofrontal cortex (OFC), the anterior cingulate cortex (ACC), and the dorsomedial (DMPFC), dorsolateral (DLPFC) and ventrolateral (VLPFC) areas of the prefrontal cortex have been consistently implicated in cognitive control processes (Sui, Pearlson et al. 2015), including decision-making and emotion regulation (Phillips, Ladouceur et al. 2008; Kupfer, Frank et al. 2012). In mood disorders, these prefrontal cortical areas form part of the limbic–cortical–striatal–pallidal–thalamic circuits that are hypothesized to be dysfunctional in MDD and BD based on neuroimaging studies (Drevets 2000; Price and Drevets 2012). A number of

previous studies of resting-state FC in BD samples found increased resting-state FC in the prefrontal cortices, particularly within ventral prefrontal cortex in BD (Chepenik, Raffo et al. 2010). Another ICA-defined FNC analysis reported that BD subjects showed increased FC in emotion evaluation regions such as the bilateral medial prefrontal cortex, and in "affective working memory network" including the DLPFC and VLPFC, during an affective working memory task (Passarotti, Ellis et al. 2012). Abnormal medial prefrontal cortex connectivity between ICA components were also found during the resting-state in the BD group in multiple previous studies (Ongur, Lundy et al. 2010; Calhoun, Sui et al. 2011). Our findings with stronger FC in BD subjects within the prefrontal cortical areas highlighted in Module 1 not only replicated our recent results on the same dataset with different analysis approaches (He, Yu et al. 2016), but also are in line with prior resting-state FC studies.

Another interesting finding was that two subcortical regions, the putamen and thalamus, were grouped together into Module 1, potentially consistent with the anatomical circuits formed between the prefrontal cortex, the striatum and the thalamus, as well as with previous evidence that dysfunction within these circuits plays a major role in the pathophysiology of BD (Strakowski, DelBello et al. 2005). Fronto-limbic abnormalities in BD also have been supported from the view of FC by a number of task-based fMRI studies (de Almeida, Versace et al. 2009; Versace, Thompson et al. 2010), but may be complex and difficult to be detected during resting-date (Vargas, Lopez-Jaramillo et al. 2013; Stoddard, Gotts et al. 2016). A few FC studies that probe limbic regions directly found abnormal prefrontal-limbic connectivity in resting BD subjects (Chepenik, Raffo et al. 2010; Anticevic, Brumbaugh et al. 2013; Torrisi, Moody et al.

113

2013). No significant group difference in fronto-limbic FC was observed in our previous FNC study on the same data set. Our results from the modular analysis performed herein on the FNC component thus may provide a more sensitive method for detecting prefrontal-limbic dysfunction in BD patients during rest.

7.4.2   GMD Abnormality in MDD

Beside the joint group-discriminative IC5, GMD-IC2 was identified as modality-specific group-discriminative IC, where group difference was only found in GMD. In our study, both BD and MDD exhibited higher mixing weights associated with GMD-IC2 compared to HC, but no statistical difference was detected between the patients in two disorders. The amygdale and anterior hippocampus form central structures of the limbic system and play major roles in emotion regulation, episodic memory, and responses to stressors, threats and appetitive stimuli (Aggleton 1992; Burgess, Maguire et al. 2002). Consistent with their functional roles, deficits of amygdala related to mood disorders such as BD and MDD are widely supported from a variety of neuroimaging approaches (Videbech 2000; Price and Drevets 2012).

Although many structural studies on the BD group demonstrated reduced amygdala volume compared to healthy subjects (Blumberg, Kaufman et al. 2003; Foland-Ross, Brooks et al. 2012; Phillips and Swartz 2014), other studies reported amygdala in BD were either enlarged (Haldane, Cunningham et al. 2008) or unchanged (Almeida, Akkal et al. 2009). (Drevets 2003; Savitz, Nugent et al. 2010) provided evidence that speculate the disagreement at least partly be explained by the putative neurotrophic / neuroprotective effects of some mood stabilizer treatments in BD. With medication effects controlled, Savitz et al. found amygdala volumes declined in unmedicated BD in

contrast to HC (Savitz, Nugent et al. 2010). Instead of selecting ROI a priori, our analysis approach was data-driven. The IC of gray matter density demonstrated similar trend of amygdala reduction in unmedicated BD compared to HC. However, the group difference did not reach statistical significance after FDR correction, potentially reflecting the biological heterogeneity within these phenotypes (Savitz, Dantzer et al. 2015; Savitz, Drevets et al. 2015).

On the other hand, the reduction in amygdala volume in MDD appears generally consistent with a variety of recent analyses (Tang, Wang et al. 2007; Zou, Deng et al. 2010; Bora, Fornito et al. 2012; Sacher, Neumann et al. 2012), and our results that GMD-IC2 of MDD exhibits significant change compared to HC is in accordance with them. In addition to the amygdala abnormality, GMD-IC2 includes part of culmen and declive regions of the cerebellum as well. Simultaneous cerebellar and amygdala reduction in MDD was also reported in prior gray matter density studies (Lee, Tae et al. 2011; Peng, Liu et al. 2011). Recent studies have shown that the cerebellum plays a role in emotion regulation and cognition (Bugalho, Correa et al. 2006; Baldacara, Borgio et al. 2008; Phillips, Hewedi et al. 2015), and also have implicated the cerebellum in MDD based on findings of altered structure (Yucel, Nazarov et al. 2013; Zhao, Wang et al. 2016) and function (Liu, Zeng et al. 2012; Ma, Zeng et al. 2013).

7.4.3 Classifications based on selected ICs

As an exploration, the group discriminative features extracted from multimodal analysis were evaluated using classification. Classifiers yielded highly accurate and reliable performance with cross-validation. Even though no significant difference was found between BD and MDD during statistical test on mixing profiles of individual ICs,

classifiers still distinguished the two disorders with relatively high accuracy by combining the high-dimensional features from two modalities, indicating classification methods provide a mechanism for evaluating predictive power of the results which null hypothesis testing does not (Craddock, Holtzheimer et al. 2009). The classifiers trained with the combination of both modalities performed better and more stable than those trained on a single modality, suggesting that information gained through multimodal fusion can improve the potential diagnostic prediction, in accordance with (Sui, Adali et al. 2009; Yang, Liu et al. 2010). These data merit replication in future studies to determine their potential utility as diagnostic biomarkers in mood disorders (Sui, He et al. 2013).

7.4.4 Limitations

Several methodological issues limit the conclusions that can be drawn from the current study. The major issue is the small number of subjects, especially in the BD group. In order to avoid the potential confound of medication, our study was limited to subjects who were treatment-naive or unmedicated for at least three weeks. However, this strict requirement constrained the sample size of this study. Nevertheless, most recent neuroimaging studies comparing BD and MDD reviewed in (de Almeida and Phillips 2013) also included sample sizes ranging from 10 to 30 subjects per patient group. During the evaluation of biomarkers with classification, we adopted an upsampling approach on the BD samples, in order to reduce the impact of the unbalanced group sizes on the classifiers. It would be helpful to increase statistical power by including more subjects in future studies. In addition, to utilize as much information as possible, the features were derived from all subjects. Although the classification models were tested

116

with 10-fold cross validation, more solid conclusions can be drawn by examining the performance of biomarkers on new subjects which were excluded from the feature extraction process (Du, Pearlson et al. 2015; Meng, Jiang et al. 2016).

7.5 Conclusion

In conclusion, we conducted fusion analysis on the functional network connectivity and gray matter density in mood disordered and healthy control samples, providing a novel perspective to neuroimaging abnormalities in mood disorders by combining both structural and functional MRI. Both multimodal and modality-specific discriminative components were detected. Comparing to HC, BD exhibited reduced GMD in the parietal and occipital cortices, which correlated with attenuated functional connectivity within sensory and motor networks as well as hyper-connectivity in regions that are putatively engaged in cognitive control. In addition, altered GMD features were found in MDD in the amygdala and cerebellum. High accuracy in discriminating across groups was achieved by trained classification models, implying that features extracted from our fusion analysis hold the potential to ultimately serve as diagnostic biomarkers in BD and MDD research.

Chapter 8　Conclusions and Future Works

8.1　Summary

In summary, our work makes several important contributions to advance the functional connectivity analysis to neuroimaging studies, with application to help searching for biomarkers for mental disorders.

First, in Chapter 3, we examined the differences between healthy controls and patients with schizophrenia on topological properties of small-world structures of functional connectivity among working memory related brain regions. The sophisticated graph network measures provide a means of characterizing the effects of dysfunctional neural circuitry and variations in impaired connectivity across levels of dysconnectivity working memory demands in schizophrenia.

In Chapter 4, whole brain functional graphs were generated based on a subtype of functional connectivity, functional network connectivity, whose brain nodes were defined by ICA. After performing the graph analysis to resting-state fMRI collected from bipolar and major depressive disorders, we observed that, the FNC of the BD group exhibited higher connectivity strengths and also was characterized by more efficient topological structures based on measures obtained using graph theory at the functional-network-level in prefrontal cortex as well as at the whole-brain-level.

We then attempted to compare functional network connectivity with another functional measure, fractional amplitude of low frequency fluctuations, in Chapter 5.The two measures that correlated with cognitive deficits in schizophrenia were computed

separately, and spatially overlaid side by side to show the consistency across two approaches.

In addition to simply compare functional connectivity with other neuroimaging measures at result level, we further introduced a multimodal fusion framework, mCCA+jICA, which link the information from multiple imaging modalities through joint analysis. This framework was applied to explore the relationship between altered functional connectivity and gray matter density in brains of bipolar and major depressive disorder in Chapter 7. Both multimodal and modal-specific discriminative components have been detected. Our findings suggest that both overlapped and unique functional and structural deficits exist in bipolar and major depressive disorder, and the abnormalities may be utilized as potential diagnostic biomarkers.

8.2   Future Works

There are still many aspects that can be explored further regarding the existing frameworks on functional connectivity.

Currently, we characterized functional connectivity as the correlation or partial correlation between the time courses of brain regions. While correlation is preferred for its straightforward interpretation and tractability, there are other statistics that measures the temporal dependency methods that may be worth trying in future studies, such as mutual information, or coherence, which may detect the nonlinear dependencies and the resolution phase of spectral relationships,.

In additional to fuse functional connectivity and gray matter density, the N-way mCCA+jICA can be applied with other multimodal data sets, i.e., on FC and DTI to show

the relationship between functional and anatomical connectivity from the aspect of data distribution. FC map may also be substituted by extracted features from dynamic FC, i.e. power spectrum in certain bands of dynamic FC, to show connection of the fluctuation of FC through time to other imaging modalities.

For evaluating the potential use of features derived from the multimodal frameworks, we adopted classification models with 10-fold cross validation. However, this process is somehow biased as the subjects used for testing also participated in the feature extraction process. In future works, more solid conclusions can be drawn by examining the performance of biomarkers on new subjects which were fully separated from analyzing process (Du, Pearlson et al. 2015; Meng, Jiang et al. 2016).

References

Abou-Elseoud, A., T. Starck, et al. (2010). "The effect of model order selection in group PICA." <u>Human brain mapping</u> **31**(8): 1207-1216.

Achard, S. and E. Bullmore (2007). "Efficiency and cost of economical brain functional networks." <u>PLoS Comput Biol</u> **3**(2): e17.

Achard, S., R. Salvador, et al. (2006). "A resilient, low-frequency, small-world human brain functional network with highly connected association cortical hubs." <u>J Neurosci</u> **26**(1): 63-72.

Aggleton, J. P. (1992). <u>The amygdala : neurobiological aspects of emotion, memory, and mental dysfunction</u>. New York ; Chichester, Wiley-Liss.

Aha, D. W., D. Kibler, et al. (1991). "Instance-Based Learning Algorithms." <u>Machine Learning</u> **6**(1): 37-66.

Alexander-Bloch, A. F., N. Gogtay, et al. (2010). "Disrupted modularity and local connectivity of brain functional networks in childhood-onset schizophrenia." <u>Front Syst Neurosci</u> **4**: 147.

Alexander, G. E., M. R. DeLong, et al. (1986). "Parallel organization of functionally segregated circuits linking basal ganglia and cortex." <u>Annu Rev Neurosci</u> **9**: 357-381.

Allen, E. A., E. Damaraju, et al. (2014). "Tracking Whole-Brain Connectivity Dynamics in the Resting State." <u>Cerebral Cortex</u> **24**(3): 663-676.

Allen, E. A., E. B. Erhardt, et al. (2011). "A baseline for the multivariate comparison of resting-state networks." <u>Frontiers in systems neuroscience</u> **5**: 2.

Almeida, J. R., D. Akkal, et al. (2009). "Reduced gray matter volume in ventral prefrontal cortex but not amygdala in bipolar disorder: significant effects of gender and trait anxiety." Psychiatry research **171**(1): 54-68.

Almeida, J. R. C., A. Versace, et al. (2010). "Elevated Amygdala Activity to Sad Facial Expressions: A State Marker of Bipolar but Not Unipolar Depression." Biological psychiatry **67**(5): 414-421.

Anand, A., Y. Li, et al. (2005). "Activity and connectivity of brain mood regulating circuit in depression: a functional magnetic resonance study." Biological psychiatry **57**(10): 1079-1088.

Anand, A., Y. Li, et al. (2005). "Antidepressant effect on connectivity of the mood-regulating circuit: an FMRI study." Neuropsychopharmacology : official publication of the American College of Neuropsychopharmacology **30**(7): 1334-1344.

Andreasen, N. C. (1984). Scale for the Assessment of Negative Symptoms. Iowa City, IA, University of Iowa.

Andreasen, N. C. (1984). Scale for the Assessment of Positive Symptoms. Iowa City, IA, University of Iowa.

Anticevic, A., M. S. Brumbaugh, et al. (2013). "Global Prefrontal and Fronto-Amygdala Dysconnectivity in Bipolar I Disorder with Psychosis History." Biological Psychiatry **73**(6): 565-573.

Arbabshirani, M. R., K. A. Kiehl, et al. (2013). "Classification of schizophrenia patients based on resting-state functional network connectivity." Frontiers in neuroscience **7**: 133.

Ashburner, J. and K. J. Friston (1999). "Nonlinear spatial normalization using basis functions." Hum Brain Mapp **7**(4): 254-266.

Ashburner, J. and K. J. Friston (2005). "Unified segmentation." NeuroImage **26**(3): 839-851.

August, S. M., J. N. Kiwanuka, et al. (2011). "The MATRICS Consensus Cognitive Battery (MCCB): clinical and cognitive correlates." Schizophr Res **134**(1): 76-82.

Baddeley, A. (1992). "Working memory." Science **255**(5044): 556-559.

Baldacara, L., J. G. Borgio, et al. (2008). "Cerebellum and psychiatric disorders." Revista brasileira de psiquiatria **30**(3): 281-289.

Bassett, D. S. and E. Bullmore (2006). "Small-world brain networks." Neuroscientist **12**(6): 512-523.

Bassett, D. S., E. T. Bullmore, et al. (2009). "Cognitive fitness of cost-efficient brain functional networks." Proc Natl Acad Sci U S A **106**(28): 11747-11752.

Bassett, D. S., A. Meyer-Lindenberg, et al. (2006). "Adaptive reconfiguration of fractal small-world human brain functional networks." Proceedings of the National Academy of Sciences of the United States of America **103**(51): 19518-19523.

Baxter, L. R., Jr., J. M. Schwartz, et al. (1989). "Reduction of prefrontal cortex glucose metabolism common to three types of depression." Archives of General Psychiatry **46**(3): 243-250.

Beckmann, C. F., M. DeLuca, et al. (2005). "Investigations into resting-state connectivity using independent component analysis." Philosophical transactions of the Royal Society of London. Series B, Biological sciences **360**(1457): 1001-1013.

Bell, A. J. and T. J. Sejnowski (1995). "An information-maximization approach to blind separation and blind deconvolution." Neural computation **7**(6): 1129-1159.

Bench, C. J., K. J. Friston, et al. (1992). "The anatomy of melancholia--focal abnormalities of cerebral blood flow in major depression." Psychological Medicine **22**(3): 607-615.

Benjamini, Y. and Y. Hochberg (1995). "Controlling the False Discovery Rate - a Practical and Powerful Approach to Multiple Testing." Journal of the Royal Statistical Society Series B-Methodological **57**(1): 289-300.

Bertocci, M. A., G. M. Bebko, et al. (2012). "Abnormal anterior cingulate cortical activity during emotional n-back task performance distinguishes bipolar from unipolar depressed females." Psychological Medicine **42**(7): 1417-1428.

Binder, J. R., R. H. Desai, et al. (2009). "Where Is the Semantic System? A Critical Review and Meta-Analysis of 120 Functional Neuroimaging Studies." Cerebral Cortex **19**(12): 2767-2796.

Bluhm, R. L., J. Miller, et al. (2007). "Spontaneous low-frequency fluctuations in the BOLD signal in schizophrenic patients: Anomalies in the default network." Schizophrenia Bulletin **33**(4): 1004-1012.

Blumberg, H. P., J. Kaufman, et al. (2003). "Amygdala and hippocampal volumes in adolescents and adults with bipolar disorder." Archives of General Psychiatry **60**(12): 1201-1208.

Bora, E., A. Fornito, et al. (2012). "Gray matter abnormalities in Major Depressive Disorder: a meta-analysis of voxel based morphometry studies." Journal of affective disorders **138**(1-2): 9-18.

Breiman, L. (2001). "Random forests." <u>Machine Learning</u> **45**(1): 5-32.

Brotman, M. A., L. Kassem, et al. (2007). "Parental diagnoses in youth with narrow phenotype bipolar disorder or severe mood dysregulation." <u>The American journal of psychiatry</u> **164**(8): 1238-1241.

Brown, G. G., G. McCarthy, et al. (2009). "Brain-Performance Correlates of Working Memory Retrieval in Schizophrenia: A Cognitive Modeling Approach." <u>Schizophrenia Bulletin</u> **35**(1): 32-46.

Buckner, R. L., J. R. Andrews-Hanna, et al. (2008). "The brain's default network: anatomy, function, and relevance to disease." <u>Ann N Y Acad Sci</u> **1124**: 1-38.

Bugalho, P., B. Correa, et al. (2006). "[Role of the cerebellum in cognitive and behavioural control: scientific basis and investigation models]." <u>Acta medica portuguesa</u> **19**(3): 257-267.

Burgess, N., E. A. Maguire, et al. (2002). "The human hippocampus and spatial and episodic memory." <u>Neuron</u> **35**(4): 625-641.

Calhoun, V. D. and T. Adali (2012). "Multisubject independent component analysis of fMRI: a decade of intrinsic networks, default mode, and neurodiagnostic discovery." <u>IEEE reviews in biomedical engineering</u> **5**: 60-73.

Calhoun, V. D., T. Adali, et al. (2006). "Method for Multimodal analysis of independent source differences in schizophrenia: Combining gray matter structural and auditory oddball functional data." <u>Human Brain Mapping</u> **27**(1): 47-62.

Calhoun, V. D., T. Adali, et al. (2001). "A method for making group inferences from functional MRI data using independent component analysis." <u>Human brain mapping</u> **14**(3): 140-151.

Calhoun, V. D., T. Adali, et al. (2001). "Spatial and temporal independent component analysis of functional MRI data containing a pair of task-related waveforms." Human brain mapping **13**(1): 43-53.

Calhoun, V. D. and E. Allen (2013). "Extracting Intrinsic Functional Networks with Feature-Based Group Independent Component Analysis." Psychometrika **78**(2): 243-259.

Calhoun, V. D. and J. Sui (2016). "Multimodal fusion of brain imaging data: A key to finding the missing link(s) in complex mental illness." Biological Psychiatry: Cognitive Neuroscience and Neuroimaging.

Calhoun, V. D., J. Sui, et al. (2011). "Exploring the psychosis functional connectome: aberrant intrinsic networks in schizophrenia and bipolar disorder." Frontiers in psychiatry **2**: 75.

Callicott, J. H., A. Bertolino, et al. (2000). "Physiological dysfunction of the dorsolateral prefrontal cortex in schizophrenia revisited." Cereb Cortex **10**(11): 1078-1092.

Callicott, J. H., V. S. Mattay, et al. (1999). "Physiological characteristics of capacity constraints in working memory as revealed by functional MRI." Cerebral Cortex **9**(1): 20-26.

Callicott, J. H., V. S. Mattay, et al. (2003). "Complexity of prefrontal cortical dysfunction in schizophrenia: more than up or down." Am J Psychiatry **160**(12): 2209-2215.

Camchong, J., A. W. Macdonald, 3rd, et al. (2009). "Altered functional and anatomical connectivity in schizophrenia." Schizophr Bull **37**(3): 640-650.

Cardoso de Almeida, J. R. and M. L. Phillips (2013). "Distinguishing between unipolar depression and bipolar depression: current and future clinical and neuroimaging perspectives." Biological psychiatry **73**(2): 111-118.

Cerullo, M. A., J. C. Eliassen, et al. (2014). "Bipolar I disorder and major depressive disorder show similar brain activation during depression." Bipolar disorders **16**(7): 703-712.

Chawla, N. V., K. W. Bowyer, et al. (2002). "SMOTE: Synthetic minority over-sampling technique." Journal of Artificial Intelligence Research **16**: 321-357.

Chen, K., E. M. Reiman, et al. (2009). "Linking functional and structural brain images with multivariate network analyses: a novel application of the partial least square method." NeuroImage **47**(2): 602-610.

Chepenik, L. G., M. Raffo, et al. (2010). "Functional connectivity between ventral prefrontal cortex and amygdala at low frequency in the resting state in bipolar disorder." Psychiatry Research-Neuroimaging **182**(3): 207-210.

Cohen, J. D., T. S. Braver, et al. (1996). "A computational approach to prefrontal cortex, cognitive control and schizophrenia: recent developments and current challenges." Philos Trans R Soc Lond B Biol Sci **351**(1346): 1515-1527.

Comon, P. (1994). "Independent Component Analysis, a New Concept." Signal Processing **36**(3): 287-314.

Cooney, R. E., J. Joormann, et al. (2010). "Neural correlates of rumination in depression." Cognitive Affective & Behavioral Neuroscience **10**(4): 470-478.

Cordes, D., V. M. Haughton, et al. (2000). "Mapping functionally related regions of brain with functional connectivity MR imaging." AJNR. American journal of neuroradiology **21**(9): 1636-1644.

Correa, N. M., Y. O. Li, et al. (2008). "Canonical Correlation Analysis for Feature-Based Fusion of Biomedical Imaging Modalities and Its Application to Detection of Associative Networks in Schizophrenia." Ieee Journal of Selected Topics in Signal Processing **2**(6): 998-1007.

Craddock, R. C., P. E. Holtzheimer, 3rd, et al. (2009). "Disease state prediction from resting state functional connectivity." Magnetic resonance in medicine **62**(6): 1619-1628.

Damaraju, E., E. A. Allen, et al. (2014). "Dynamic functional connectivity analysis reveals transient states of dysconnectivity in schizophrenia." NeuroImage. Clinical **5**: 298-308.

Damoiseaux, J. S. and M. D. Greicius (2009). "Greater than the sum of its parts: a review of studies combining structural connectivity and resting-state functional connectivity." Brain structure & function **213**(6): 525-533.

de Almeida, J. R. C. and M. L. Phillips (2013). "Distinguishing between Unipolar Depression and Bipolar Depression: Current and Future Clinical and Neuroimaging Perspectives." Biological Psychiatry **73**(2): 111-118.

de Almeida, J. R. C., A. Versace, et al. (2009). "Abnormal Amygdala-Prefrontal Effective Connectivity to Happy Faces Differentiates Bipolar from Major Depression." Biological Psychiatry **66**(5): 451-459.

Delvecchio, G., P. Fossati, et al. (2012). "Common and distinct neural correlates of emotional processing in Bipolar Disorder and Major Depressive Disorder: a voxel-based meta-analysis of functional magnetic resonance imaging studies." European neuropsychopharmacology : the journal of the European College of Neuropsychopharmacology **22**(2): 100-113.

Dennis, E. L., N. Jahanshad, et al. (2012). "Test-retest reliability of graph theory measures of structural brain connectivity." Medical image computing and computer-assisted intervention : MICCAI ... International Conference on Medical Image Computing and Computer-Assisted Intervention **15**(Pt 3): 305-312.

Diler, R. S., J. R. C. de Almeida, et al. (2013). "Neural activity to intense positive versus negative stimuli can help differentiate bipolar disorder from unipolar major depressive disorder in depressed adolescents: A pilot fMRI study." Psychiatry Research-Neuroimaging **214**(3): 277-284.

Doris, A., E. Belton, et al. (2004). "Reduction of cingulate gray matter density in poor outcome bipolar illness." Psychiatry research **130**(2): 153-159.

Drevets, W. C. (2000). "Neuroimaging studies of mood disorders." Biological Psychiatry **48**(8): 813-829.

Drevets, W. C. (2001). "Neuroimaging and neuropathological studies of depression: implications for the cognitive-emotional features of mood disorders." Current Opinion in Neurobiology **11**(2): 240-249.

Drevets, W. C. (2003). "Neuroimaging abnormalities in the amygdala in mood disorders." Annals of the New York Academy of Sciences **985**: 420-444.

Du, Y. H., E. A. Allen, et al. (2016). "Artifact removal in the context of group ICA: A comparison of single-subject and group approaches." Human Brain Mapping **37**(3): 1005-1025.

Du, Y. H. and Y. Fan (2013). "Group information guided ICA for fMRI data analysis." NeuroImage **69**: 157-197.

Du, Y. H., H. M. Li, et al. (2012). "Identification of subject specific and functional consistent ROIs using semi-supervised learning." Medical Imaging 2012: Image Processing **8314**.

Du, Y. H., G. D. Pearlson, et al. (2015). "A group ICA based framework for evaluating resting fMRI markers when disease categories are unclear: application to schizophrenia, bipolar, and schizoaffective disorders." Neuroimage **122**: 272-280.

Dudek, D., M. Siwek, et al. (2013). "Diagnostic conversions from major depressive disorder into bipolar disorder in an outpatient setting: Results of a retrospective chart review." Journal of affective disorders **144**(1-2): 112-115.

Ehrlich, S., S. Brauns, et al. (2011). "Associations of Cortical Thickness and Cognition in Patients With Schizophrenia and Healthy Controls." Schizophr Bull.

Ehrlich, S., A. Yendiki, et al. (2011). "Striatal function in relation to negative symptoms in schizophrenia." Psychol Med: 1-16.

Elliott, R. (2003). "Executive functions and their disorders." British medical bulletin **65**: 49-59.

Erhardt, E. B., E. A. Allen, et al. (2011). "On network derivation, classification, and visualization: a response to Habeck and Moeller." Brain Connect **1**(2): 1-19.

Erhardt, E. B., S. Rachakonda, et al. (2011). "Comparison of multi-subject ICA methods for analysis of fMRI data." Human brain mapping **32**(12): 2075-2095.

Ferrier, I. N., R. Chowdhury, et al. (2004). "Neurocognitive function in unaffected first-degree relatives of patients with bipolar disorder: a preliminary report." Bipolar disorders **6**(4): 319-322.

First, M. B., R. L. Spitzer, et al., Eds. (1996). Structured Clinical Interview for DSM-IV Axis I Disorders-Patient Edition (SCID-I/P, Version 2.0). New York, New York State Psychiatry Institute.

Fisher, R. A. (1914). "Frequency distribution of the values of the correlation coefficient in samples from an indefinitely large population." Biometrika **10**: 507-521.

Foland-Ross, L. C., J. O. Brooks, et al. (2012). "Mood-state effects on amygdala volume in bipolar disorder." Journal of affective disorders **139**(3): 298-301.

Foland, L. C., L. L. Altshuler, et al. (2008). "Evidence for deficient modulation of amygdala response by prefrontal cortex in bipolar mania." Psychiatry research **162**(1): 27-37.

Fornito, A., J. Yoon, et al. (2011). "General and Specific Functional Connectivity Disturbances in First-Episode Schizophrenia During Cognitive Control Performance." Biological Psychiatry **70**(1): 64-72.

Fox, M. D., A. Z. Snyder, et al. (2005). "The human brain is intrinsically organized into dynamic, anticorrelated functional networks." Proceedings of the National Academy of Sciences of the United States of America **102**(27): 9673-9678.

Frazier, J. A., J. L. Breeze, et al. (2005). "Cortical gray matter differences identified by structural magnetic resonance imaging in pediatric bipolar disorder." Bipolar disorders **7**(6): 555-569.

Freire, L. and J. F. Mangin (2001). "Motion correction algorithms may create spurious brain activations in the absence of subject motion." Neuroimage **14**(3): 709-722.

Freire, L., A. Roche, et al. (2002). "What is the best similarity measure for motion correction in fMRI time series?" IEEE transactions on medical imaging **21**(5): 470-484.

Friston, K. J. (2002). "Beyond phrenology: What can neuroimaging tell us about distributed circuitry?" Annual Review of Neuroscience **25**: 221-250.

Friston, K. J. (2011). "Functional and effective connectivity: a review." Brain connectivity **1**(1): 13-36.

Ginestet, C. E. and A. Simmons (2010). "Statistical parametric network analysis of functional connectivity dynamics during a working memory task." Neuroimage **55**(2): 688-704.

Girvan, M. and M. E. J. Newman (2002). "Community structure in social and biological networks." Proceedings of the National Academy of Sciences of the United States of America **99**(12): 7821-7826.

Goldman-Rakic, P. S. (1994). "Working memory dysfunction in schizophrenia." J Neuropsychiatry Clin Neurosci **6**(4): 348-357.

Green, M. F., C. E. Bearden, et al. (2012). "Social Cognition in Schizophrenia, Part 1: Performance Across Phase of Illness." Schizophrenia Bulletin **38**(4): 854-864.

Green, M. F., R. S. Kern, et al. (2004). "Longitudinal studies of cognition and functional outcome in schizophrenia: implications for MATRICS." Schizophr Res **72**(1): 41-51.

Green, M. F., K. H. Nuechterlein, et al. (2004). "Approaching a consensus cognitive battery for clinical trials in schizophrenia: the NIMH-MATRICS conference to select cognitive domains and test criteria." Biol Psychiatry **56**(5): 301-307.

Greicius, M. D., K. Supekar, et al. (2009). "Resting-State Functional Connectivity Reflects Structural Connectivity in the Default Mode Network." Cerebral Cortex **19**(1): 72-78.

Grotegerd, D., A. Stuhrmann, et al. (2014). "Amygdala excitability to subliminally presented emotional faces distinguishes unipolar and bipolar depression: an fMRI and pattern classification study." Human brain mapping **35**(7): 2995-3007.

Groves, A. R., C. F. Beckmann, et al. (2011). "Linked independent component analysis for multimodal data fusion." NeuroImage **54**(3): 2198-2217.

Guimera, R. and L. A. N. Amaral (2005). "Functional cartography of complex metabolic networks." Nature **433**(7028): 895-900.

Haldane, M., G. Cunningham, et al. (2008). "Structural brain correlates of response inhibition in Bipolar Disorder I." Journal of psychopharmacology **22**(2): 138-143.

Hampson, M., N. R. Driesen, et al. (2006). "Brain connectivity related to working memory performance." J Neurosci **26**(51): 13338-13343.

Hampson, M., B. S. Peterson, et al. (2002). "Detection of functional connectivity using temporal correlations in MR images." Hum Brain Mapp **15**(4): 247-262.

Hashemi, R. H., W. G. Bradley, et al. (2003). <u>MRI : the basics</u>. Philadelphia, Pa. ; London, Lippincott Williams & Wilkins.

He, H., J. Sui, et al. (2012). "Altered small-world brain networks in schizophrenia patients during working memory performance." <u>PloS one</u> **7**(6): e38195.

He, H., Q. Yu, et al. (2016). "Resting-state functional network connectivity in prefrontal regions differs between unmedicated patients with bipolar and major depressive disorders." <u>Journal of affective disorders</u> **190**: 483-493.

He, Y., Z. Chen, et al. (2009). "Neuronal networks in Alzheimer's disease." <u>Neuroscientist</u> **15**(4): 333-350.

He, Y., Z. J. Chen, et al. (2007). "Small-world anatomical networks in the human brain revealed by cortical thickness from MRI." <u>Cereb Cortex</u> **17**(10): 2407-2419.

Heinrichs, R. W. and K. K. Zakzanis (1998). "Neurocognitive deficit in schizophrenia: a quantitative review of the evidence." <u>Neuropsychology</u> **12**(3): 426-445.

Hirschfeld, R. M., L. Lewis, et al. (2003). "Perceptions and impact of bipolar disorder: how far have we really come? Results of the national depressive and manic-depressive association 2000 survey of individuals with bipolar disorder." <u>The Journal of clinical psychiatry</u> **64**(2): 161-174.

Hirschfeld, R. M. A. and L. A. Vornik (2005). "Bipolar disorder - Costs and comorbidity." <u>American Journal of Managed Care</u> **11**(3): S85-S90.

Ho, B. C. and N. C. Andreasen (2001). "Long delays in seeking treatment for schizophrenia." <u>Lancet</u> **357**(9260): 898-900.

Humphries, M. D. and K. Gurney (2008). "Network 'small-world-ness': a quantitative method for determining canonical network equivalence." <u>PLoS One</u> **3**(4): e0002051.

Hyverinen, A., J. Karhunen, et al. (2001). <u>Independent Component Analysis</u> New York, Wiley.

Jafri, M. J., G. D. Pearlson, et al. (2008). "A method for functional network connectivity among spatially independent resting-state components in schizophrenia." <u>Neuroimage</u> **39**(4): 1666-1681.

James, C. J. and C. W. Hesse (2005). "Independent component analysis for biomedical signals." <u>Physiological measurement</u> **26**(1): R15-39.

Jenkinson, M., P. Bannister, et al. (2002). "Improved optimization for the robust and accurate linear registration and motion correction of brain images." <u>Neuroimage</u> **17**(2): 825-841.

Jie, N. F., M. H. Zhu, et al. (2015). "Discriminating Bipolar Disorder From Major Depression Based on SVM-FoBa: Efficient Feature Selection With Multimodal Brain Imaging Data." <u>Ieee Transactions on Autonomous Mental Development</u> **7**(4): 320-331.

John, H. G. L., P (1995). <u>Estimating Continuous Distributions in Bayesian Classifiers</u>. Eleventh Conference on Uncertainty in Artificial Intelligence, San Mateo.

Johnson, S. L., G. McKenzie, et al. (2008). "Ruminative Responses to Negative and Positive Affect Among Students Diagnosed with Bipolar Disorder and Major Depressive Disorder." <u>Cognitive Therapy and Research</u> **32**(5): 702-713.

Judd, L. L., H. S. Akiskal, et al. (2003). "A prospective investigation of the natural history of the long-term weekly symptomatic status of bipolar II disorder." Archives of General Psychiatry **60**(3): 261-269.

Judd, L. L., H. S. Akiskal, et al. (2002). "The long-term natural history of the weekly symptomatic status of bipolar I disorder." Archives of General Psychiatry **59**(6): 530-537.

Kaiser, M. and C. C. Hilgetag (2004). "Modelling the development of cortical systems networks." Neurocomputing **58**: 297-302.

Kang, S. S., S. R. Sponheim, et al. (2011). "Disrupted functional connectivity for controlled visual processing as a basis for impaired spatial working memory in schizophrenia." Neuropsychologia **49**(10): 2836-2847.

Karlsgodt, K. H., D. C. Glahn, et al. (2007). "The relationship between performance and fMRI signal during working memory in patients with schizophrenia, unaffected co-twins, and control subjects." Schizophr Res **89**(1-3): 191-197.

Keerthi, S. S., S. K. Shevade, et al. (2001). "Improvements to Platt's SMO algorithm for SVM classifier design." Neural computation **13**(3): 637-649.

Kegeles, L. S., Frankle, W.G., Gil, R., Narendran, R., Slifstein, M., Hwang, D.R., Cangiano, C., Haber, S.N., Abi-Dargham, A., and Laruelle, M.C. (2006). "Schizophrenia is associated with increased synaptic dopamine in associative rather than limbic regions of the striatum: implications for mechanisms of action of antipsychotic drugs." J. Nucl. Med. **47**: 139.

Kempton, M. J., Z. Salvador, et al. (2011). "Structural neuroimaging studies in major depressive disorder. Meta-analysis and comparison with bipolar disorder." Archives of General Psychiatry **68**(7): 675-690.

Kettenri.Jr (1971). "Canonical Analysis of Several Sets of Variables." Biometrika **58**(3): 433-&.

Kim, D. I., D. S. Manoach, et al. (2009). "Dysregulation of working memory and default-mode networks in schizophrenia using independent component analysis, an fBIRN and MCIC study." Hum Brain Mapp **30**(11): 3795-3811.

Kim, D. I., J. Sui, et al. (2010). "Identification of imaging biomarkers in schizophrenia: a coefficient-constrained independent component analysis of the mind multi-site schizophrenia study." Neuroinformatics **8**(4): 213-229.

Kim, M. A., E. Tura, et al. (2010). "Working memory circuitry in schizophrenia shows widespread cortical inefficiency and compensation." Schizophr Res **117**(1): 42-51.

Kiviniemi, V., J. H. Kantola, et al. (2003). "Independent component analysis of nondeterministic fMRI signal sources." NeuroImage **19**(2 Pt 1): 253-260.

Kiviniemi, V., T. Starck, et al. (2009). "Functional segmentation of the brain cortex using high model order group PICA." Human brain mapping **30**(12): 3865-3886.

Konarski, J. Z., R. S. Mcintyre, et al. (2008). "Volumetric neuroimaging investigations in mood disorders: bipolar disorder versus major depressive disorder." Bipolar disorders **10**(1): 1-37.

Kupfer, D. J. (2005). "The increasing medical burden in bipolar disorder." JAMA : the journal of the American Medical Association **293**(20): 2528-2530.

Kupfer, D. J., E. Frank, et al. (2012). "Major depressive disorder: new clinical, neurobiological, and treatment perspectives." Lancet **379**(9820): 1045-1055.

Latora, V. and M. Marchiori (2001). "Efficient behavior of small-world networks." Physical review letters **87**(19).

Latora, V. and M. Marchiori (2003). "Economic small-world behavior in weighted networks." European Physical Journal B **32**(2): 249-263.

Lauritzen, S. L. (1996). Graphical models. Oxford, Clarendon.

Le Bihan, D. (2003). "Looking into the functional architecture of the brain with diffusion MRI." Nature Reviews Neuroscience **4**(6): 469-480.

Lee, H. Y., W. S. Tae, et al. (2011). "Demonstration of decreased gray matter concentration in the midbrain encompassing the dorsal raphe nucleus and the limbic subcortical regions in major depressive disorder: an optimized voxel-based morphometry study." Journal of affective disorders **133**(1-2): 128-136.

Li, Y. O., T. Adali, et al. (2007). "Estimating the number of independent components for functional magnetic resonance imaging data." Hum Brain Mapp **28**(11): 1251-1266.

Li, Y. O., T. Adali, et al. (2009). "Joint Blind Source Separation by Multi-set Canonical Correlation Analysis." IEEE transactions on signal processing : a publication of the IEEE Signal Processing Society **57**(10): 3918-3929.

Liao, W., Z. Q. Zhang, et al. (2010). "Altered Functional Connectivity and Small-World in Mesial Temporal Lobe Epilepsy." Plos One **5**(1): -.

Lin, F. H., A. R. McIntosh, et al. (2003). "Multivariate analysis of neuronal interactions in the generalized partial least squares framework: simulations and empirical studies." NeuroImage **20**(2): 625-642.

Liu, L., L. L. Zeng, et al. (2012). "Altered cerebellar functional connectivity with intrinsic connectivity networks in adults with major depressive disorder." PLoS ONE **7**(6): e39516.

Liu, Y., M. Liang, et al. (2008). "Disrupted small-world networks in schizophrenia." Brain **131**(Pt 4): 945-961.

Lochhead, R. A., R. V. Parsey, et al. (2004). "Regional brain gray matter volume differences in patients with bipolar disorder as assessed by optimized voxel-based morphometry." Biological Psychiatry **55**(12): 1154-1162.

Lynall, M. E., D. S. Bassett, et al. (2010). "Functional connectivity and brain networks in schizophrenia." The Journal of neuroscience : the official journal of the Society for Neuroscience **30**(28): 9477-9487.

Lyoo, I. K., M. J. Kim, et al. (2004). "Frontal lobe gray matter density decreases in bipolar I disorder." Biological Psychiatry **55**(6): 648-651.

Lyoo, I. K., Y. H. Sung, et al. (2006). "Regional cerebral cortical thinning in bipolar disorder." Bipolar disorders **8**(1): 65-74.

Ma, Q., L. L. Zeng, et al. (2013). "Altered cerebellar-cerebral resting-state functional connectivity reliably identifies major depressive disorder." Brain research **1495**: 86-94.

Manoach, D. S. (2003). "Prefrontal cortex dysfunction during working memory performance in schizophrenia: reconciling discrepant findings." <u>Schizophr Res</u> **60**(2-3): 285-298.

Manoach, D. S., R. L. Gollub, et al. (2000). "Schizophrenic subjects show aberrant fMRI activation of dorsolateral prefrontal cortex and basal ganglia during working memory performance." <u>Biological Psychiatry</u> **48**(2): 99-109.

Manoach, D. S., D. Z. Press, et al. (1999). "Schizophrenic subjects activate dorsolateral prefrontal cortex during a working memory task, as measured by fMRI." <u>Biol Psychiatry</u> **45**(9): 1128-1137.

Marrelec, G., A. Krainik, et al. (2006). "Partial correlation for functional brain interactivity investigation in functional MRI." <u>Neuroimage</u> **32**(1): 228-237.

Mars, R. B., S. Jbabdi, et al. (2011). "Diffusion-Weighted Imaging Tractography-Based Parcellation of the Human Parietal Cortex and Comparison with Human and Macaque Resting-State Functional Connectivity." <u>Journal of Neuroscience</u> **31**(11): 4087-4100.

Maslov, S. and K. Sneppen (2002). "Specificity and stability in topology of protein networks." <u>Science</u> **296**(5569): 910-913.

McCarthy, G., A. M. Blamire, et al. (1994). "Functional magnetic resonance imaging of human prefrontal cortex activation during a spatial working memory task." <u>Proc Natl Acad Sci U S A</u> **91**(18): 8690-8694.

McKeown, M. J., S. Makeig, et al. (1998). "Analysis of fMRI data by blind separation into independent spatial components." <u>Human brain mapping</u> **6**(3): 160-188.

McKeown, M. J. and T. J. Sejnowski (1998). "Independent component analysis of fMRI data: examining the assumptions." Human brain mapping **6**(5-6): 368-372.

Meng, X., R. Jiang, et al. (2016). "Predicting individualized clinical measures by a generalized prediction framework and multimodal fusion of MRI data." Neuroimage.

Michael, A. M., M. D. King, et al. (2011). "A Data-Driven Investigation of Gray Matter-Function Correlations in Schizophrenia during a Working Memory Task." Front Hum Neurosci **5**: 71.

Micheloyannis, S., E. Pachou, et al. (2006). "Small-world networks and disturbed functional connectivity in schizophrenia." Schizophr Res **87**(1-3): 60-66.

Milo, R., S. Shen-Orr, et al. (2002). "Network motifs: simple building blocks of complex networks." Science **298**(5594): 824-827.

Mitchell, P. B., K. Wilhelm, et al. (2001). "The clinical features of bipolar depression: a comparison with matched major depressive disorder patients." The Journal of clinical psychiatry **62**(3): 212-216; quiz 217.

Montgomery, S. A. and M. Asberg (1979). "New Depression Scale Designed to Be Sensitive to Change." British Journal of Psychiatry **134**(Apr): 382-389.

Moussa, M. N., C. D. Vechlekar, et al. (2011). "Changes in cognitive state alter human functional brain networks." Frontiers in Human Neuroscience **5**.

Murray, C. J. L., A. D. Lopez, et al. (1996). The Global burden of disease : a comprehensive assessment of mortality and disability from diseases, injuries, and risk factors in 1990 and projected to 2020. Geneva, World Health Organization.

Narrow, W. E., D. S. Rae, et al. (2002). "Revised prevalence estimates of mental disorders in the United States: using a clinical significance criterion to reconcile 2 surveys' estimates." Archives of General Psychiatry **59**(2): 115-123.

Newman, M. E. J. (2004). "Fast algorithm for detecting community structure in networks." Physical Review E **69**(6).

Nolte, J. (2009). The human brain : an introduction to its functional anatomy. Philadelphia, PA, Mosby/Elsevier.

Oldfield, R. C. (1971). "The assessment and analysis of handedness: the Edinburgh inventory." Neuropsychologia **9**(1): 97-113.

Ongur, D., M. Lundy, et al. (2010). "Default mode network abnormalities in bipolar disorder and schizophrenia." Psychiatry Research-Neuroimaging **183**(1): 59-68.

Owen, A. M., K. M. McMillan, et al. (2005). "N-back working memory paradigm: a meta-analysis of normative functional neuroimaging studies." Hum Brain Mapp **25**(1): 46-59.

Pachou, E., M. Vourkas, et al. (2008). "Working memory in schizophrenia: an EEG study using power spectrum and coherence analysis to estimate cortical activation and network behavior." Brain Topogr **21**(2): 128-137.

Palva, S., S. Monto, et al. (2010). "Graph properties of synchronized cortical networks during visual working memory maintenance." Neuroimage **49**(4): 3257-3268.

Parent, A. and L. N. Hazrati (1995). "Functional-Anatomy of the Basal Ganglia .1. The Cortico-Basal Ganglia-Thalamo-Cortical Loop." Brain Research Reviews **20**(1): 91-127.

Park, B., D. S. Kim, et al. (2014). "Graph independent component analysis reveals repertoires of intrinsic network components in the human brain." PLoS ONE **9**(1): e82873.

Park, S. and P. S. Holzman (1992). "Schizophrenics Show Spatial Working Memory Deficits." Archives of General Psychiatry **49**(12): 975-982.

Passarotti, A. M., J. Ellis, et al. (2012). "Reduced functional connectivity of prefrontal regions and amygdala within affect and working memory networks in pediatric bipolar disorder." Brain connectivity **2**(6): 320-334.

Pavuluri, M. N., M. M. O'Connor, et al. (2007). "Affective neural circuitry during facial emotion processing in pediatric bipolar disorder." Biological psychiatry **62**(2): 158-167.

Pavuluri, M. N., M. M. O'Connor, et al. (2008). "An fMRI study of the interface between affective and cognitive neural circuitry in pediatric bipolar disorder." Psychiatry Research-Neuroimaging **162**(3): 244-255.

Peng, J., J. Liu, et al. (2011). "Cerebral and cerebellar gray matter reduction in first-episode patients with major depressive disorder: a voxel-based morphometry study." European journal of radiology **80**(2): 395-399.

Perlstein, W. M., C. S. Carter, et al. (2001). "Relation of prefrontal cortex dysfunction to working memory and symptoms in schizophrenia." American Journal of Psychiatry **158**(7): 1105-1113.

Petrides, M., B. Alivisatos, et al. (1993). "Functional activation of the human frontal cortex during the performance of verbal working memory tasks." Proc Natl Acad Sci U S A **90**(3): 878-882.

Phillips, J. R., D. H. Hewedi, et al. (2015). "The cerebellum and psychiatric disorders." Frontiers in public health **3**: 66.

Phillips, M., C. Ladouceur, et al. (2008). "A neural model of voluntary and automatic emotion regulation: implications for understanding the pathophysiology and neurodevelopment of bipolar disorder." Molecular Psychiatry **13**(9): 833-857.

Phillips, M. L. and H. A. Swartz (2014). "A critical appraisal of neuroimaging studies of bipolar disorder: toward a new conceptualization of underlying neural circuitry and a road map for future research." The American journal of psychiatry **171**(8): 829-843.

Poldrack, R. A. (2010). "Mapping Mental Function to Brain Structure: How Can Cognitive Neuroimaging Succeed?" Perspectives on Psychological Science **5**(6): 753-761.

Potkin, S. G., J. A. Turner, et al. (2009). "Working memory and DLPFC inefficiency in schizophrenia: the FBIRN study." Schizophr Bull **35**(1): 19-31.

Power, J. D., K. A. Barnes, et al. (2012). "Spurious but systematic correlations in functional connectivity MRI networks arise from subject motion." Neuroimage **59**(3): 2142-2154.

Price, J. L. and W. C. Drevets (2012). "Neural circuits underlying the pathophysiology of mood disorders." Trends in Cognitive Sciences **16**(1): 61-71.

Raffo, M., M. Hampson, et al. (2004). "Functional connectivity between ventral prefrontal cortex and amygdala in bipolar disorder." Biological psychiatry **55**: 229s-229s.

Reichardt, J. and S. Bornholdt (2006). "Statistical mechanics of community detection." Physical Review E **74**(1).

Rigucci, S., G. Serafini, et al. (2010). "Anatomical and functional correlates in major depressive disorder: the contribution of neuroimaging studies." The world journal of biological psychiatry : the official journal of the World Federation of Societies of Biological Psychiatry **11**(2 Pt 2): 165-180.

Rissling, A. J., S. Makeig, et al. (2010). "Neurophysiologic markers of abnormal brain activity in schizophrenia." Curr Psychiatry Rep **12**(6): 572-578.

Roffman, J. L., R. L. Gollub, et al. (2008). "MTHFR 677C --> T genotype disrupts prefrontal function in schizophrenia through an interaction with COMT 158Val --> Met." Proc Natl Acad Sci U S A **105**(45): 17573-17578.

Ronhovde, P. and Z. Nussinov (2009). "Multiresolution community detection for megascale networks by information-based replica correlations." Physical Review E **80**(1).

Rubinov, M., S. A. Knock, et al. (2009). "Small-World Properties of Nonlinear Brain Activity in Schizophrenia." Human Brain Mapping **30**(2): 403-416.

Rubinov, M. and O. Sporns (2010). "Complex network measures of brain connectivity: uses and interpretations." Neuroimage **52**(3): 1059-1069.

Rykhlevskaia, E., G. Gratton, et al. (2008). "Combining structural and functional neuroimaging data for studying brain connectivity: A review." Psychophysiology **45**(2): 173-187.

Sacher, J., J. Neumann, et al. (2012). "Mapping the depressed brain: a meta-analysis of structural and functional alterations in major depressive disorder." Journal of affective disorders **140**(2): 142-148.

Salvador, R., A. Martinez, et al. (2008). "A simple view of the brain through a frequency-specific functional connectivity measure." Neuroimage **39**(1): 279-289.

Savitz, J., R. Dantzer, et al. (2015). "Neuroprotective kynurenine metabolite indices are abnormally reduced and positively associated with hippocampal and amygdalar volume in bipolar disorder." Psychoneuroendocrinology **52**: 200-211.

Savitz, J., W. C. Drevets, et al. (2015). "Putative neuroprotective and neurotoxic kynurenine pathway metabolites are associated with hippocampal and amygdalar volumes in subjects with major depressive disorder." Neuropsychopharmacology : official publication of the American College of Neuropsychopharmacology **40**(2): 463-471.

Savitz, J., A. C. Nugent, et al. (2010). "Amygdala volume in depressed patients with bipolar disorder assessed using high resolution 3T MRI: The impact of medication." Neuroimage **49**(4): 2966-2976.

Sawaguchi, T. and P. S. Goldman-Rakic (1991). "D1 dopamine receptors in prefrontal cortex: involvement in working memory." Science **251**(4996): 947-950.

Saykin, A. J., R. C. Gur, et al. (1991). "Neuropsychological function in schizophrenia. Selective impairment in memory and learning." Arch Gen Psychiatry **48**(7): 618-624.

Simpson, E. H., C. Kellendonk, et al. (2010). "A possible role for the striatum in the pathogenesis of the cognitive symptoms of schizophrenia." Neuron **65**(5): 585-596.

Smith, S. M. (2004). "Overview of fMRI analysis." British Journal of Radiology **77**: S167-S175.

Spencer, K. M., P. G. Nestor, et al. (2004). "Neural synchrony indexes disordered perception and cognition in schizophrenia." Proceedings of the National Academy of Sciences of the United States of America **101**(49): 17288-17293.

Sporns, O. (2011). Networks of the brain. Cambridge, Mass. ; London, MIT Press.

Sporns, O. and J. D. Zwi (2004). "The small world of the cerebral cortex." Neuroinformatics **2**(2): 145-162.

Spreng, R. N., R. A. Mar, et al. (2009). "The Common Neural Basis of Autobiographical Memory, Prospection, Navigation, Theory of Mind, and the Default Mode: A Quantitative Meta-analysis." Journal of cognitive neuroscience **21**(3): 489-510.

Stam, C. J., B. F. Jones, et al. (2007). "Small-world networks and functional connectivity in Alzheimer's disease." Cereb Cortex **17**(1): 92-99.

Stein, J. L., L. M. Wiedholz, et al. (2007). "A validated network of effective amygdala connectivity." NeuroImage **36**(3): 736-745.

Stephen, J. M., B. A. Coffman, et al. (2013). "Using joint ICA to link function and structure using MEG and DTI in schizophrenia." Neuroimage **83**: 418-430.

Sternberg, S. (1966). "High-speed scanning in human memory." Science **153**(736): 652-654.

Stoddard, J., S. J. Gotts, et al. (2016). "Aberrant intrinsic functional connectivity within and between corticostriatal and temporal-parietal networks in adults and youth with bipolar disorder." Psychological Medicine **46**(7): 1509-1522.

Strakowski, S. M., C. M. Adler, et al. (2012). "The functional neuroanatomy of bipolar disorder: a consensus model." Bipolar disorders **14**(4): 313-325.

Strakowski, S. M., M. P. DelBello, et al. (2005). "The functional neuroanatomy of bipolar disorder: a review of neuroimaging findings." Molecular Psychiatry **10**(1): 105-116.

Strimbu, K. and J. A. Tavel (2010). "What are biomarkers?" Current Opinion in Hiv and Aids **5**(6): 463-466.

Stuss, D. T. and D. F. Benson (1984). "Neuropsychological Studies of the Frontal Lobes." Psychological bulletin **95**(1): 3-28.

Sui, J., T. Adali, et al. (2010). "A CCA+ICA based model for multi-task brain imaging data fusion and its application to schizophrenia." Neuroimage **51**(1): 123-134.

Sui, J., T. Adali, et al. (2009). "An ICA-based method for the identification of optimal FMRI features and components using combined group-discriminative techniques." Neuroimage **46**(1): 73-86.

Sui, J., T. Adali, et al. (2012). "A review of multivariate methods for multimodal fusion of brain imaging data." Journal of neuroscience methods **204**(1): 68-81.

Sui, J., H. He, et al. (2013). "Three-way (N-way) fusion of brain imaging data based on mCCA+jICA and its application to discriminating schizophrenia." NeuroImage **66**: 119-132.

Sui, J., H. He, et al. (2013). "Combination of Resting State fMRI, DTI, and sMRI Data to Discriminate Schizophrenia by N-way MCCA + jICA." <u>Frontiers in human neuroscience</u> **7**: 235.

Sui, J., R. Huster, et al. (2014). "Function-structure associations of the brain: Evidence from multimodal connectivity and covariance studies." <u>Neuroimage</u> **102**: 11-23.

Sui, J., G. Pearlson, et al. (2011). "Discriminating schizophrenia and bipolar disorder by fusing fMRI and DTI in a multimodal CCA+ joint ICA model." <u>NeuroImage</u> **57**(3): 839-855.

Sui, J., G. D. Pearlson, et al. (2015). "In Search of Multimodal Neuroimaging Biomarkers of Cognitive Deficits in Schizophrenia." <u>Biological Psychiatry</u> **78**(11): 794-804.

Sui, S. G., Y. Zhang, et al. (2010). "Abnormal cerebellum density in victims of rape with post-traumatic stress disorder: Voxel-based analysis of magnetic resonance imaging investigation." <u>Asia-Pacific Psychiatry</u> **2**(3): 129-135.

Sweeney, J. A., J. A. Kmiec, et al. (2000). "Neuropsychologic impairments in bipolar and unipolar mood disorders on the CANTAB neurocognitive battery." <u>Biological Psychiatry</u> **48**(7): 674-684.

Tang, Y., L. Kong, et al. (2013). "Decreased functional connectivity between the amygdala and the left ventral prefrontal cortex in treatment-naive patients with major depressive disorder: a resting-state functional magnetic resonance imaging study." <u>Psychological Medicine</u> **43**(9): 1921-1927.

Tang, Y., F. Wang, et al. (2007). "Reduced ventral anterior cingulate and amygdala volumes in medication-naive females with major depressive disorder: A voxel-

based morphometric magnetic resonance imaging study." Psychiatry research **156**(1): 83-86.

Tang, Y. Y., Q. B. Zhao, et al. (2008). "The effects of neuron heterogeneity and connection mechanism in cortical networks." Physica a-Statistical Mechanics and Its Applications **387**(23): 5952-5957.

Taylor Tavares, J. V., L. Clark, et al. (2008). "Neural basis of abnormal response to negative feedback in unmedicated mood disorders." NeuroImage **42**(3): 1118-1126.

Torrisi, S., T. D. Moody, et al. (2013). "Differences in resting corticolimbic functional connectivity in bipolar I euthymia." Bipolar disorders **15**(2): 156-166.

Tregellas, J. R., J. Smucny, et al. (2014). "Intrinsic Hippocampal Activity as a Biomarker for Cognition and Symptoms in Schizophrenia." Am J Psychiatry.

Tzourio-Mazoyer, N., B. Landeau, et al. (2002). "Automated anatomical labeling of activations in SPM using a macroscopic anatomical parcellation of the MNI MRI single-subject brain." NeuroImage **15**(1): 273-289.

van den Heuvel, M. P. and H. E. Hulshoff Pol (2010). "Exploring the brain network: a review on resting-state fMRI functional connectivity." Eur Neuropsychopharmacol **20**(8): 519-534.

van den Heuvel, M. P., R. C. W. Mandl, et al. (2009). "Functionally Linked Resting-State Networks Reflect the Underlying Structural Connectivity Architecture of the Human Brain." Human Brain Mapping **30**(10): 3127-3141.

van den Heuvel, M. P., C. J. Stam, et al. (2009). "Efficiency of Functional Brain Networks and Intellectual Performance." <u>Journal of Neuroscience</u> **29**(23): 7619-7624.

Van Dijk, K. R., T. Hedden, et al. (2010). "Intrinsic functional connectivity as a tool for human connectomics: theory, properties, and optimization." <u>Journal of neurophysiology</u> **103**(1): 297-321.

Van Dijk, K. R. A., M. R. Sabuncu, et al. (2012). "The influence of head motion on intrinsic functional connectivity MRI." <u>Neuroimage</u> **59**(1): 431-438.

Van Essen, D. C. and D. Dierker (2007). "On navigating the human cerebral cortex: Response to 'in praise of tedious anatomy'." <u>Neuroimage</u> **37**(4): 1050-1054.

Varela, F., J. P. Lachaux, et al. (2001). "The brainweb: phase synchronization and large-scale integration." <u>Nature reviews. Neuroscience</u> **2**(4): 229-239.

Vargas, C., C. Lopez-Jaramillo, et al. (2013). "A systematic literature review of resting state network-functional MRI in bipolar disorder." <u>Journal of affective disorders</u> **150**(3): 727-735.

Veer, I. M., C. F. Beckmann, et al. (2010). "Whole brain resting-state analysis reveals decreased functional connectivity in major depression." <u>Frontiers in systems neuroscience</u> **4**.

Versace, A., W. K. Thompson, et al. (2010). "Abnormal Left and Right Amygdala-Orbitofrontal Cortical Functional Connectivity to Emotional Faces: State Versus Trait Vulnerability Markers of Depression in Bipolar Disorder." <u>Biological Psychiatry</u> **67**(5): 422-431.

Videbech, P. (2000). "PET measurements of brain glucose metabolism and blood flow in major depressive disorder: a critical review." Acta psychiatrica Scandinavica **101**(1): 11-20.

Wang, H., L. Douw, et al. (2010). "Effect of tumor resection on the characteristics of functional brain networks." Phys Rev E Stat Nonlin Soft Matter Phys **82**(2 Pt 1): 021924.

Wang, L., D. F. Hermens, et al. (2012). "A systematic review of resting-state functional-MRI studies in major depression." Journal of affective disorders **142**(1-3): 6-12.

Wang, L., P. D. Metzak, et al. (2010). "Impaired efficiency of functional networks underlying episodic memory-for-context in schizophrenia." J Neurosci **30**(39): 13171-13179.

Watts, D. J. and S. H. Strogatz (1998). "Collective dynamics of 'small-world' networks." Nature **393**(6684): 440-442.

White, T., D. O'Leary, et al. (2001). "Anatomic and functional variability: the effects of filter size in group fMRI data analysis." Neuroimage **13**(4): 577-588.

White, T., M. Schmidt, et al. (2011). "Disrupted Functional Brain Connectivity during Verbal Working Memory in Children and Adolescents with Schizophrenia." Cerebral Cortex **21**(3): 510-518.

Whittaker, J. (1990). Graphical models in applied multivariate statistics. Chichester [England] ; New York, Wiley.

Witten, I. H., E. Frank, et al. (2011). "Introduction to Weka." Data Mining: Practical Machine Learning Tools and Techniques, 3rd Edition: 403-406.

Xia, M., J. Wang, et al. (2013). "BrainNet Viewer: a network visualization tool for human brain connectomics." PLoS ONE **8**(7): e68910.

Xu, L., K. M. Groth, et al. (2009). "Source-Based Morphometry: The Use of Independent Component Analysis to Identify Gray Matter Differences With Application to Schizophrenia." Human Brain Mapping **30**(3): 711-724.

Yan, C. G., R. C. Craddock, et al. (2013). "Addressing head motion dependencies for small-world topologies in functional connectomics." Frontiers in human neuroscience **7**.

Yang, H. H., J. Y. Liu, et al. (2010). "A hybrid machine learning method for fusing fMRI and genetic data: combining both improves classification of schizophrenia." Frontiers in Human Neuroscience **4**.

Young, R. C., J. T. Biggs, et al. (1978). "A rating scale for mania: reliability, validity and sensitivity." The British journal of psychiatry : the journal of mental science **133**: 429-435.

Yu, Q., S. M. Plis, et al. (2011). "Modular Organization of Functional Network Connectivity in Healthy Controls and Patients with Schizophrenia during the Resting State." Frontiers in systems neuroscience **5**: 103.

Yu, Q., J. Sui, et al. (2013). "Disrupted correlation between low frequency power and connectivity strength of resting state brain networks in schizophrenia." Schizophrenia research **143**(1): 165-171.

Yu, Q., J. Sui, et al. (2011). "Altered Topological Properties of Functional Network Connectivity in Schizophrenia during Resting State: A Small-World Brain Network Study." PLoS One **6**(9): e25423.

Yu, Q., J. Sui, et al. (2011). "Altered small-world brain networks in temporal lobe in patients with schizophrenia performing an auditory oddball task." Front Syst Neurosci **5**: 7.

Yucel, K., A. Nazarov, et al. (2013). "Cerebellar vermis volume in major depressive disorder." Brain structure & function **218**(4): 851-858.

Zhao, L. P., Y. Wang, et al. (2016). "Cerebellar microstructural abnormalities in bipolar depression and unipolar depression: A diffusion kurtosis and perfusion imaging study." Journal of affective disorders **195**: 21-31.

Zhu, X., X. Wang, et al. (2012). "Evidence of a dissociation pattern in resting-state default mode network connectivity in first-episode, treatment-naive major depression patients." Biological psychiatry **71**(7): 611-617.

Zou, K., W. Deng, et al. (2010). "Changes of brain morphometry in first-episode, drug-naive, non-late-life adult patients with major depression: an optimized voxel-based morphometry study." Biological Psychiatry **67**(2): 186-188.

Zou, Q. H., C. Z. Zhu, et al. (2008). "An improved approach to detection of amplitude of low-frequency fluctuation (ALFF) for resting-state fMRI: fractional ALFF." J Neurosci Methods **172**(1): 137-141.